الجمهورية الجزائرية الديمقراطية الشعبية

وزارة التعليم العالي و البحث العلمي

جامعة تيسمسيلت

THÈSE

En vue de l'obtention du Diplôme de Doctorat LMD

Présentée par : ZEFFANE Soumia

Intitulé:*Élaboration et Etude des Propriétés Structurales, Electroniques et Magnétiques des Alliages de Heusler : Application en Spintronique*

Faculté	***: Sciences et de la Technologie***
Département	***: Sciences de la matière***
Domaine	***: Sciences de la matière***
Filière	***: Physique***
Spécialité	***: Nano-physique***

Devant le Jury Composé de :

Membres de Jury	***Grade***	***Qualité***	***Domiciliation***
BENALIA Salah Eddine	***Pr***	***Président***	***U. Tissemsilt***
DAHMANE Fethallah	***Pr***	***Encadreur***	***U. Tissemsilt***
MOKHTARI Mohamed	***MCA***	***Co-Encadreur***	***U. Tissemsilt***
BOUDIA Keltouma	***Pr***	***Examinateur***	***U. Tissemsilt***
RACHED Habib	***Pr***	***Examinateur***	***U. Chlef***
RIGHI Haroun	***MCA***	***Examinateur***	***U. Batna -1***

*Année Universitaire : **2022/2023***

الجمهورية الجزائرية الديمقراطية الشعبية

وزارة التعليم العالي و البحث العلمي

جامعة تيسمسيلت

THESIS

With the View to Obtaining the LMD Doctoral Diploma

Presented by : Soumia ZEFFANE

***Entitled**: Elaboration and Study of the Structural, Electronic, and Magnetic Properties of Heusler Alloys: Application in Spintronics*

Faculty	***: Sciences and Technology***
Departement	***: Sciences of Matter***
Domain	***: Sciences of Matter***
Filière	***: Physics***
Spécialité	***: Nano-physics***

In front of the jury composed of:

Members of the Jury	*Grade*	*Position*	*Affiliation*
Salah Eddine BENALIA	***Prof***	***Chairman***	***U. Tissemsilt***
Fethallah DAHMANE	***Prof***	***Supervisor***	***U. Tissemsilt***
Mohamed MOKHTARI	***MCA***	***Co-supervisor***	***U. Tissemsilt***
Keltouma BOUDIA	***Prof***	***Examiner***	***U. Tissemsilt***
Habib RACHED	***Prof***	***Examiner***	***U. Chlef***
Haroun RIGHI	***MCA***	***Examiner***	***U. Batna -1***

*Academic Year :**2022/2023***

Dedication

To all the people I love.

Acknowledgments

I would like to express my deepest gratitude and appreciation to my supervisor **Professor Fethallah DAHMENE** for his guidance, monitoring, support, devotion to helping me, and immense knowledge. I have been very fortunate to have an inspiring supervisor who made my research journey far easier and more productive.

I am greatly indebted to **Doctor Mohamed MOKHTARI** for his great amounts of encouragement, advice, and help.

I would like to further thank my colleague **Miss. Fatima SOFRANI** for everything she has done for me.

Special thanks are due to **Professor Salah Eddine BENALIA**, **ProfessorKeltouma BOUDIA**,**ProfessorHabib RACHED**, and **DoctorHaroun RIGHI** for accepting to be part of the panel of examination and judging the research work to be complete for its defense.

Abstract

In this work of reaserch, we investigated the structural, electronic and magnetic properties of the full Heusler compounds Mn_2YSn (Y= Mo,Nb, Zr) and pressure effects on the structural, electronic, and magnetic properties of Mn_2YSn (Y= Ru, Rh, and Pd) Heusler alloys.This study was carried out by employing state of an art first-principles computational approach named "full potential (FP) linearized (L) augmented plane wave (APW)"as designed with "density functional theory (DFT)"using the generalized gradient approximation and executed in WIEN2k computational code.We found that the calculated lattice constants are in good agreement with the theoretical values. For Mn_2YSn (Y= Mo,Nb, Zr),we observed that the Cu_2MnAl-type structure is more stable than the Hg_2CuTi type. Mn_2MoSn have a metallic character in both Hg_2CuTi and Cu_2MnAl type structures. The total spin magnetic moment obeys the Slater-Pauling rule. Half-metal exhibits 100% spin polarization at the Fermi level. The obtained results show that Mn_2RuSn, Mn_2RhSn and Mn_2PdSn compounds are stable in the Hg_2CuTi- type structure. Furthermore, under pressure effect Mn_2RuSn, Mn_2RhSn and Mn_2PdSn compounds become half metals at about 10 GPa, 10 GPa and 20 GPa, respectively.

Keywords: Heusler alloys, DFT,half metallic, Ferromagnetics.

Résumé

Dans ce travail de recherche, nous avons étudié les propriétés structurales, électroniques et magnétiques des composés Heusler complets Mn_2YSn (Y= Mo, Nb, Zr) et les effets de la pression sur les propriétés structurales, électroniques et magnétiques de Mn_2YSn (Y= Ru, Rh , et Pd) alliages Heusler. Cette étude a été réalisée en utilisant une approche informatique de premier principe appelée "Full potential- linearized augmented plane wave" (FP) linéarisé (L) onde plane augmentée (APW)" telle que conçue avec la "théorie fonctionnelle de la densité (DFT)" en utilisant l'approximation de gradient généralisée et exécutée dans le code de calcul WIEN2k. Nous avons constaté que les constantes de réseau calculées sont en bon accord avec les valeurs théoriques. Pour Mn_2YSn (Y= Mo, Nb, Zr), nous avons observé que la structure de type Cu_2MnAl est plus stable que celle de type Hg_2CuTi. Mn_2MoSn a un caractère métallique dans les structures de type Hg_2CuTi et Cu_2MnAl. Le moment magnétique de spin total obéit à la règle de Slater-Pauling. Le demi-métal présente une polarisation de spin de 100% au niveau de Fermi. Les résultats obtenus montrent que les composés Mn_2RuSn, Mn_2RhSn et Mn_2PdSn sont stables dans la structure de type Hg_2CuTi. De plus, sous l'effet de la pression, les composés Mn_2RuSn, Mn_2RhSn et Mn_2PdSn deviennent des demi-métaux à environ 10 GPa, 10 GPa et 20 GPa, respectivement.

Mots-clés : Alliages Heusler.DFT, semi-métallique, Ferromagnétique

ملخص

في هذا العمل البحثي ، درسنا الخصائص الهيكلية والإلكترونية والمغناطيسية لمركبات هوسلر الكاملة Mn_2YSn (Y= Mo, Nb ,Zr) وتأثيرات الضغط على الخصائص الهيكلية والإلكترونية والمغناطيسية لـ Mn_2YSn (Y=Ru,Rh ,Pd) سبائك هوسلر. تم إجراء هذه الدراسة من خلال استخدام أحدث نهج حسابي للمبادئ الأولى يسمى "الموجة المستوية الخطية (L) ذات الإمكانات الكاملة "(APW) (FP) كما تم تصميمه باستخدام "نظرية الكثافة الوظيفية "(DFT) باستخدام تقريب التدرج المعمم ويتم تنفيذه في الكود الحسابي WIEN2k .ثوابت الشبكة المحسوبة تتوافق جيدًا مع القيم النظرية. بالنسبة إلى Mn_2YSn (Y= Mo, Nb , Zr) ، لاحظنا أن بنية Cu_2MnAl أكثر استقرارًا من بنية Hg_2CuTi. Mn_2MoSn له طابع معدني في كل من هياكل من النوع Hg_2CuTi و Cu_2MnAl. تخضع عزم الدوران المغناطيسي الكلي لقاعدة سلاتر-بولينج. يعرض نصف المعدن استقطابًا بنسبة 100٪ على مستوى فيرمي. أظهرت النتائج التي تم الحصول عليها أن مركبات Mn_2RuSn و Mn_2RhSn و Mn_2PdSn مستقرة في هيكل من النوع Hg_2CuTi .علاوة على ذلك، تحت تأثير الضغط، تصبح مركبات Mn_2RuSnو Mn_2RhSn و Mn_2PdSnنصف معادن عند حوالي 10 GPa و 10 GPa و 20 GPaعلى التوالي

الكلمات المفتاحية: سبائك هوسلر ، DFT، نصف معدنية ، مغناطيسية حديدية

Table of Contents

List of Tables

List of Figures

List of Abbreviations

DFT	Density Functional Theory
HF	Hartree- Fock
HK	Hohenberg and Kohn
KS	Kohn-Sham
LDA	Local Density Approximation
GGA	Generalized gradient approximation
LAPW	The linearized Augmented Plane Wave method
FP-LAPW	Full potential- linearized augmented plane wave
MT	Muffin-tin
R_{MT}	sphere Radius ´´Muffin-Tin´´
E_{xc}	Exchange energy and correlation
DOS	Density Of State
TDOS	Total Density Of State
PDOS	Partial Density Of State
FM	Ferromagnetic
HM	Half-Metallic
AFM	Antiferromagnetic
C_b	Conduction band
V_b	Valence band
E_F	Fermi level
BZ	Brillouin Zone
E_f	formation Energy

GENERAL INTRODUCTION

Introduction

The full Heusler are among a group of materials called Heusler alloys; they got this name from its first discoverer.Heusler materials have been shown their diverse properties for spin-up and spin-down channels. These materials attracted considerable attraction from the research community when F. Heusler exposed the ferromagnetic character of the Cu_2MnAl though no one constituent of this ternary compound had ferromagnetic nature **[1]**

Half-Metallic (HM) materials are known as these materials behave differently in both spin bands(spin-up, spin-down), the one spin band shows metallic behaviour, while the other spin band presents semiconductor behaviour **[2, 3]**. Moreover, Heusler materials have been shown their diverse properties for spin-up and spin-down channels.

Ameliorating the performance of spintronic devices is indispensable for advancing modern technology**[4]**. Half Metallic Ferromagnets (HMFs) are interesting spin-polarized materials and, thus, are ideal for application in spintronic devices **[5]**. Half-metal magnets have got broad attention. They are utilized in the manufacturing of electronic gadgets because of their wide band gap in minority spins, magnetic random access memory effect, high data processing rate and low consumption of electric power and gradually increasing density **[6, 7]**.

Numerous half-metallic ferromagnets have been predicted and verified experimentally since NiMnSn was predicted in1983 by De Groot et al **[8]**. Ferromagnetic materials display diverse electronic properties in the spin-up and spin dn bands, with metallic properties in one spin band and insulator or semiconductor properties in another, thus leading to 100% spin polarization at the Fermi level **[9-11]**. Heusler alloys are a class of inter-metallic compounds, with simple structures and unique properties**[12]**.

In 1903, a German scientist Heusler found that the atoms in the alloy Cu_2MnAl were non-magnetic (NM), but the alloys showed an adjustable magnetism through heat treatment and chemical components. During the past few decades, Heusler alloys have been favorable candidates for multifunctional materials because of their many excellent properties, such as:

Magnetocaloric effect[13, 14], Giant magnetoresistance[15], magnetic field-drive shape memory effects[16], half-metallicity, Hall effects[17]. In addition, some Heusler compounds are exhibiting excellent thermoelectric properties[18].

Since that time, many Mn-based Heusler materials have been investigated including the materials cited in the ensuing references reported in the literature previously[19]. Recently, research on Heusler compounds/alloys has been extended and included all Mn_2RhZ systems (Z=Ga, Al, In, Ge, Si, Sb, and Sn)[20], Mn_2PdZ(Z=In, Sn) [21]. Mn_2PtCo [22], Mn_2YZ(Y = Ni, Cu, and Zn; Z = Ga, Ge, and As)[23]. Hoat et al[24].

Additionally, a very interesting class of Heusler alloys that has received considerable theoretical studies is the HM, Mn_2YZ, these materials are much more favorable than their ferromagnetic counterparts in magneto-electronic applications[25]. One important application of Mn_2YZ Heusler alloys is spintronic materials, many Mn2-based Heusler alloys have been reported to be half-metals or spin gapless semiconductors (SGSs) such as Mn_2CoAl inverse Heusler alloy under pressure[26],Mn_2CoZ (Z=Al,Ga,In,Si,Ge,Sn,Sb)[27] Mn_2VZ (Z = Al, Ga, In, Si, Ge, Sn)[28],Mn_2CoAl[29].

In order to understand the different properties, we present in this thesis numerical investigations based on a study of the first principle of the structural, electronic, and magnetic properties of Mn_2YSn (Y= Mo,Nb, Zr) and Mn_2YSn (Y= Ru, Rh, and Pd), This thesis is divided into three chapters. In chapter 1 we give general and theoretical information on heusler alloys and spintronic, in chapter 2 we take up the basic ideas of DFT as implemented in the Wien2k code,Chapter three is divided into two parts.In the first part, We present an investigation of the structural, electronic, and magnetic properties and half-metallic behavior of Mn_2YSn (Y=Mo, Nb, Zr).

In the second part, This study includes the pressure effect on the structural, electronic, and magnetic properties as well as the metallic behaviour of Mn_2YSn (Y=Ru, Rh, and Pd).

References

1. Heusler, F., W. Starck, and E. Haupt, Magnetisch-chemische studien. Verh. Dtsch. Phys. Ges, 1903. 5: p. 219-232.
2. Itoh, H. and J. Inoue, Spin polarization at the interface and tunnel magnetoresistance. Journal of magnetism and magnetic materials, 2001. 226: p. 930-932.
3. Žutić, I., J. Fabian, and S.D. Sarma, Spintronics: Fundamentals and applications. Reviews of modern physics, 2004. 76(2): p. 323.
4. Paudel, R., et al., Half-metallicity and magnetism of CoFeHfGe novel quaternary Heusler alloy in bulk form as well as (100) and (001) surfaces: an ab initio study. Journal of Physics and Chemistry of Solids, 2020. 136: p. 109190.
5. Guha, S., et al., Crystal structure and magnetic properties study on ferromagnet $Fe_2MnSi0.75Al0.25$ Heusler alloy. Physica B: Condensed Matter, 2020. 579: p. 411805.
6. Anjami, A., et al., Ab-initio study of mechanical, half-metallic and optical properties of Mn_2ZrX (X= Ge, Si) compounds. Results in physics, 2017. 7: p. 3522-3529.
7. Kervan, S. and N. Kervan, Half-metallic properties of the $CuHg_2Ti$-type Mn2ZnSi full-Heusler compound. Current Applied Physics, 2013. 13(1): p. 80-83.
8. De Groot, R., et al., New class of materials: half-metallic ferromagnets. Physical review letters, 1983. 50(25): p. 2024.
9. Addadi, Z., et al., Electronic and Ferromagnetic Properties of 3 d (V)-Doped (BaS) Barium Sulfide. Journal of Superconductivity and Novel Magnetism, 2017. 30: p. 917-923.
10. Dahmane, F., et al., First principles study of the electronic structures and magnetic properties of transition metal-doped cubic indium nitride. Materials science in semiconductor processing, 2014. 21: p. 66-73.
11. Dahmane, F., et al., Electronic structure, magnetism and stability of Co_2CrX (X= Al, Ga, In) ab initio study. Modern Physics Letters B, 2016. 30(01): p. 1550265.
12. Zhou, Y., et al., The structural, electronic, magnetic and mechanical properties of d0 binary Heusler alloys XF_3 (X= Be, Mg, Ca, Sr, Ba). Journal of Physics and Chemistry of Solids, 2020. 138: p. 109246.
13. Wu, Y., et al., Magneto-structural transition and magnetocaloric effect of $Ni_{50-x}Tb_xMn_{30}Ga_{20}$ (x= 0− 1) alloys. Intermetallics, 2017. 89: p. 100-104.

14. Liu, J., et al., Giant magnetocaloric effect driven by structural transitions. Nature materials, 2012. 11(7): p. 620-626.

15. Yu, S., et al., Large magnetoresistance in single-crystalline Ni 50 Mn 50− x In x alloys (x= 14–16) upon martensitic transformation. Applied Physics Letters, 2006. 89(16): p. 162503.

16. Kainuma, R., et al., Magnetic-field-induced shape recovery by reverse phase transformation. Nature, 2006. 439(7079): p. 957-960.

17. Dubenko, I., et al., Giant Hall effect in Ni-Mn-In Heusler alloys. Physical Review B, 2009. 80(9): p. 092408.

18. Gavrea, R., et al., Investigations on compensated ferrimagnetism in the Mn2Co0. 5V0. 5Al Heusler alloy. Solid State Communications, 2020. 309: p. 113812.

19. Weht, R. and W.E. Pickett, Half-metallic ferrimagnetism in Mn_2VAl. Physical Review B, 1999. 60(18): p. 13006.

20. Ren, Z., et al., Site preference and electronic structure of Mn_2RhZ (Z= Al, Ga, In, Si, Ge, Sn, Sb): a theoretical study. Mater. Sci.-Pol., 2016(0).

21. Xu, X., et al., Magnetic properties of Mn_2PdSn and Mn_2PdIn. Journal of Magnetism and Magnetic Materials, 2016. 401: p. 618-624.

22. Kaur, N., V. Srivastava, and S.A. Dar, GGA based study on electronic structure and thermoelectric properties of Mn_2PtCo full-Heusler compound. Indian Journal of Physics, 2022. 96(1): p. 71-77.

23. Wu, Z., et al., Influence of Symmetry from Crystal Structure and Chemical Environments of Magnetic Ions on the Fully Compensated Ferrimagnetism of Full Heusler Cr_2YZ and Mn_2YZ Alloys. Symmetry, 2022. 14(5): p. 988.

24. Hoat, D., et al., Mn_2CoX (X= P and As) full-Heusler compounds for spintronic applications: Half-metallicity and elastic properties. Physics Letters A, 2020. 384(24): p. 126589.

25. Abada, A., et al., First principles study of a new half-metallic ferrimagnets Mn_2-based full Heusler compounds: Mn_2ZrSi and Mn_2ZrGe. Journal of Magnetism and Magnetic Materials, 2015. 388: p. 59-67.

26. Chen, X.R., et al., Structural, electronic, elastic, and thermodynamic properties of the spin-gapless semiconducting Mn_2CoAl inverse Heusler alloy under pressure. physica status solidi (b), 2015. 252(12): p. 2830-2839.

27. Liu, G., et al., Mn_2co z (z= al, ga, in, si, ge, sn, sb) compounds: Structural, electronic, and magnetic properties. Physical Review B, 2008. 77(1): p. 014424.

28. Özdogan, K., et al., Search for half-metallic ferrimagnetism in V-based Heusler alloys Mn_2VZ (Z= Al, Ga, In, Si, Ge, Sn). Journal of Physics: Condensed Matter, 2006. 18(10): p. 2905.

29. Ouardi, S., et al., Realization of spin gapless semiconductors: The Heusler compound Mn_2CoAl. Physical review letters, 2013. 110(10): p. 100401.

CHAPTER I : GENERAL INFORMATION ON HEUSLER ALLOYS

I.1 Introduction

The ferromagnetic manganese alloys were discovered by F. Heusler in 1898 and named after him. They contain in addition to manganese or Manganese-Copper, one more element, viz., Aluminum, Tin, Arsenic, Antimony, Bismuth, and Boron. Of these various alloys, the Aluminum-Manganese Bronzes show by far the strongest ferromagnetism; they have mostly been investigated for this reason, and the following considerations are, in the first instance, to be limited to this group of alloys **[1]**.

Because of its potential applicability to the next generation of electronic devices, there has been a lot of interest in the development of spintronic devices in the last 30 years. The charge of the electron is the carrier of information in traditional electronic devices. The discovery of ferromagnetic half-metals, in which the electron's spin operates as the information carrier, was a significant step forward in the discipline **[2]**.

I.2 Heusler Alloys

I.2.1. Classification of Heusler Alloys

Based on their chemical makeup, Heusler alloys are divided into three groups. The Half-Heuslers are the first family. The chemical composition of the alloys in this family is XYZ. The Full-Heuslers are the second family, and the alloys in this family have the chemical formula X_2YZ **[3],[4]**, Z is a group III to V element, whereas X and Y are transition metals.

In certain situations, however, Y is substituted with a rare earth metal or an alkaline earth metal. The LiMgPdSn type quaternary Heusler compounds, also known as LiMgPdSb type quaternary Heusler compounds, are another family of filled Heusler. They are quaternary transition metal compounds having the chemical formula (XX_0) YZ, with transition metal atoms X, X_0, and Y.

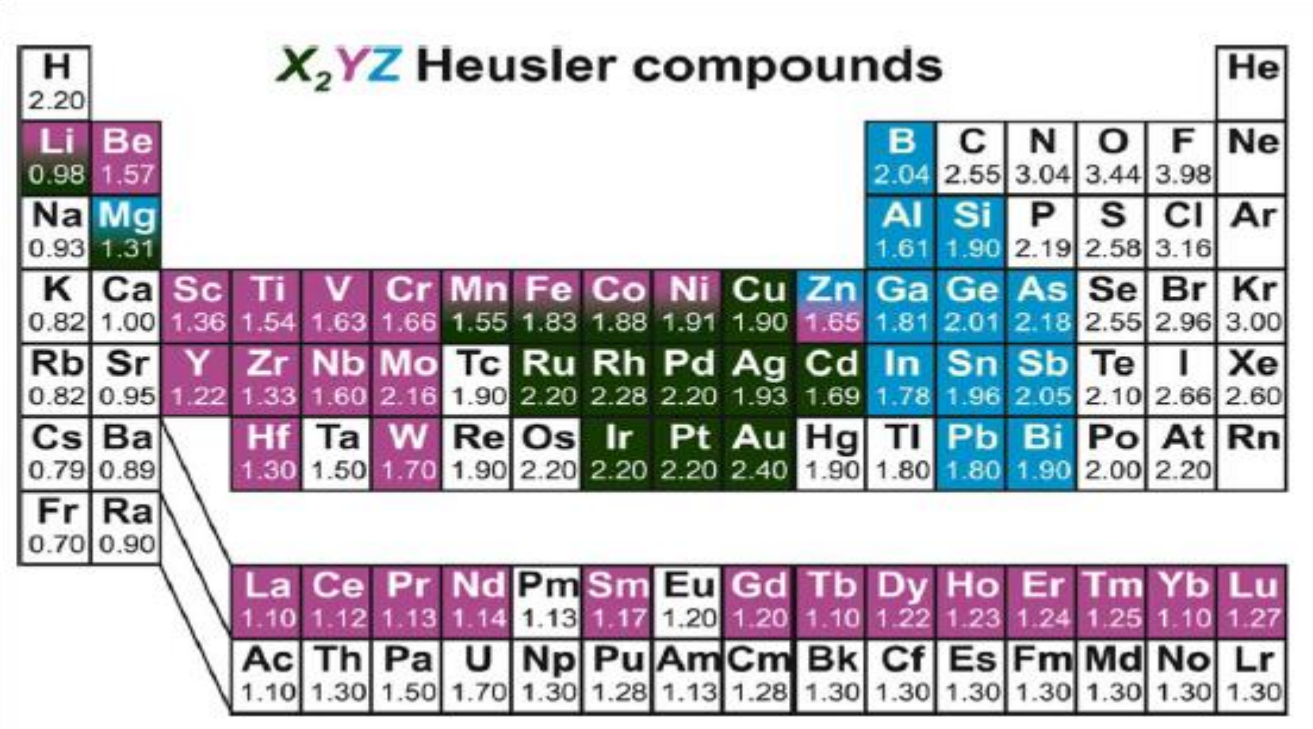

Figure.I.1: Main combinations of Heuslers alloy formation

I.2.1.1. Half Heusler

This type of alloys has a chemical formula like XYZ, and they are made up of 2 components, one covalent and the other ionic. The cationic character of the X and Y atoms is distinct, but the anionic character of the Z atom is possible **[5-7]**.

The electronegativity of these elements is used as a sorting parameter, with the most electropositive element at the start of the formula and the most electronegative one at the finish. The main group element, a transition metal, or a rare earth element can be X and Y. Element Z, like Ge, Sn, and Sb, belongs to a major group but is found in the second half of the periodic table **[8, 9]**.

- **Crystal structure**

The first family of alloys (Half-Heuslers) crystallizes in a non-centrosymmetric cubic structure (space group N° 216, F-43m, C1b) that may be generated from the ZnS type tetrahedral structure by filling

The sites octahedral lattice. The interpenetration of three face-centered cubics (fcc) sublattices, each of which is occupied by atoms X, Y, and Z, characterizes this form of semi-Heusler structure **[10]**.The positions held are as follows: 4a (0, 0, 0), 4b (1/2, 1/2, 1/2), et 4c (1/4, 1/4, 1/4).

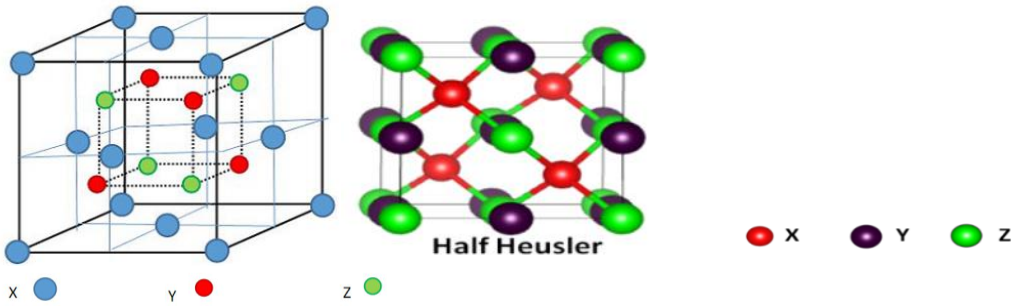

Figure.I.2: Crystal structure of Half Heusler alloy XYZ

I.2.1.2. Full Heusler

Heusler alloys were once thought to be intermetallic alloys, however, their atomic order feature makes them more appropriately characterized as intermetallic compounds. The Heuslers' general formula is X_2YZ, where X and Y are transition metals and Z is a periodic table element from Group III, IV, or V.In certain situations, however, Y is substituted with a rare earth metal or an alkaline Earthmetal **[6]**.

Table.1.1:occupations of sites, general formula, type of structure, space group of half and full heusler alloys **[11]**.

site occupancy	**site occupancy**	**site occupancy**			**site occupancy**
		ICSD	**SB**	**Pearson**	
X, Y, Z	XYZ	LiAlSi	C1b	cF16	F-43m(N^0.216)
X=X`,Y , Z	X_2YZ	Cu_2MnAl	$L2_1$	cF16	Fm-3m (N^0.225)
X, X´=Y , Z	$XX´_2Z$	$CuHg_2Ti$	X	cF16	F-43m (N^0.216)
X , X`,Y, Z	XX`YZ	LiMgPdSn	Y	cF16	F-43m (N^0.216)

- **Crystal structure**

The structure distinguishes Full-Heuslers alloys. $L2_1$ is the most well-known Heusler structure, in which all of the atoms are well-arranged yet there are other forms resulting from disorder in the atom distribution on the network's sites. This disorder in the structure has a variety of effects on the electronic structure, as well as magnetic and transport characteristics **[12, 13]**.

In full Heusler alloys, several forms of disordered structures have been discovered, including the $L2_1$ (Cu_2MnAl) and X(Hg_2CuTi) structures **[14]**.

- **$L2_1$ (Cu_2MnAl) Type structure**

This structure is defined by the group space Fm-3m (N° 225) **[15, 16]**.and is made up of four cubic cells with centered faces (fcc): two cells are occupied by the atom X, one cell is reserved for the atom Y, and the last cell is reserved for the atom Z. The perfect arrangement of atoms in this structure is shown in **Figure.I.3**.

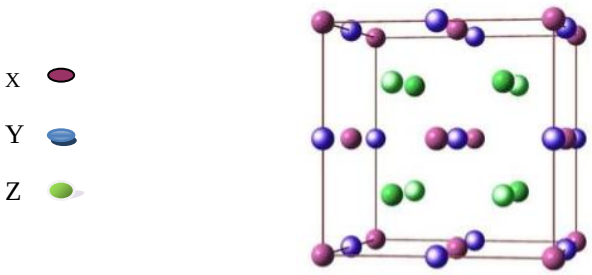

$L2_1(Cu_2MnAl)$

Figure.I.3: Full-Heusler representations of cubic meshes.

- **X (Hg_2CuTi) Type structure**

Because one of the X or Y sites changes position, this structure is known as the inverse Heuslers alloys. This sort of structure is less common. The space group F-43m (N° 216) is designated to it **[17]**.

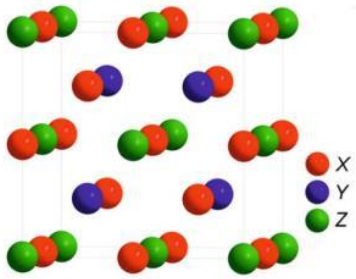

X (Hg_2CuTi)

As illustrated in **Figure.I.4**, this inverse Heusler structure is common in Mn_2-based materials with Z (Y) > Z (Mn). Mn_2CoSn, also known as (MnCo)MnSn **[18, 19]** , is a well-studied case.

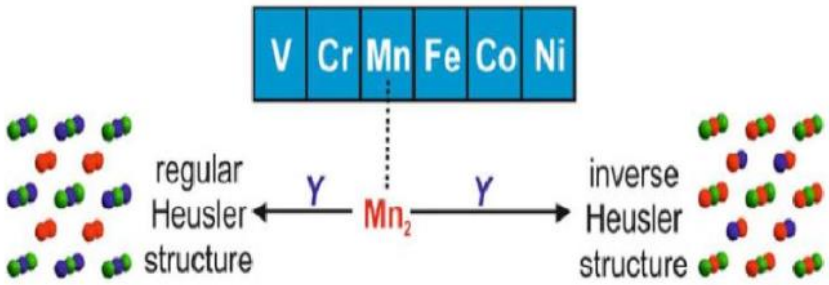

Figure.I.4: The two structures (regular and inverse) for Heusler alloys based on Mn_2 depending on the position of the element Y.

I.2.1.3. Quaternary Heusler Alloys

The LiMgPdSn type, also known as quaternary-Heusler compounds of the LiMgPdSb type, is another filled-Heuslerfamily. They are transition metal quaternary compounds having the chemical formula (XX_0) YZ, where X, X_0, and Y are transition metal atoms.

The valence of the X element is lower than that of the X atoms, while the valence of the Y element is lower than that of both X and X. The atomic sequence along the diagonal of the fcc cube is X-Y-X-Z, which is the most energetically stable **[20]**.

There have been a few LiMgPdSn-type half-metallic compounds explored **[21,22]**. A substantial number of such compound have recently become the subject of research **[23]**.

The electrical and magnetic characteristics of 60 LiMgPdSntype multifunctional quaternary Heusler compounds were studied using first-principles electronic structure computations in **[24]**. With a few exceptions, the majority of the compounds were half-metals that followed the same Slater-Pauling law as full-Heusler compounds, Mt = Zt - 24. The same hybridization approach as in full Heusler compounds was shown to be the driving factor behind the Slater-Paling rule.

- **Crystal structure**

A new series of quaternary Heuslers alloys which are composed of 4 different atoms with a stoichiometry of type 1,1,1,1, can be obtained by replacing one of the X atoms in the formula X_2YZ with another X' atom.

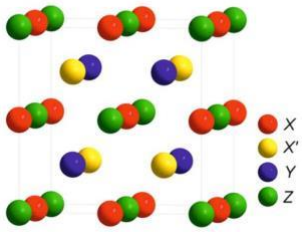

Figure.I.5: Structure of the quaternary Heusler alloy (LiMgPdSn).

I.3. Half-metallic Heusler Alloys

Half-metallic ferromagnets (HMF) are a relatively new family of materials that have generated a lot of attention recently because of their potential uses in spin electronics (also known as Spintronic) **[25]**.

In the early 1980sGroot et al **[26]**, who were interested in the computation of the band structure of half-Heusler alloys: NiMnSb **[26]**, used the term half-metallicity for the first time. For majority spin electrons (up) and minority spin electrons (down), ordinary ferromagnetic materials have an electronic density of states at the Fermi level.

Minority spins and majority spins have fundamentally different conduction characteristics in half-metallic materials (P=1). They have a metallic property in one spin direction (non-zero density of state at the Fermi level) and a semiconducting or even insulating property in the other spin direction, This is shown schematically in **Figure.I.6**, resulting in a 100 percent(100%)spin polarization rate.

The bandgap is an important factor of half-metals, and it is stated that three types of half-metals may be separated based on the nature of the bandgap: covalent band gaps, charge-transfer band gaps, and d - d band gaps **[27]**. Because the origin of half-metallicity differs in each group, this distinction is crucial. The crystal structure is intimately linked to covalent band gaps. NiMnSb is a popular example **[28]**. It crystallizes in the Heusler C1b structure, which is similar to the zincblende structure in that the third element fills one of the vacant spots (Ni). Mn and Sb must both occupy tetrahedral coordination sites. The semiconducting spin direction has the same band structure, interactions, and bonding as group III–V semiconductors such as GaAs. Conduction occurs in very wide bands in the metallic spin direction, with an effective mass that is about equivalent to the free-electron mass. In highly magnetic compounds, charge-transfer band gaps are found when the transition metal's d bands are empty for the minority spin direction and the itinerants, p electrons of the transition metal have been localized on the anions. The d-d band gap causes gaps between crystal-field split bands in materials with a d-d bandgap. The Fermi level may be positioned in a gap for just one spin direction due to exchange splitting.

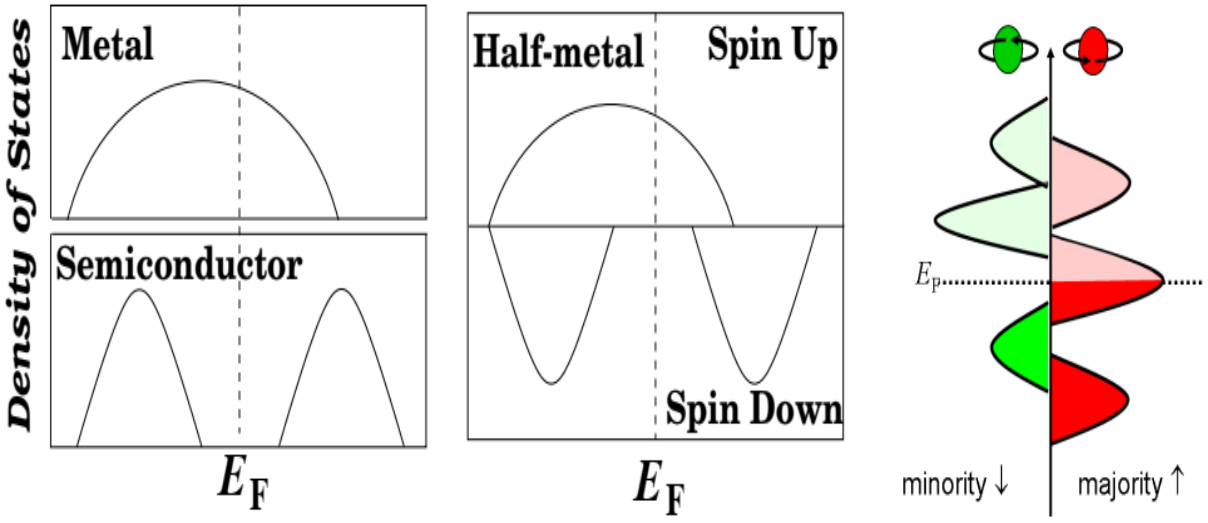

Figure.I.6: Schematic representation of the density of states for metal with respect to normal metals and semiconductors **[29]**.

I.4. Magnetic behavior of full Heusler

In the full-Heusler compounds (X_2YZ), the situation is completely different because of the existence of the two X atoms which occupy the tetrahedral sites and which allow a magnetic interaction between the latter two, thus the formation of a second sub- magnetic lattice plus delocalizes (**Figure.I.7**).X_2YZ type Heuslers compounds exhibit a wide range of magnetic phenomena and orders as a result of these two separate magnetic sublattices, including ferrimagnetism, ferromagnetism, antiferromagnetism, and half-metallic ferromagnetism.

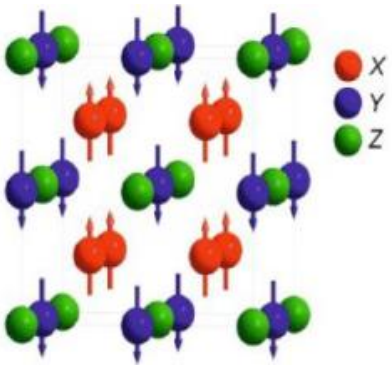

Figure.I.7: Full-Heusler compound of formula X2YZ (structure $L2_1$**[30].**

I.5. Feromagnetism

The susceptibility of ferromagnetic materials to external magnetic fields is substantial and positive. They have a significant attraction to magnetic fields and may keep their magnetic characteristics even when the external magnetic field is removed. Ferromagnetic materials have a net magnetic moment because their atoms contain few unpaired electrons. Magnetic domains are responsible for their strong magnetic characteristics. The magnetic force in these domains is significant because vast numbers of atoms are oriented parallel in these domains.

The domains of ferromagnetic material are virtually randomly ordered when it is not magnetized, and the net magnetic field of the portion is globally equal to zero. The domains align when a magnetizing force is applied, resulting in a high magnetic field in the component. Ferromagnetic metals include (iron, nickel, and cobalt).

The magnetic moments in a ferromagnetic material interact with one another and tend to line up parallel to one another. The term "exchange interaction" refers to the interaction of moments with one another. The moments are grouped in complicated geometries termed magnetic domains in the absence of an applied field (**figure.I.8**). The total energy of the system is reduced as a result of this design. A multiplicity of moments are aligned with one another inside a domain, and the direction of the lyrics changes rapidly across domains.

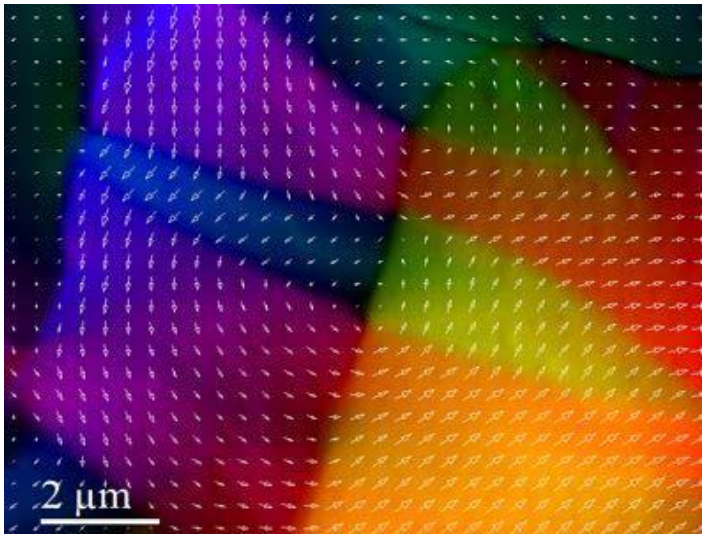

Figure.I.8:Image of the magnetic domains made by Transmission Electron Microscopy in Lorentz mode of a ferromagnetic sample of Co_2MnSi **[31]**.

In general, the magnetism at saturation reaches a maximum value at T = 0 K, corresponding to the elementary parallelism of the moments, declines steadily as the temperature rises, and disappears at a temperature known as the Curie temperature **[32,33]**.

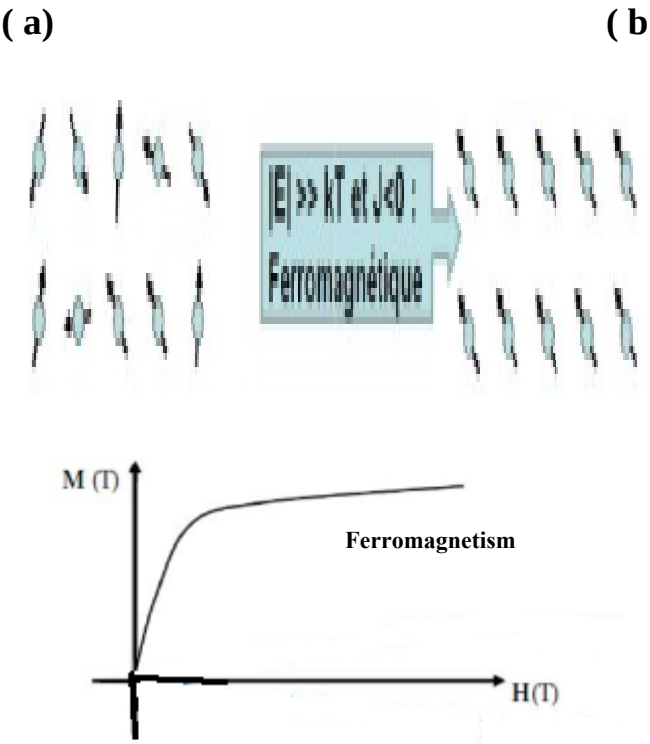

Figure.I.9: Ferromagnetism: (a) Lattice of spins - (b) Field variation of the magnetization as a function of the magnetic field M (T).

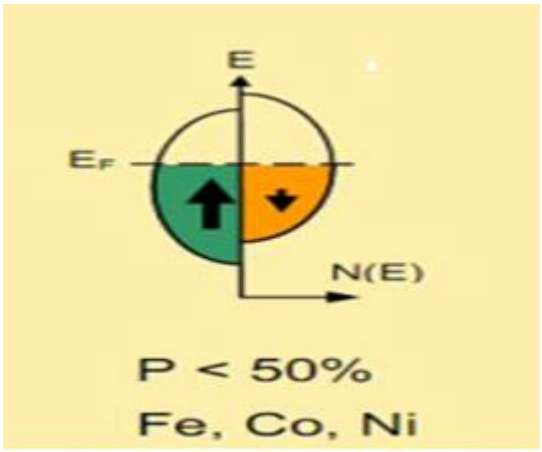

Figure.I.10: Schematic representation of the density of state and spin polarization of a ferromagnetic material[34]..

I.6. Antiferromagnets:

The lowest energy state of an antiferromagnetic substance corresponds to an antiparallel alignment of magnetic moments. This causes the moments to group together into two sub-lattices of equal and opposing magnetization, resulting in a total magnetization of zero in the absence of a field **[35]**.

When the temperature increases, the alignment of the moments is disturbed by the thermal agitation and the magnetic susceptibility χ_m increases up to a temperature T_N called the Néel temperature. Above the Néel temperature, these materials become paramagnetic. Materials with low Neel temperature (70…293) K are used for the realization of magnetic circuits with high reluctance.

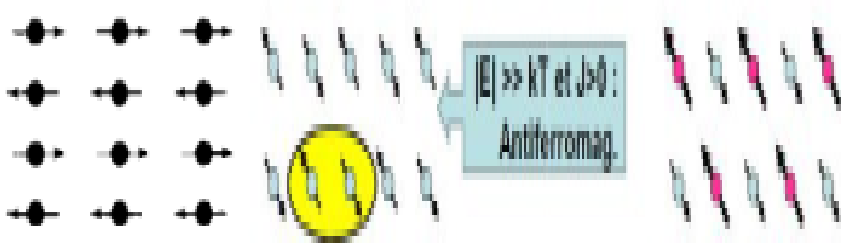

Figure.I.11: Antiferromagnets: spin network

I.7. Slater pauling rule

Slater and Pauling discovered that the average number of valence electrons (Nv) per atom may be used to determine the magnetic moment m of 3d elements and their binary alloys **[36,37]**. Based on m, the materials are split into two zones (Nv). The area of low valence electron concentrations (Nv≤ 8) and localized magnetism is the first zone of the Slater-Pauling curve. The bccs are the most closely related structures discovered here. The realm with high valence electron concentrations (Nv ≥ 8) and itinerant magnetism is the second domain. Systems with closed structures are seen in this area (cfc and hcp). Iron is at the intersection of localized and itinerant magnetis.

The Slater-Pauling curve for transition metals and various alloys is shown in Figure I.17. In the localized region of this curve, Heusler alloys are found. As a result, we concentrate on this portion of the curve. The magnetic moment is calculated using the following equation:

$$\boldsymbol{M = N_v - 2n_{\downarrow}} \qquad \text{(I.1)}$$

The number of electrons in the minority states is denoted by $\mathbf{2n_{\downarrow}}$. Because the minority density of states is at its lowest, the number of electrons in the minority d-band is forced to be about three. The magnetic moment in the confined area of the Slater-Pauling curve may be determined by ignoring the **s** and **p** electrons:

$$\boldsymbol{M \approx N_v - 6} \text{(I.2)}$$

This means that the magnetic moment per atom is just the average number of valence electrons minus six. The magnetic moment per atom is therefore equal to the average number of valence electrons minus six. Ferromagnetic semi-metals have a gap in the minority densities of states at the Fermi level by definition. The number of occupied minority states must be an integer as a result of this gap, which is perfectly proven for the case $M = N_v - 6$ **[38,39]**.

If the average concentration of valence electrons is not an integer, this rule might result in non-integer numbers. As a result, using the number of valence electrons per formula unit is frequently more convenient. The Slater-Pauling rule for semiHeusler compounds with three atoms per unit formula is:

$$\boldsymbol{M_{XYZ} = N_v - 18} \qquad \text{(I.3)}$$

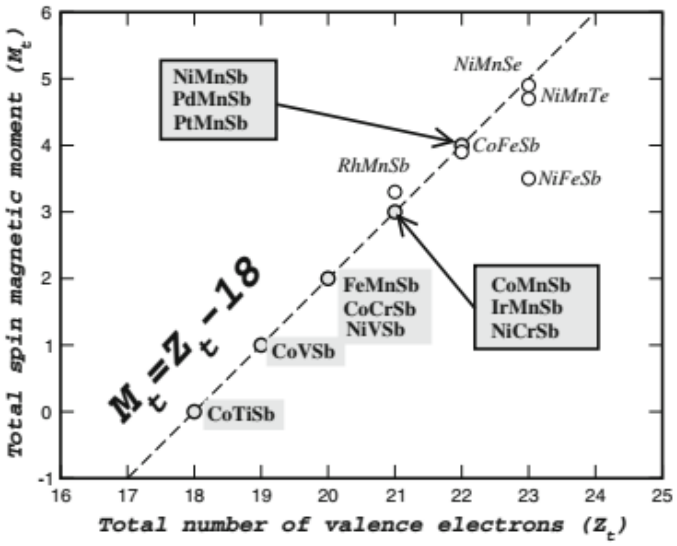

Figure.I.12: Calculated total spin moments for all the studied half Heusler alloys**[40]**.

We have presented the computed total spin magnetics for the semi-Heusler alloys as a function of the total number of valence electrons in this figure. The dotted line depicts the rule that these compounds follow. If N_v- 18, the total moment Mt is an integer number if the values 0, 1, 2.3, 4, and 5 are assumed. The semiconductor phase is represented by 0 and the maximum moment when the 10 majority states are filled by 5.

First, we changed the valence of a transition metal atom with a lower value (magnetic). Using the observed lattice constants of two Mn compounds, we substitute V, Cr, and Fe for Mn in the compounds NiMnSb and CoMnSb.The total spin magnetic moment is computed perfectly with the total charge for all of these compounds, and they all exhibit half-metallicity.

There are four atoms per cell in Heusler X_2YZ materials, resulting in the formula :

$$M_{X2YZ} = N_v - 24 \qquad \text{(I.4)}$$

We plotted the total spin magnetic moments for all compound investigated against the total amount of valence electrons in Figure I.5. The half-metallicity rule: M =N_v- 24 of complete Heusler alloys is shown by the dotted line. When all majority d states are occupied, the greatest possible moment is 7μβ.

In addition to the standard Full-Heusler compound, the inverse Full-Heusler compound Hg_2TiCu have been explored. The chemical formula for these compounds is X_2YZ, however, the valence of the transition metal atom X is less than the valence of the transition metal atom **[41].**

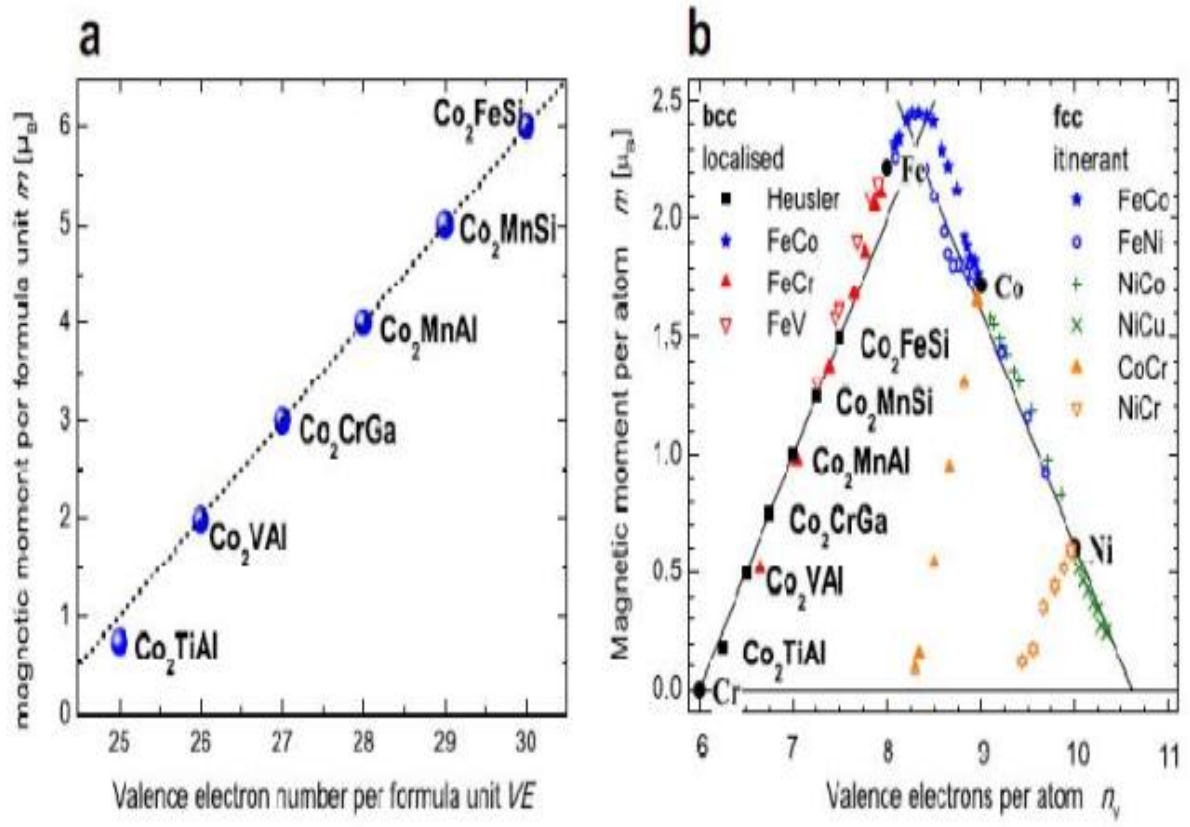

Figure.I.13:(a) the magnetic moment per formula unit of Heusler compounds based on Co_2 is proportional to the number of valence electrons and follows the Slater Pauling curve which is illustrated in**(b)**. Values of 3d transition metals and their alloys are given for comparison. (Note: $A_{1-x}B_x$ alloys are given as AB) **[42]**.

I.8.Spintronic

The regulation of charge currents, negative charge electrons, and positive charge holes is the foundation of traditional electronics, which has infiltrated our daily lives. It is well understood that electrons have their own magnetic moment, referred to as the spin moment or spin.

Spintronics, also known as spin electronics, proposes that information be encoded using both the charge and the spin of the electron. The spin, which has never been employed in traditional microelectronics applications, causes novel physical phenomena that open up new possibilities in terms of integrability, switching speed, energy consumption, and information non-volatility. In this regard, spintronics has piqued the scientific community's interest as a viable alternative to traditional electronics, which now confronts significant physical challenges owing to component size reductions .The d bands of up electrons and down electrons in ferromagnetic materials are asymmetrical, meaning that the density of electronic states for spins up and down is different. After that, we talk about the majority and minority spin. This means that an electron traveling through a ferromagnetic material will scatter differently depending on its spin state, resulting in different electrical resistance for spins up and spins down. The number of electrons in an electric current traveling through a ferromagnetic material is thus adjusted, and the current is said to be spin-polarized. The phenomena of Giant Magnetoresistance (GMR) and Tunnel Magnetoresistance (TMR) are based on this effect **[43]**.

In the last two and a half decades, this sector has seen a lot of fascinating technical advancements. The use of giant magnetoresistance (GMR) or, more recently, tunneling magnetoresistance (TMR) in current hard drive read heads to provide high-density storage on a magnetic platter is perhaps the most well-known use of spintronics. Binasch et al **[44]**.and Baibich et al **[45]**.GMR was separately reported in 1988 when multilayers of ferromagnetic (FM) and non-magnetic (NM) materials showed (Kou, De Boer, et al. 1998) ed "giant" disparities in magnetoresistance depending on the magnetic alignment of the ferromagnetic layers in their studies. A non-magnetic substance is layered between ferromagnetic slabs in a conventional GMR configuration, and the current flows perpendicular to the planes. The

current perpendicular to plane (CPP) heterostructure is what this configuration is termed. The GMR effect is caused by the thickness of the ferromagnetic layers in comparison to the mean free path of electrons in the two spin channels (λ↑andλ↓, respectively).

The magnetic orientation of the layers affects which spin scatters with the smaller mean path when the multilayer thickness is between the mean free path sizes (for example, let λ↓ <<t << λ↑). Electrons with spins in the same direction (up spin channel) scatter less due to the parallel alignment of the magnetic moments in the two ferromagnetic layers. Because of the short mean free route, the opposing spin channel has a significantly higher chance of scattering. The equivalent resistance is low in the parallel arrangement because a low resistance is paralleled with high resistance. Because the fields are aligned antiparallel, both spin channels undergo significant scattering in one of the ferromagnetic layers. The resistance is greater in this setup than in the parallel configuration. The two magnetic moment alignments in the CPP setup are shown schematically in **Figure.I.15**.

The value of the magnetoresistance MR is defined by the difference in resistance (or conductance G) between parallel (↑↑) and antiparallel (↑↓) configurations:

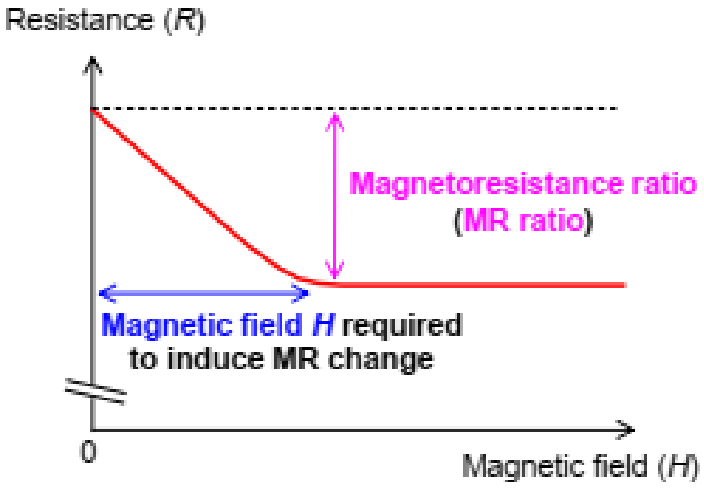

Figure.I.14: Magneto-Resistance ; MR **[46]**.

$$MR = \frac{R\uparrow\downarrow - R\uparrow\uparrow}{R\uparrow\uparrow} \qquad (I.5)$$

$$MR = \frac{G\uparrow\downarrow - G\uparrow\uparrow}{G\uparrow\uparrow} \qquad (I.6)$$

Where $R_{\uparrow\downarrow}$ and $R_{\uparrow\uparrow}$ are the resistivity for the antiparallel configuration and the parallel configuration respectively.

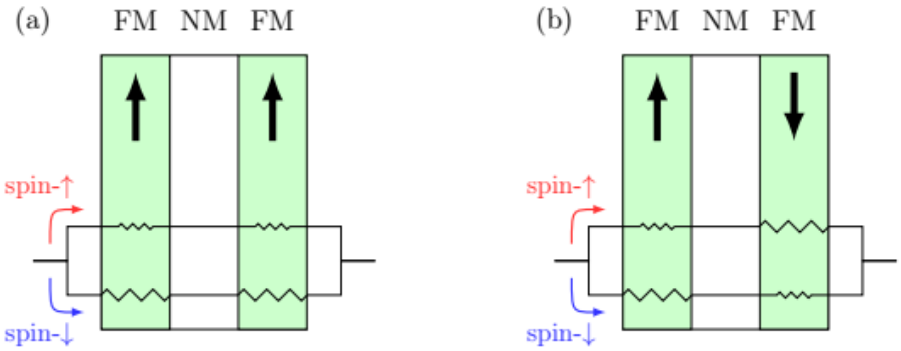

Figure.I.15: GMR devices in the CPP configuration. Two ferromagnetic (FM) layers sandwich a non-magnetic (NM) layer. One FM layer is pinned, while the other is free to change alignment. The size of the resistor symbol denotes the relative resistance of the ferromagnetic layer. **(a)** With parallel alignment, spin-up current flows more easily and the overall resistance is low. **(b)** When the two ferromagnetic layers have antiparallel moments, both spin channels experience high resistance in one of the two layers. The overall resistance is high.

I.8.1. Tunnel Magneto-resistance

In Ferro/Insulator/Ferro systems, TMR may be seen. Depending on the design of ferromagnetic materials, it expresses itself as a variable in electrical resistance, of current traveling through the insulation through tunnel effect. The TMR is connected to the difference in states accessible for spin ups and spin downs on each side of the barrier due to solely quantum conduction between the two ferromagnetic materials.

The Magnetic Tunnel Junction (MTJ) is the device most widely employed in modern technologies (e.g. MRAM memories), which leverage TMR.

It's made up of two ferromagnetic electrodes separated by a dielectric barrier, most often MgO or Al_2O. Despite the fact that the initial observations of this phenomenon were made in 1975 by Although Julliere **[43]** made the first observations of this phenomenon in 1975, it was not until 1995, aided by the work of Moodera et al. on Co/Al_2O_3/ CoFe stacks **[47]**, that TMR saw a resurgence of attention and interest. Many teams have been studying TMR with various types of ferromagnetic materials since the 2000s.

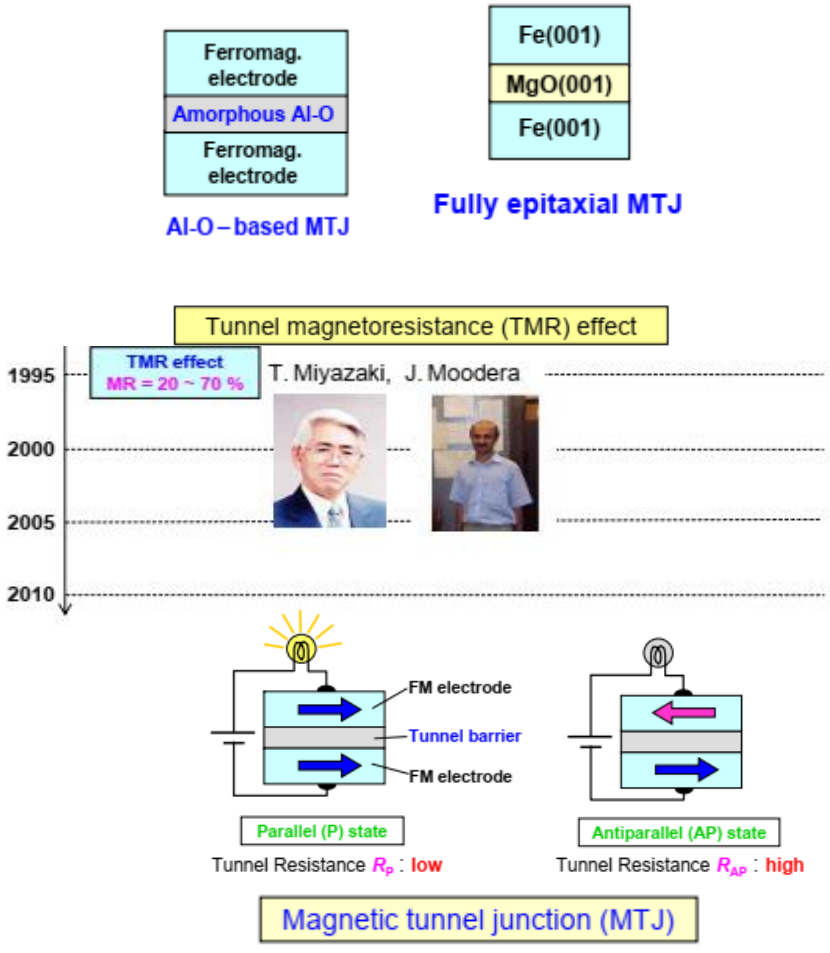

Figure.I.16: Magnetic tunnel junction **[46]**.

The TMR would potentially be infinite and the current would be 100 percent(100%) polarized if a material has zero electron density at Fermi energy for one kind of spin but non-zero for the other (half-metallic materials). Fe_3O4, CrO_2, and Heusler alloys are some of the most well-known materials expected to be half-metallic. In recent years, the latter has piqued people's curiosity.

MTJs using Heusler alloy electrodes have been shown to exhibit high TMRs, despite this (330 percent at room temperature **[48]**),

I.8.2. Giant Magnetoresistance

P. Grünberg **[49]** and A. Fert **[44]** discovered the giant magnetoresistance (GMR) effect in multilayers in 1986, which revolutionized the area of information technology.They were awarded the Nobel Prize in Physics in 2007 for this groundbreaking discovery. The spin valve is a mechanism that makes use of the GMR phenomena and is frequently utilized in hard disk drive heads. The spin valve is found in hard disk drives. A spin valve is usually made up of a Ferro/Metal/Ferro stack, with ferromagnetic materials serving as electrodes. GMR is seen in CIP formation, although it has a bigger impact on CPP creation**[50]**. GMR spin valves have resulted in a significant improvement in storage density, but when new technologies with extraordinarily fast speeds emerge, GMR is being phased out in favor of spin-dependent tunneling devices. Replacing the metal spacer with a bead of insulating material results in an increase in magnetoresistance by a factor of 10 compared to GMR spin valves. As the effect is based on the tunneling of electrons through an insulating barrier, these new devices are known as TMR tunnel magnetoresistance devices (**Figure.I.17**) **[51]**.

Figure.I.17: Illustration of basic devices for spintronics, GMR multilayers.

Ferromagnetic semi-metallic oxides and ferromagnetic semi-metallic metals, such as Heusler compounds, are potential options. Because of their high potential for novel electrode materials in spintronic devices, such as tunnel junctions devices (MTJs) **[52-58]**, giant magnetoresistance (GMR) devices **[59-60]**, and spin injection of ferromagnetic electrodes in semiconductors, Co_2-based heusler materials have been extensively studied **[6]**.

I.9. Transition metals

The fifty-six has currently known transition chemical elements all have a partly filled d or f electronic sub-shell, either in their single element form or in their stable oxidized state. Deep levels with unfinished deep levels have comparable qualities. They have a high melting point and density when they are in the state of simple bodies. They can have unusual physical characteristics (ferromagnetism, superconductivity). Their capacity to create extraordinarily resistant alloys or solid solutions with one other or with certain non-metals (H, C, N, O) has earned them a crucial position in advanced metallurgy (special steels), aeronautics (titanium alloys), and nuclear physics (batteries). With the exception of noble metals, transition elements are strongly electropositive and dissolve in mineral acids. Their oxidation produces a number of stable degrees and gives them paramagnetic characteristics.

The presence of many valences explains their proclivity for forming non-stoichiometric phases, as well as the unique physical features of a few compounds and complexes, which are commonly exploited in the industry (ferrites in computer science, doped garnets for laser emission for example). The numerous uses of transition elements and their derivatives make them crucial economic materials, which explains why they have received so much attention **[61,62]**.

I.9.1. Manganese

(L. Magnes, magnet, manganese dioxide magnetic characteristics; Manganese (a degraded form of magnesia), atomic weight Mn. 54.938049; atomic number: 25; melting point: 1246°C; boiling point: 2061°C; valence 1, 2, 3.4, 6, or 7. The metal is made via electrolysis or reduction of magnesium oxide, sodium, or aluminum. It's gray-white and looks like iron. Chemically reactive, the metal decomposes slowly in cold water.

Manganese is included in a variety of key alloys. Manganese enhances steel rolling, toughness, stiffness, wear resistance, and hardness. It creates extremely ferromagnetic alloys with aluminum and antimony, especially with modest levels of copper **[63]**.

Only with specific treatment is manganese ferromagnetic metal. There are four allotropic types of pure metal. Gamma manganese is flexible, soft, simple to cut, and bendable, while alpha manganese is stable at room temperature. In dry cells, carbon dioxide (pyrolusite) is employed as a depolarizer and to "discolor" green-colored glass **[63]**.

Manganese, which is responsible for the color of real amethyst, alone gives glass an amethyst hue. The dioxide is also used to make oxygen and chlorine, as well as to dry black paint. Permanganate is a powerful oxidant used in quantitative analysis and medicine **[63].**

I.10.Tin (Sn) Post-Transition Metal

Tin is a chemical element with the atomic number 50 and the symbol Sn (from the Latin stannum). It belongs to the periodic table's subgroup IV b. Between germanium, very little metallic, and lead, it is found. Gray tin (form) is one of the numerous crystalline forms available, one of which is not metallic.

White tin (silvery grey) is a soft metal that is simple to roll into very thin sheets (tin foil) and is unaffected by air in its natural state. Tin makes about 0.003 percent of the earth's crust (an intermediate rate between those of copper and lead). SnO_2 oxide (cassiterite) and complex sulfides such as $Sn_3Pb_5Sb_2S_{14}$ (frankeite) and

SnCu2FeS4 are the most common forms (stannite)... The deposits are typically poor: alluvial deposits arising from the alteration of magmatic rocks (granites, rhyolites), where cassiterite, the primary ore, is concentrated in veins, account for four-fifths of the world's tin production.

Tin mining produces roughly 250,000 tonnes per year across the world. More than 60% of the market is dominated by three countries: China (almost 40%), Indonesia, and Peru. These seven countries,along with Australia, Malaysia, Bolivia, and Brazil, produce nearly all of the world's tin**[69]** .

Figure.I.18: Periodic Table of the Elements, Post Transition Metals.

I.10.1. Metal properties

Tin (Sn) melts at 231.9 ^{0}C and vaporizes at 2270 ^{0}C. Gray tin (variety) is related to its higher equivalents in column IV of the periodic table, silicon and germanium, due to its low density (5.75 g/m3), structure, semiconducting, and diamagnetic characteristics. White tin (variety) has a high density (7.31 g/m3), electrical conductivity (near to that of iron), and paramagnetism, which are all metal characteristics.

The transition point is 13.2°C, although the rate of change from white to gray tin is gradual. Pewter leprosy is a condition that happens when pewter items are exposed to cold: black blotches of gray pewter form on the metal's surface. Transformation is inhibited by the presence of traces of lead, antimony, or bismuth. Pewter resists corrosion by forming a protective oxide coating on the surface. Acids and bases have little effect on them when it is cold.

It is used to coat steel because of its indestructibility (tinning). Tinplate is steel that has been protected by immersion in molten tin or an electrolytic bath containing tin salts. It is used primarily in the fabrication of cans **[69]**.

I.11 Applications of Heusler alloys for spintronics

Heusler alloys have piqued interest in recent decades due to a variety of characteristics that make them ideal for device applications. The half-metallic nature is one of the qualities that has led to the increased interest in these alloys. De Groot and colleagues predicted this characteristic for the Half-Heuslers in 1983 **[28]**. Galanakis and colleagues **[64][65]** predicted in 2002 that Full-Heusler alloys are also half-metals. They are, in fact, great candidates for electrodes in Magnetic Tunnel Junctions because of this property.

According to recent research, utilizing Heusler materials as electrodes in MTJs can result in high TMR values. With a Co_2FeAl electrode, Wang et al.measured a value of 330 % **[48]**. With Co2MnSi electrodes and a MgO barrier, Ishikawa and colleagues achieved a value of 182% **[66]**.

Although these TMR values are impressive, they are still well below theoretical predictions. This demonstrates that the processes that occur in the Heusler are not fully understood, hence the ongoing interest in these alloys. The high Curie temperature of these alloys, particularly Full-Heusler alloys, is another noteworthy feature. This is due to a strong interatomic interaction between the multiple species that make up the alloy, which explains why Full-Heuslers have higher Curie temperatures than Half-Heuslers since its lattice has no empty sites. The Curie temperature has been determined to be 985 K in the Co2MnSi alloy and higher than 1100 K in the Co2FeGa alloy . Unlike other half-metals, such as magnetite (Fe_3O4), which has a Curie temperature close to ambient temperature, Heusler alloys have a high Curie temperature, which makes them suitable for device applications in terms of thermal stability. In addition to these benefits, Heusler alloys are projected to have a low magnetic damping factor in theory. Indeed, according to Liu and al , The magnetic damping parameter of the Co_2MnSi alloy is 0.6×10^{-4}, according to theory. Because the damping factor is strongly connected to the material's frequency response, these alloys might potentially replace YIG in contemporary microwave devices.

With a value of 1 $x10^{-3}$ b, the Co_2FeAl alloy has the lowest documented experimental results. and the Co_2MnSi alloy **[67]**, which has a value of $3x10^{-3}$. The values obtained on Heusler alloys are distant from theoretical expectations, albeit modest. This discrepancy is frequently ascribed to crystalline flaws or disorders in the materials. However, there are still numerous processes in these alloys that are poorly understood, and a deeper knowledge should help them better meet the demands of modern technologies.

Another noteworthy property of some Heusler alloys is their ability to alter the form in response to an applied field. The crystalline mesh is bent by a magnetic field, and when the field is removed, the alloy recovers to its original shape. The Ni_2MnGa alloy, which can deform up to 9% under relatively modest fields, has been intensively explored for this property, known as magnetic shape memory.

I.12 Conclusion

Because of the wide range of spintronic applications, we will concentrate on Heusler alloys and their many forms. Spin valves for GMR applications and magnetic tunnel junctions for TMR applications should come first. These investigations should make it possible to enhance the characteristics of the materials, and reported more to the scientific community, in addition, these materials might serve as a basis for the creation of materials that can compete with spin polarizers of high efficiency at room temperature.

In the year 1898, Heusler alloys were found for the first time (de, Erve). Friedrich Heusler **[68]** initially explored a series of chemicals called half-Heusler (with a general formula XYZ) and complete Heusler (X_2YZ) in 1903. Transition metals X and Y, and group III or V elements Z, make up these materials. These materials, according to Koyashi, have fascinating features, such as half-metallicity and a high curie temperature. we see that the number of publications is continually rising, reaching 920 in 2016 **[45]**.

References

1. Heusler, F. and E. Take, The nature of the Heusler alloys. Transactions of the Faraday Society, 1912. **8**(October): p. 169-184.
2. Paudel, R., et al., Half-metallicity and magnetism of CoFeHfGe novel quaternary Heusler alloy in bulk form as well as (100) and (001) surfaces: an ab initio study. Journal of Physics and Chemistry of Solids, 2020. **136**: p. 109190.
3. Asfour, I., et al., Theoretical Study of the Electronic and Thermodynamic Properties of Co_2CrZ (Z= Ga, Al). 2018.
4. Prokeš, K., et al., Reduced magnetic moments in UNiSi. Journal of alloys and compounds, 1998. **269**(1-2): p. 43-49.
5. POPULAIRE, E., Mlle BAHNES Aicha, 2018, Université de Mostaganem, These de Doctorat.
6. ZENASNI, H., , 2013. Université de Telemcen,These de Doctorat.
7. Sakurada, S. and N. Shutoh, Effect of Ti substitution on the thermoelectric properties of (Zr, Hf) NiSn half-Heusler compounds. Applied Physics Letters, 2005. **86**(8): p. 082105.
8. Spina, L., et al., Compositional and structural variations in the ternary system Li–Al–Si. Zeitschrift für Kristallographie-Crystalline Materials, 2003. **218**(11): p. 740-746.
9. Hohl, H., et al., Efficient dopants for ZrNiSn-based thermoelectric materials. Journal of Physics: Condensed Matter, 1999. **11**(7): p. 1697.
10. Galanakis, I. and P. H Dederichs, Half-metallicity and Slater-Pauling behavior in the ferromagnetic Heusler alloys. Half-Metallic Alloys: Fundamentals and Applications, 2005: p. 1-39.
11. Graf, T., et al., Crystal structure of new Heusler compounds. Zeitschrift für anorganische und allgemeine Chemie, 2009. **635**(6-7): p. 976-981.
12. Miura, Y., M. Shirai, and K. Nagao, Ab initio study on stability of half-metallic Co-based full-Heusler alloys. Journal of applied physics, 2006. **99**(8): p. 08J112.
13. Sakuraba, Y., et al., Huge spin-polarization of L21-ordered Co2MnSi epitaxial Heusler alloy film. Japanese journal of applied physics, 2005. **44**(8L): p. L1100.
14. Graf, T., C. Felser, and S.S. Parkin, Simple rules for the understanding of Heusler compounds. Progress in solid state chemistry, 2011. **39**(1): p. 1-50.

15.Heusler,O.,KristallstrukturundFerromagnetismusderMangan-Aluminium-Kupferlegierungen. Annalen der Physik, 1934. **411**(2): p. 155-201.

16. Bradley, A.J. and J. Rodgers, The crystal structure of the Heusler alloys. Proceedings of the royal society of london. Series A, Containing Papers of a Mathematical and Physical Character, 1934. **144**(852): p. 340-359.

17. Hesse, W., M. Jansen, and W. Schnick, Recent results in solid state chemistry of ionic ozonides, hyperoxides, and peroxides. Progress in solid state chemistry, 1989. **19**(1): p. 47-110.

18. Surikov, V., V. Zhordochkin, and T.Y. Astakhova, Hyperfine fields in a new Heusler alloy Mn_2CoSn. Hyperfine Interactions, 1990. **59**: p. 469-472.

19. Lakshmi, N., A. Pandey, and K. Venugopalan, Hyperfine field distributions in disordered Mn_2CoSn and Mn_2NiSn Heusler alloys. Bulletin of Materials Science, 2002. **25**: p. 309-313.

20. Alijani, V., et al., Quaternary half-metallic Heusler ferromagnets for spintronics applications. Physical Review B, 2011. **83**(18): p. 184428.

21. Dai, X., et al., New quarternary half metallic material CoFeMnSi. Journal of Applied Physics, 2009. **105**(7): p. 07E901.

22. Izadi, S. and Z. Nourbakhsh, Structural, Electronic and Magnetic Properties of Nanolayer and Bulk of MnCo 2 Si and MnFeCoSi Compounds. Journal of superconductivity and novel magnetism, 2011. **24**: p. 825-831.

23. Xu, G., et al., A new spin gapless semiconductors family: Quaternary Heusler compounds. Europhysics Letters, 2013. **102**(1): p. 17007.

24. Özdoğan, K., E. Şaşıoğlu, and I. Galanakis, Slater-Pauling behavior in LiMgPdSn-type multifunctional quaternary Heusler materials: Half-metallicity, spin-gapless and magnetic semiconductors. Journal of Applied Physics, 2013. **113**(19): p. 193903.

25. Žutić, I., J. Fabian, and S.D. Sarma, Spintronics: Fundamentals and applications. Reviews of modern physics, 2004. **76**(2): p. 323.

26. Siewierska, K., et al., Imaging domains in a zero-moment half metal. IEEE Transactions on Magnetics, 2018. **55**(2): p. 1-4.

27. Fang, C.M., G. De Wijs, and R. De Groot, Spin-polarization in half-metals. Journal of Applied Physics, 2002. **91**(10): p. 8340-8344.

28. De Groot, R., et al., New class of materials: half-metallic ferromagnets. Physical review letters, 1983. **50**(25): p. 2024.

29. Galanakis, I., P. Mavropoulos, and P. Dederichs, Introduction to half-metallic Heusler alloys: electronic structure and magnetic properties. arXiv preprint cond-mat/0510276, 2005.

30. HEHN, M., F. MONTAIGNE, and A. SCHUHL, Magnétorésistance géante et électronique de spin. Techniques de l'ingénieur. Electronique, 2002. **3**(E2135): p. 1-15.

31. Ortiz Hernandez, G., Elaboration et étude des propriétés physiques de couches minces monocristallines d'alliage de Heusler à faible amortissement magnétique pour composants hyperfréquences, 2013, Université de Toulouse, Université Toulouse III-Paul Sabatier.

32. Duc, N., et al., Exchange interactions in rare earth—transition metal compounds. Journal of magnetism and magnetic materials, 1993. **124**(3): p. 305-311.

33. Radwanski, R., J. Franse, and S. Sinnema, Effective anisotropy constants in rare earth-3d intermetallics. Journal of magnetism and magnetic materials, 1987. **70**(1-3): p. 313-315.

34. Duc, N., et al., Exchange interactions in rare earth—transition metal compounds. Journal of magnetism and magnetic materials, 1993. **124**(3): p. 305-311.

35. Hu, J., et al., Determination of magnetocrystalline anisotropy constants from a hard magnetic material with polycrystalline structure. Solid state communications, 1994. **89**(9): p. 799-801.

36. Slater, J.C., The ferromagnetism of nickel. Physical Review, 1936. **49**(7): p. 537.

37. Pauling, L., The nature of the interatomic forces in metals. Physical Review, 1938. **54**(11): p. 899.

38. Kübler, J., Chap. 1, 2000, Oxford University Press Oxford, UK.

39. Wurmehl, S., et al., Geometric, electronic, and magnetic structure of Co_2FeSi: Curie temperature and magnetic moment measurements and calculations. Physical Review B, 2005. **72**(18): p. 184434.

40. ASFOUR, I., Étude des propriétés physique des alliages Heusler et Half-Heusler, 2018.

41. Özdog, K. and I. Galanakis, First-principles electronic and magnetic properties of the half-metallic antiferromagnet Cr_2MnSb. Journal of magnetism and magnetic materials, 2009. **321**(15): p. L34-L36.

42. HAMRI, B., Investigation théorique des propriétés structurales, électroniques et magnétiques des alliages heusler Ti2VZ (Z= Ge, Sn, Pb), 2016.

43. Julliere, M., Tunneling between ferromagnetic films. Physics letters A, 1975. **54**(3): p. 225-226.

44. Baibich, M.N., et al., Giant magnetoresistance of (001) Fe/(001) Cr magnetic superlattices. Physical review letters, 1988. **61**(21): p. 2472.

45. Binasch, G., et al., Enhanced magnetoresistance in layered magnetic structures with antiferromagnetic interlayer exchange. Physical review B, 1989. **39**(7): p. 4828.

46. Yuasa, S., et al., Tunnel Magnetoresistance Effect and Its Applications, Japan Science and Technology Agency, http://www. jst. go. jp/sicp/ws2009 ….

47. Moodera, J., et al., Geometrically enhanced magnetoresistance in ferromagnet–insulator–ferromagnet tunnel junctions. Applied physics letters, 1996. **69**(5): p. 708-710.

48. Wang, W., et al., Giant tunneling magnetoresistance up to 330% at room temperature in sputter deposited Co_2FeAl/MgO/CoFe magnetic tunnel junctions. Applied Physics Letters, 2009. **95**(18): p. 182502.

49. Grünberg, P., et al., Layered magnetic structures: evidence for antiferromagnetic coupling of Fe layers across Cr interlayers. Physical review letters, 1986. **57**(19): p. 2442.

50. Ball, P., Meet the spin doctors. Nature, 2000. **404**(6781): p. 918-921.

51. Moodera, J.S., J. Nassar, and G. Mathon, Spin-tunneling in ferromagnetic junctions. Annual Review of Materials Science, 1999. **29**(1): p. 381-432.

52. Inomata, K., et al., Large tunneling magnetoresistance at room temperature using a Heusler alloy with the B_2 structure. Japanese journal of applied physics, 2003. **42**(4B): p. L419.

53. Kämmerer, S., et al., Co 2 Mn Si Heusler alloy as magnetic electrodes in magnetic tunnel junctions. Applied Physics Letters, 2004. **85**(1): p. 79-81.

54. Graf, T., S.S. Parkin, and C. Felser, Heusler compounds—A material class with exceptional properties. IEEE Transactions on Magnetics, 2010. **47**(2): p. 367-373.

55. Ishikawa, T., et al., Spin-dependent tunneling characteristics of fully epitaxial magnetic tunneling junctions with a full-heusler alloy co 2 mn si thin film and a mgo tunnel barrier. Applied physics letters, 2006. **89**(19): p. 192505.

56. Tsunegi, S., et al., Tunnel magnetoresistance in epitaxially grown magnetic tunnel junctions using Heusler alloy electrode and MgO barrier. Journal of Physics D: Applied Physics, 2009. **42**(19): p. 195004.

57. Taira, T., et al., Spin-dependent tunnelling characteristics of fully epitaxial magnetic tunnel junctions with a Heusler alloy Co_2MnGe thin film and a MgO barrier. Journal of Physics D: Applied Physics, 2009. **42**(8): p. 084015.

58. Birsan, A., Electronic structure and magnetism of new scandium-based full Heusler compounds: Sc_2CoZ (Z= Si, Ge, Sn). Journal of Alloys and Compounds, 2014. **598**: p. 230-235.

59. Yakushiji, K., et al.Current-perpendicular-to-plane magnetoresistance in epitaxial Co_2 Mn Si⁄ Cr⁄ Co $_2$ Mn Si trilayers. Applied physics letters, 2006. **88**(22): p. 222504.

60. Nikolaev, K., et al., "All-Heusler alloy" current-perpendicular-to-plane giant magnetoresistance. Applied Physics Letters, 2009. **94**(22): p. 222501.

61. Thomas, J.M., Turning points in catalysis. Angewandte Chemie International Edition in English, 1994. **33**(9): p. 913-937.

62. Massa, W. and R.O. Gould, Crystal structure determination. 2004.

63. Lide, D.R., Atomic, molecular, and optical physics; ionization potentials of atoms and atomic ions, 2003,CRC press: Boca Raton, Florida.

64. Galanakis, I., P. Dederichs, and N. Papanikolaou, Origin and properties of the gap in the half-ferromagnetic Heusler alloys. Physical Review B, 2002. **66**(13): p. 134428.

65. MEBSOUT, R., Investigation théorique des propriétés électroniques, magnétiques et thermodynamiques des alliages Co_2MnZ [Z= Al, Ga], 2016.

66. Ishikawa, T., et al., Half-metallic electronic structure of Co 2 MnSi electrodes in fully epitaxial Co_2MnSi/MgO/Co 2 MnSi magnetic tunnel junctions investigated by tunneling spectroscopy. Journal of Applied Physics, 2009. **105**(7): p. 07B110.

67. Yilgin, R., et al., Anisotropic intrinsic damping constant of epitaxial Co2MnSi Heusler alloy films. Japanese journal of applied physics, 2007. **46**(3L): p. L205.

68. Heusler, F., Verhandlungen Dtsch. Phys. Ges, 1903. **5**: p. 219

69. Claude FOUASSIER, Michel PÉREYRE, « ÉTAIN », *E*ncyclopædia Universalis [en ligne], URL : https://www.universalis.fr/encyclopedie/etain/ 21 mai 2022.

CHAPTRE II : CALCULATION METHODS

II.1. The DFT method

II.1.1.Introduction

Methods of the abinitio type rely on resolving the Schrödinger equation. With the use of these techniques, it is possible to ascertain a system's physical and chemical properties, such as its electronic structure, ionization energy.

Given how difficult it is to resolve the multi-particle Schrödinger equation, it may be simplified into a system of single-particle equations, which is easier to solve numerically, especially with the help of a few approximations. The primary techniques for resolving these equations will be briefly discussed in this chapter. The process on which the Wien2k code utilized in this study is based will be discussed in the sections that follow.

II.1.2. Schrödinger equation

The solution of the time-dependent Schrödinger equation serves as the foundation for theoretical research on the electronic characteristics of materials :

$$\Psi(\{r_i\},\{R_I\},t) = i\hbar\frac{\partial}{\partial t}\Psi(\{r_i\},\{R_I\},t) \qquad \text{(II.1)}$$

The multi-particle wave function $\Psi(\{r_i\},\{R_I\},t)$ is being used to describe the system, and the system's Hamiltonian is *H*. The set $\{ri\}$ contains the variables defining the location of the electrons, whereas $\{R_I\}$ contains those characterizing the position of the nuclei.

The time-independent Schrödinger equation (steady state) may be used to determine the ground state of the system's wave function, which contains a lot of degrees of freedom **[1]** :

$$H\Psi(\{ri\},\{RI\}) = E\Psi\{ri\},\{RI\}) \qquad \text{(II.2)}$$

where E is the ground state energy described by the eigenfunctionψ. Generally, the Hamiltonian operator is written:

$$H = T_e(r) + T_n(R) + V_{ee}(r) + V_{nn}(R) + V_{ne}(r, R) \qquad \text{(II.3)}$$

The kinetic energy operators of electrons and nuclei are T_e and T_n, respecti

vely, whereas the repulsion energy operators between electrons and nuclei are V_{ee} and V_{nn}, and the attraction energy operator between nuclei and electrons is Vn_e. You can write these operators (in electrostatic units like$4\pi\varepsilon_0 = 1$)) :

$$\hat{T}_n = -\frac{\hbar^2}{2}\sum_i \frac{\nabla^2 \overrightarrow{R_i}}{M_n} \text{ ,} \hat{T}_e = -\frac{\hbar^2}{2}\sum_i \frac{\nabla^2 \vec{r}_i}{m_e} \qquad \text{(II.4)}$$

$$\hat{V}_{n-n} = \frac{1}{8\pi\varepsilon_0}\sum_{i=j} \frac{e^2}{|\vec{R}_i - \vec{R}_j|} \quad \text{and} \quad \hat{V}_{e-e} = \frac{1}{8\pi\varepsilon_0}\sum_{i=j} \frac{e^2}{|\vec{r}_i - \vec{r}_j|} \qquad \text{(II.5)}$$

$$\hat{V}_{n-e} = -\frac{1}{4\pi\varepsilon_0}\sum_{i=j} \frac{e^2 Z_i}{|\vec{R}_i - \vec{r}_j|} \qquad \text{(II.6)}$$

Where $\hbar = h/2\pi$ and h the Planck constant, m the mass of an electron, M the mass of the nucleus and Z its charge.The Born-Oppenheimer (BO) approximation, which separates the motion of electrons and nuclei by splitting the system into two paired subsystems, one for electrons and the other for kernels **[2]**, may then be used to simplify Equation (II.3):

$$\Psi \approx \Psi_{BO} = \Psi_{elec} \times \Psi_{noyaux} \text{(II.7)}$$

In fact, because the mass of the electrons is much lower than that of the protons, it is possible to think of them as instantly reorganising for a particular location of the nuclei. Therefore, T_n.

may be disregarded and V_{NN} is constant for the two parts of equation (II.3) that rely only on the nuclei. The Schrödinger equation may then be resolved for these nucleus positions.

The resulting electronic and nuclear Hamiltonians are expressed as follows:

$$H_{elec}=T_e(r)+V_{ee}(r)+V_{ne}(r,R) \qquad \text{(II.8)}$$

$$H_n = T_n(R) + V_{nn}(R) \approx V_{NN}(R) \qquad \text{(II.9)}$$

II.1.3 Born-Oppenheimer approximation :

The velocity of nuclei is substantially slower since their mass is far greater than that of electrons **[3]**.The ground state of any instantaneous ion configuration may be thought of as the electronic system at any given time.The motions of electrons and nuclei may be distinguished using this approximation, sometimes referred to as the adiabatic (Born-Oppenheimer) approximation. It is thus possible to factor the overall wave function of the system of electrons and nuclei as the result of adding the wave functions for the nuclei and the individual electrons.

The theory is generally seen to be intriguing, however, there are some circumstances, like the plairon theory of manganites, where the connection of the electrical movement to that of the nuclei is crucial.

In cases where the electronic ground state is almost degenerate, the adiabatic approximation is invalid.

In the adiabatic approximation, the electronic Hamiltonian is written as:

$$\widehat{H} = \sum_{i=1}^{N} -\frac{\hbar^2}{2m_e}\nabla_i^2 + \frac{1}{2}\sum_{J=1,j\neq i}^{N}\frac{e^2}{|r_i-r_j|} - \sum_I \frac{e^2 Z_I}{|\vec{r}_i-\vec{R}_j|} \qquad \text{(II.10)}$$

The first component was the kinetic energy of electron i the second was the Coulomb interaction between electron i and the other electrons, mark j, and the third and final term was

the external potential resulting from the nucleus. The atomic numbers of the nuclei in places $R_I$are Z_I. The electronic system's Schrödinger equation is therefore expressed as follows:

$$H\Psi = E\Psi \qquad \text{(II.11)}$$

Where E is the energy of the electronic system in the external potential and is the multi-electron wave function. However, the issue becomes excessively complex due to the electron-electron interaction, necessitating the use of alternative approximations.Most of these approximations attempt to transform the issue of N electrons acting in concert into the case of N-independent quasi-particles in an active field. Then, one-particle wave functions are used to express the many-body wave function.

II.1.4 Hartree approximation :

According to this approximation, which was developed by DOUGLAS HARTREE in 1928 **[4]**, each electron in the poly-electronic system may be characterised by a different wave function. It becomes apparent that each electron is subject to a global potential that is generated by both the potential of confinement and the potential of the other electrons. This results in the global wave function ψ ($\vec{r}_1$, $\vec{r}_2$,……,$\vec{r}_N$) being broken down into a collection of elementary wave functions that each describe the state of a specific electron **[5]** :

$$\Psi(\vec{r}_1, \vec{r}_2, \dots\dots, \vec{r}_N) = \Psi_1(\vec{r}_1)\Psi_2(\vec{r}_2)\dots\dots\Psi_N(\vec{r}_N) \qquad \text{(II.12)}$$

According to this approximation, each electron moves independently in the mean-field produced by the nuclei and their surrounding electrons.

The Hartree equation, often known as the Schrödinger equation for a particle, has the following form:

$$\widehat{H_i}\Psi_i = E_i\Psi_i \qquad \text{(II.13)}$$

$$\text{and :} \quad \widehat{H_i} = -\frac{1}{2}\Delta_i + V_{ext} + V_i(\vec{r}) \qquad \text{(II.14)}$$

$V_i(\vec{r})$ is the Hartree potential for the i [th] electron, which takes the role of the electrostatic electron-electron interaction with all other electrons **[6]**. V_{ext} $(\vec{r})$ reflects both the potential owing to nucleus-nucleus interactions and those of other electrons-nuclei in the system.

Thispotential is derived from the assumption that each electron has an associated electron density, $\tilde{\rho}_j$. The chance that an electron exists is represented by this density.

$$V_i(\vec{r}) = \int d^3\,\vec{r}' \,\frac{\tilde{\rho}_i(\overrightarrow{r'})}{|\vec{r}-\vec{r}'|} \qquad \text{(II.15)}$$

The electron density $\tilde{\rho}_i(\vec{r})$ in equation (II.15) is given by

$$\tilde{\rho}_i(\overrightarrow{r}) = \sum_{\substack{j=0 \\ j\neq 0}}^{Ne} \left|\Psi_j\,(\overrightarrow{r})\right|^2 \qquad \text{(II.16)}$$

Sum was extended to the occupied N_e mono-electronic states.

The Hartree equation for a mono-electronic system may be found by inserting equations (II.4), (II.15), and (II.16) into equation (II.13):

$$\left(-\frac{1}{2}\Delta_i + V_{ext} + V_i(\vec{r})\right)\Psi_i\,(\overrightarrow{r}) + \sum_{\substack{j=1 \\ i\neq j}}^{Ne} \int d^3\vec{r}\,\frac{\left|\Psi_j\,(\overrightarrow{r'})\right|^2}{|\vec{r}-\vec{r}'|}\Psi_i\,(\overrightarrow{r}) = E_i\Psi_i(\vec{r}) \qquad \text{(II.17)}$$

According to the equation of (II.15), the Hartree potential $V_i(\vec{r})$, which establishes the monoelectronic wave functions $\Psi_i(\vec{r})$, is stated in terms of these identical wave functions (II.16). Because of this, this method is known as the self-consistent field approximation **[5]**.

If there are a lot of occupied single-electron states N_e involved, finding a self-consistent solution with Hartree's formulation requires assuming that the single-electron density $\tilde{\rho}_i(\vec{r})$ is equal to the overall electron density $\tilde{\rho}(\vec{r})$.

$$\tilde{\rho}_i(\overrightarrow{r}) = \sum_{\substack{j=0 \\ j\neq 0}}^{Ne} \left|\Psi_j\ (\overrightarrow{r})\right|^2 \qquad \text{(II.18)}$$

II.1.5. Hartree–Fock approximation :

Because the associated functions are not antisymmetric by the exchange of two electrons, Fock [7]demonstrated in 1930 that the solutions of the Hamiltonian of the equation (II.9) are inconsistent with the PAULI exclusion principle. By, for instance, exchanging two electrons, the electronic wave function is described as being anti-symmetric:

$$\Psi(r_1, r_2, \ldots\ldots, r_i, \ldots\ldots, r_j, \ldots\ldots r_{Ne}) = -\Psi(r_1, r_2, \ldots\ldots, r_i, \ldots\ldots, r_j, \ldots\ldots r_{Ne}) \qquad \text{(II. 19)}$$

The Pauli exclusion principle, which states that two electrons with the same quantum number cannot both concurrently occupy the same quantum state, is therefore obeyed by such a description. The electron ***i***, however, perfectly occupies the state ***i*** in the Hartree formulation of the wave function, hence this is not the case.

By demonstrating that the Pauli Principle is upheld if the wave function is expressed in the form of a determinant known as "**Slater's determinant**" [8], Hartree and Fock [9]have expanded on this idea.

$$\psi_c(r_1\sigma_1, \ldots, r_N\sigma_N) = \frac{1}{\sqrt{N!}} \begin{vmatrix} \psi_1(r_1\sigma_1)\psi_1(r_2\sigma_2) \ldots & \psi_1(r_N\sigma_N) \\ \ldots & \\ \psi_1(r_1\sigma_1)\psi_1(r_2\sigma_2) \ldots & \psi_1(r_N\sigma_N) \\ \psi_2(r_1\sigma_1)\psi_2(r_2\sigma_2) \ldots & \psi_2(r_N\sigma_N) \\ \psi_N(r_1\sigma_1)\psi_N(r_2\sigma_2) \ldots & \psi_N(r_N\sigma_N) \end{vmatrix} \qquad \text{(II. 20)}$$

whereσ represents the spin.

The function ψ given by equation (II.20) leads to the Hartree-Fock equations for a one-particle system [10]. Large numbers of electrons in the system being studied make it challenging to solve these Hartree-Fock equations. In addition to the energy terms from the Hartree-Fock approximation (AHF), the electron-electron interactions also result in additional energy components, known as correlation energy terms by Wigner [11]

II.1.6. Density functional theory

The complexity of solving Schrödinger's equation is greatly reduced by the Born-Oppenheimer approximation, but the remaining issue still involves many bodies and cannot be solved because the total wave function of the system depends on the coordinates of every electron and cannot be separated into contributions to a single particle because of their mutual interaction.

To properly solve the Schrödinger equation for actual materials, further approximations are necessary. The most significant in terms of history is that of Hartree Fock (HF), which provides a superior solution that fulfils the (problematic) restriction and may be extended to the exact resolution of the equation by using a so-called Slater determinant **[12]**.

However, it is quite difficult to numerically solve the H F technique for solids. This method was not employed in our work, but Hohenberg and Kohn**[13]** and Kohn and Sham **[14]**developed the theory of functional density, or density functional theory, which was another significant advance in physical calculations (1964 and 1965).

II.1.6.1. Basic principles

The first model based on the use of electron density as a basic variable to characterise the system's features was put out by Thomas and Fermi.However, this model had some flaws since he incorrectly characterised the quantitative characteristics of molecules and solids. About 40 years later, other pioneers like Slater, Hohenberg, and Kohn put out a more thorough and correct hypothesis. They explicitly established the DFT as the method to calculate the density of the ground state and the electron density as the parameter characterising the electronic system. It is a strategy that has the dual benefits of being sufficiently exact and able to handle a variety of difficulties.

II.1.6.2 First theorem of Hohenberg and Kohn:

An electronic Hamiltonian H_{el} describes an electronic system. by minimising the function $E[\psi]$, the energy and wave function of the ground state are derived.The external potential V_{ext} (r) fixes H_{el}fully for a system with N electrons. The Hamiltonian is determined exclusively by the external potential and the quantity of electrons, which subsequently provides access to the ground state's energy and wave function **[12, 15, 16]**.

An atomic system may be observed from an electronic perspective in two different ways: either via its nucleus through the external potential or through its electronic cloud via the electron density.

The assumption that a given electron density correlates to a certain external potential is theoretically motivated by the first theorem of Hohenberg and Kohn. The electron density$\tilde{\rho}$(r), determines the external potential v_{ext} $(\vec{r}\ )$, up to a constant. The wave function and all other physical characteristics of the system are uniquely determined by the electron density $\tilde{\rho}$(r), which also fixes the number of electrons.The first theorem of Hohenberg and Kohn uses as variables the electron density, the number of electrons N but also the interatomic distances R_a

$$\rho \Rightarrow \{N, Z, R\alpha\} \Rightarrow H \Rightarrow \psi fondamentale \Rightarrow E\ fondamentale \qquad \text{(II.7)}$$

By separating the dependent and independent components of the system (N,V_{ext}), we may recast the total energy as a function of the electron density $\rho(\overrightarrow{r})$, $E = E[\rho(\overrightarrow{r})]$:

$$E[\rho(\overrightarrow{r})] = T_{el}[\rho(\overrightarrow{r})] + V_{el-el}[\rho(\overrightarrow{r})] + V_{moy-el}\rho(\overrightarrow{r}) \qquad \text{(II.21)}$$

$$= F_{HK}[\rho(\overrightarrow{r})] + \int \rho(\overrightarrow{r})\, V_{ext}\,(\vec{r})\, d^3\vec{r} \qquad \text{(II.22)}$$

$$\text{with : } F_{HK}[\rho(\overrightarrow{r})] = T_{el}[\rho(\overrightarrow{r})] + V_{el-el}[\rho(\overrightarrow{r})] \qquad \text{(II.23)}$$

The kinetic energy of the T_{el} electrons and the potential energy as a result of the interaction between the electrons are both included in the functional F_{HK}, sometimes referred to as the

Hohenberg-Kohn functional, which is independent of the system. Their precise phrases are unknown. However, the Hartree energy may be used to infer the name $V_{el\text{-}el}$:

$$V_{el-el} = \frac{1}{2}\int \frac{\rho(\vec{r})\rho(\vec{r}')}{\left\|(\vec{r})-\vec{r}\right\|} d^3\vec{r}\, d^3\vec{r}' \qquad \text{(II.24)}$$

II.1.6.3. Second theorem of Hohenberg and Kohn:

To confirm that the electron density under consideration is in fact that of the ground state, Hohenberg and Kohn's second theorem is established. This theorem's conclusion may be expressed as follows: The energy $E[\rho test\ ]$ is larger than or equal to the energy associated with the ground state electron density $E[\rho_{fond}]$ for any test density meeting the requisite boundary conditions $\rho\, test \geq 0$ and $\int \rho test\ (r)\ d^{\,3}r = N$. It is also associated with an external potential V_{ext}.

The variational principle is described in this theorem for an energy that is a function of the electron density $E[\rho]$ and not a function of wave, $E[\psi]$,**[17]**.By interpreting the two theorems, we can assert that the electron density of the ground state may be used to determine all the attributes of a system specified by an external potential, V_{ext}.

Second, if and only if the associated electron density equals that of the ground state, the energy of the system $E[\rho]$ will be at its lowest value. This variant recipe can only be used to look for the energy of the ground state. This argument is restricted to the ground state for a specific symmetry, to be more exact.

II.1.7. The Kohn-Sham equations

The DFT is made usable as a tool by the equations of Kohn and Sham, published in 1965 **[18]**. They make it simple to determine the ground state density. The portion of the total energy that is present in the precise solution but lacking from the Hartree-Fock solution is the correlation energy. According to the precise Hamilton and Hartree-Fock, the total energy functionals $Ee[\rho]$ and $E_{HF}[\rho]$ are, respectively:

$$E_e = T + V \qquad \text{(II.25)}$$

$$E_{HF} = T_0 + \underbrace{(V_H + V_x)}_{V} \qquad \text{(II.26)}$$

Here,T and Vstand for the kinetic and potential energies of electrons, respectively. $T_0$is a function of the kinetic energy of an electron gas that is not interacting, while $V_H$stands for the Hartree contribution and $V_x$for exchange energy. When (II.26) is subtracted from (II.25), the correlation contribution function reads:

$$V_c = T - T_0 \qquad \text{(II.27)}$$

The portion of the total energy exchange that is present in the Hartree-Fock solution but absent from the Hartree solution is defined as the contribution. Naturally with the Hartree function provided by:

$$E_H = T_0 + V_H \qquad \text{(II.28)}$$

It can be defined as:

$$V_x = V - V_H \qquad \text{(II.29)}$$

We can rewrite the Hohenberg-Kohn functional as follows:

$$F_{HK} = T + V + T_0 - T_0 \qquad \text{(II.30)}$$

$$= T_0 + V + \underbrace{(T - T_0)}_{V_c} \qquad \text{(II.31)}$$

$$= T_0 + V + V_c + V_H - V_H \qquad \text{(II.32)}$$

$$= T_0 + V_H + V_C + \underbrace{(V - V_H)}_{V_x} \qquad \text{(II.33)}$$

$$= T_0 + V_H + \underbrace{(V_x + V_C)}_{V_{xc}} \qquad \text{(II.34)}$$

Here, V_{xc} is the functional exchange-correlation energy, which includes contributions from both the exchange and the correlation. The functional energy may be written formally as follows:

$$E_{V_{ext}}[\rho] = T_0[\rho] + V_H[\rho] + V_{xc}[\rho] + V_{ext}[\rho] \qquad \text{(II.35)}$$

We can now use Hohenberg-Kohn's second theorem to find the state density. The Hamiltonian - calledn"the Kohn-Sham Hamiltonian" is:

$$\hat{H}_{KS} = \hat{T}_0 + \hat{V}_H + \hat{V}_{xc} + \hat{V}_{ext} \qquad \text{(II.36)}$$

$$\begin{pmatrix} \cdots \\ \langle \phi_i^b | H_{sp} | \phi_j^b \rangle - \varepsilon_m \langle \phi_i^b | \phi_j^b \rangle \\ \cdots \end{pmatrix} \begin{pmatrix} C_1^m \\ \cdot \\ \cdot \\ \cdot \\ C_p^m \end{pmatrix} = \begin{pmatrix} 0 \\ \vdots \\ \vdots \\ \vdots \\ 0 \end{pmatrix} \qquad \text{(II.37)}$$

Where the exchange-correlation potential is given by the functional derivative:

$$\hat{V}_{xc} = \frac{\partial V_{xc}[\rho]}{\partial \rho} \qquad \text{(II.38)}$$

Kohn and Sham's theorem can now be formulated as follows: The exact ground state density $\rho(\vec{r})$of an N-electron system is:

$$\rho(r) = \sum_{i=1}^{N} \phi_i\,(\vec{r})^* \phi_i(\vec{r}) \qquad \text{(II.39)}$$

Where the one-particle wave functions are the least energetic solutions *N* of the Kohn-Sham equation:

$$\widehat{H}_{Ks}\phi_i = \varepsilon_i \phi_i \qquad \text{(II.40)}$$

II.1.7.1. The exchange-correlation functional :

Due to the lack of information provided by the DFT on the exchange-correlation functional's structure, the approximation used to determine it must be adaptable to various systems.

The consequences of interactions between electrons fall into three categories:

1. The antisymmetry of the total wave function leads to the exchange effect, also known as the Fermi correlation. It is equivalent to the fact that there is no chance that two electrons with the same spin will be in the same location. The charge of the electron in no way plays a role in this phenomenon, which is closely connected to the Pauli principle. Due to the antisymmetry of the Slater determinant used to describe the wave function *Ψ*, the Hartree-Fock approximation naturally accounts for it.
2. The electron's charge is what causes the coulomb correlation. It has to do with the electron repulsion in the $1/|r\text{-}r'|$ system. It is not spin-dependent, in contrast to the exchange effect. The Hartree-Fock theory does not take into account this effect(Figure II.1) **[19]**.
3. The third result results from the formulation of electronic wave functions as independent particles. This "self-interaction" adjustment should result in a count of the number of electron pairs that is accurate.

In addition to all of this, the Kohn-Sham technique imposes the exchange-correlation term to facilitate the correction of the kinetic energy term. Because of the wave functions' artificial independence, even if the density of the hypothetical system under consideration is the same as that of the real system, the calculated kinetic energy is different from the real energy.

A few approximations are used in the computation of the energy and the exchange-correlation potential.

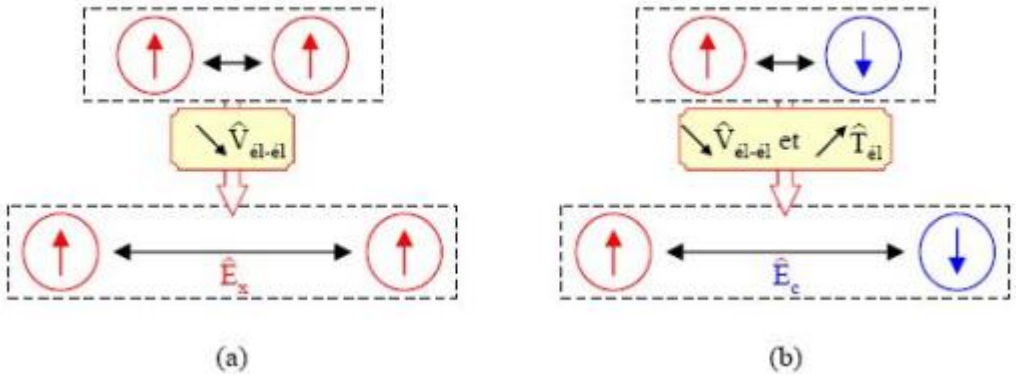

Figure.II.1:Representation of exchange and correlation effects [19].

II.1.7.2. Local Density Approximation (LDA) :

The most common approximation of the exchange and correlation functional is the LDA, where E_{xc} is the exchange and correlation energy of a homogeneous electron gas of density $\rho(r)$.

$$E_{xc}[\rho]=\int \rho(r)\,\varepsilon_{xc}(\rho(r))dr \qquad \text{(II.41)}$$

The local electron density approximation is:

$$E_{xc}[\rho]=\int \rho(r)\,\varepsilon_{xc}(\rho)dr \qquad \text{(II.42)}$$

Here, ε_{xc} is the contribution of exchange and correlation in the total energy (per electron) of a homogeneous gas of electrons in interaction with the density $\rho(r)$. This approximation is quite
good when $\rho(r)$ varies slowly **[20]**.

II.1.7.3. The Generalized Gradient Approximation (GGA):

The LDA and LSDA approaches are based on the electron gas model and therefore assume a uniform electron density. However, atomic or molecular systems are most often very different from a homogeneous electron gas. In general, we can consider that all real systems are inhomogeneous, that is to say that the electron density has a spatial variation. The so-called GGA methods, sometimes also called non-local methods, have been developed in such a way as to take into account this density variation by expressing not only the exchange and correlation energies as a function of the density but also of its gradient (its first derivative).
In general, the exchange-correlation energy depends not only on the density at each point, but also on its gradient. It is usually given as follows:

$$E_{xc}^{GGA}[\rho] = \int f[\rho(\vec{r}), \nabla\rho(\vec{r})]d^3\vec{r} \qquad \text{(II. 43)}$$

$\nabla\rho(\overrightarrow{r})$: express the gradient of the electron density.

The GGA is available in many iterations. the ones created by Perdew and Wang **[21, 22]**and Perdew, Burke, and Ernzerhof **[23, 24]**are the most often utilised. The GGA approach frequently yields more accurate answers for total energies, cohesion energies, equilibrium volumes, and incompressibility moduli than the LDA. However, insulators' and semiconductors' prohibited bandwidths continue to be far too small.

II.1.7.4. The GGA+U approximation :

The biggest issue with Kohn and Sham's methodology is that non-symmetric techniques have been devised to enhance the exchange and correlation functionals. In materials like the metal-oxide transition, where electrons frequently interact locally, the issues are more difficult to solve.These systems provide an explanation for the metal-insulator transitions and other phenomena connected to the correlation **[25]**. Within the scope of the so-called GGA+U

correlation (Anisimov, et al. 1991) **[26]**,an effort has been made to enhance the findings by combining the calculations of the approximation (GGA or LDA) with the repulsion term of Hubbard U (Coulomb repulsion) **[27]**.Strongly correlated systems appear to respond more naturally to models of the Hamiltonian kind, such as the Mott-Hubbard model **[28]**or Anderson impurity model **[29]**.

The Coulomb repulsion *U* between identical-atom electrons and kinetic energy, (which is dependent on the band with determined by the jump integral t), are explicitly opposed in the Mott-Hubbard model. The type and position of an electron will depend on the ratio between these two energies.

II.1.8. Solving the Kohn-Sham equations

The Kohn and Sham equations must be solved in a self-consistent manner (self-consistent field, or "SCF") in order to calculate a self-consistent potential or self-consistent electron density **[30]**.

The usual procedure is described in the diagram of (**figure.II.3**).

For the initial iteration, we begin with a test densityρ_{int}Typically, one first calculates the matrix of

Kohn-Sham by superimposing the atomic densities, then one solves the equations for the coefficients of expansion to produce the orbitals of Kohn-Sham, and last one calculates the new density ρ_{out} .

$$\rho_{in}^{i+1} = (1-\alpha)\rho_{in}^{i} + \alpha\rho_{out}^{i} \qquad \text{(II.45)}$$

i: represents the nth iteration.

α: A mixing parameter.

Thus the iterative procedure can be continued until convergence is achieved.

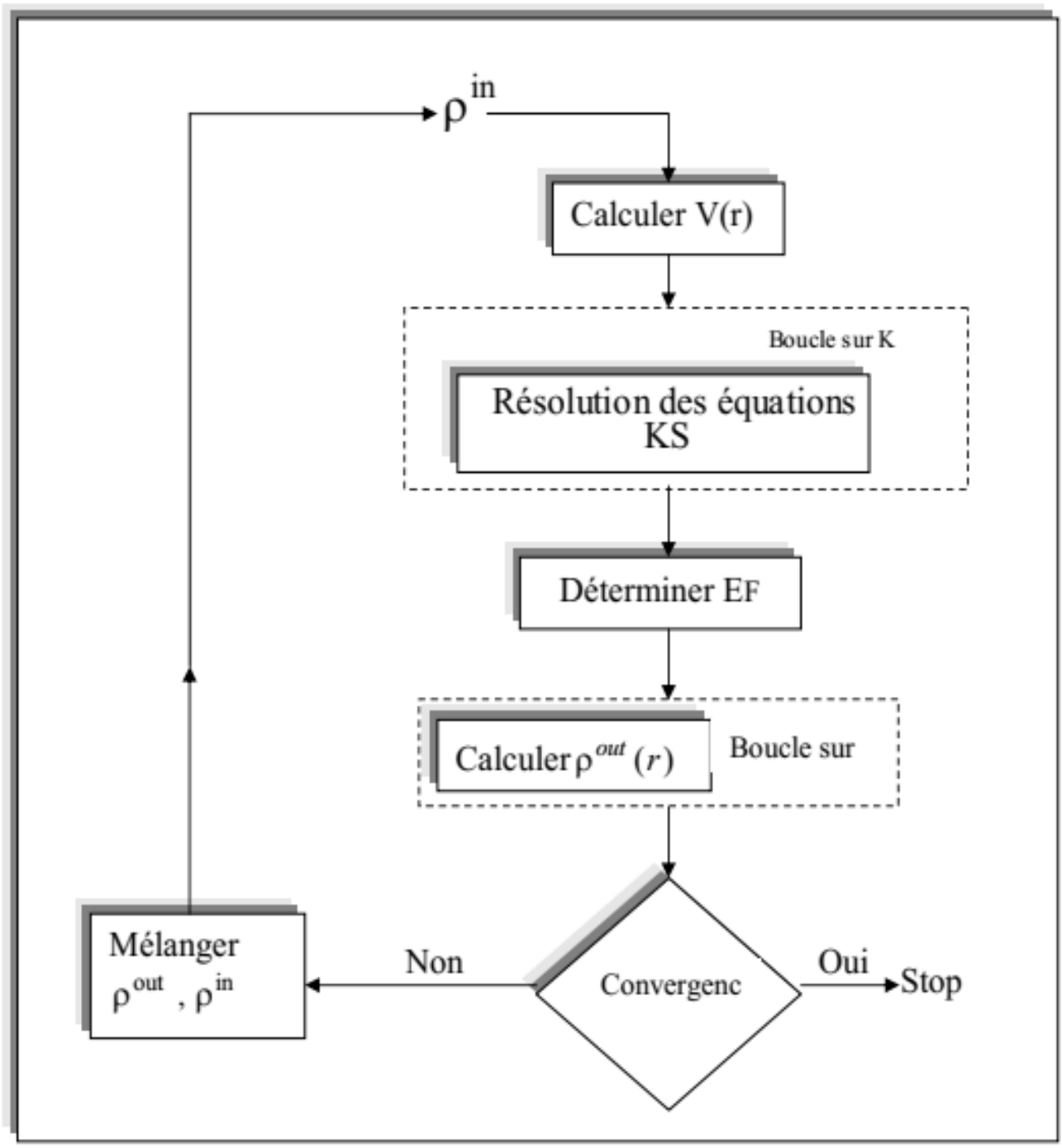

Figure.II.2: Cycle self consist of calculations [31].

II.2. Linearized augmented plane wave method (FP-LAPW)

II.2.1. Introduction

One of the most challenging issues is the study of the many condensed matter physics properties, such as the identification of band structures, cohesive energy, charge density, etc. However, we are able to model these properties, particularly the electronic structure of solids, using a number of calculation techniques.Because they are based on various approximations, they have benefits and disadvantages, especially in terms of precision and numerical details (calculation speed and information storage memory).

These techniques for the most complicated systems include:

- The tight-binding method (LCAO) (linear combination of atomic orbitals), where atomic orbitals are expressed as the product of eigenfunctions of angular momentum and radial orbitals.
- The OPW technique used by Herring **[32]**is based on the separation between the crystal potential outside the ion core and the potential of the ion core.
- Its foundation is the orthogonalization concept found in the Phillips cancellation theorem (1958) **[33]**.
- The "muffin-tin" form of the potential is used as the basis for the augmented plane wave technique (APW), which has spherical symmetry.The linear augmented plane wave technique (LAPW) and the linear Muffin-Tin orbital (LMTO) method are the methods that resulted from the approach (APW).
- The basis in the first instance consists of linearized augmented plane waves, whereas the basis in the second case consists merely of radial functions (Hankel functions).

II.2.2. The augmented plane wave (APW) method

In his paper, Salter **[10, 34, 35]**presents the APW (Augmented Plane Wave) approach. He developed augmented plane waves (APW) **[36]** in 1937 as a basis function for resolving the Kohn and Sham equations for a single electron. According to this approach (APW), the primitive cell is split into two different sorts of regions:

- “Muffin-Tin” (MT) spheres concentrated around all constituent atomic locations and Rα rays.

- A remaining interstitial region.

The potential and wave functions near the atomic nucleus have the "Muffin-Tin" (MT) form, which exhibits spherical symmetry inside a sphere with a radius of Ra. The potential and wave functions between atoms can be regarded as smooth. As a consequence, depending on the area being considered, the wave functions of the crystal are created using different bases: plane waves in the interstitial region and radial solutions of the Schrödinger equation inside the MT sphere (**Figure.II.4**).

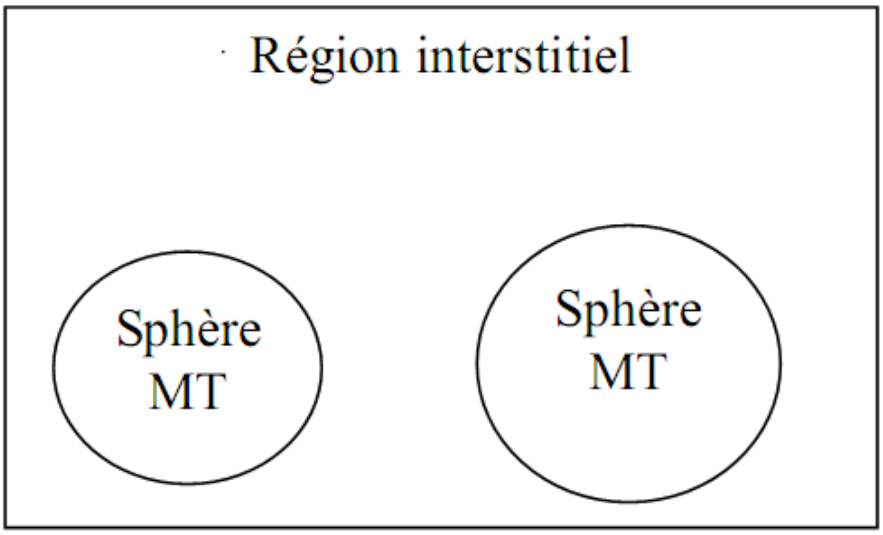

Figure.II.3: Muffin-Tin "MT" Potential Representation[37].

$$\Phi(r) = \begin{cases} \frac{1}{\Omega^{1/2}} \sum_G C_G e^{i(G+K)r} r < R_\alpha \\ \sum_{lm} A_{lm} U_l(r) Y_{lm}(r) r > R_\alpha \end{cases} \quad \text{(II.46)}$$

Where: $R\alpha$ represents the radius of the sphere MT and Ω the volume of the cell.

C_G and $A_{lm}$the development coefficients in spherical harmonics Y_{lm}.

The function $U_l(r)$ is a solution of the Schrödinger equation for the radial part which is written in the form:

$$\left\{-\frac{d^2}{dr^2} + \frac{l(l+1)}{r^2} V(r) - E_l\right\} r U_l(r) = 0 \qquad \text{(II.47)}$$

The Muffin-tin potential is represented by *V(r)*, and the linearization energy is by E_l. Any correct condition of the heart is orthogonal to the radial functions. This orthogonality disappears at the limit of the sphere **[38]** as shown by the following Schrödinger equation:

$$(E_1 - E_2)rU_1U_2 = U_2\frac{d^2U_1}{dr^2} - U_1\frac{d^2U_2}{dr^2} \qquad \text{(II.48)}$$

Where U_1 and U_2 are the radial solutions for the energies E_1 and E_2.

Slater supports the selection of these functions by pointing out that while the potential is constant, plane waves are Schrödinger's equation solutions. When $E_l$is an eigenvalue and the potential is spherical, the radial functions are solutions.

The coefficients A_{lm} must be developed in accordance with the coefficient C_G of the plane waves present in the interstitial areas in order to guarantee the continuation of the function Φ(r) at the surface of the sphere MT. As a result of the calculations:

$$\left\{A_{lm} = \frac{4\pi i^2}{\Omega^{1/2}U_l(R_\alpha)}\sum_G j_l\left(|K+G|R_\alpha\right)Y_{lm}^*(K+G)\right\} \qquad \text{(II.49)}$$

The origin is assumed to be in the sphere's centre, and the A_{lm} coefficients are calculated using the plane wavesC_G. The APW method's variation coefficients are known as the energy parameters E_l. We acquire augmented planes (APWs) as a result of the individual functions designated by G being compatible with the radial functions in the sphere.

The Schrödinger equation in spheres can be solved by the APWs functions, but only for the energy E_l, which must match the energy of the band of index *G*.

The APW method presents some difficulties related to the function $U_l(r)$ present in equation (II.41).The value of $U_l(r)$can reach zero at the surface of the sphere MT depending on the value of the parameter E_l, which would result in a separation of the radial functions from the plane wave functions.To address this issue, the APW approach has undergone a number of revisions, most notably those made by Koelling **[39]**and Andersen **[40]**.In order to create the

LAPW technique, this modification involves displaying the wave functionΦ(r) inside the spheres by combining linearly the radial functions *Ul(r)* and their derivatives with respect to the energy $U'_l(r)$.

II.2.3. Principle of the LAPW method

The basis functions for the MT spheres in the LAPW technique are linear combinations of the radial functions $U_l(r)Y_{lm}(r)$and their energy-related derivatives $\dot{U}_l(r)Y_{lm}(r)$. The APW (II.40) method defines the functions U_l as follows, and the function $\dot{U}_l(r)Y_{lm}(r)$. must meet the following requirement:

$$\left\{-\frac{d^2}{dr^2}+\frac{l(l+1)}{r^2}+V(r)-E_l\right\}r\dot{U}_l(r)=rU_r(r) \qquad \text{(II.50)}$$

These radial functions $U_l(r)$ and$\dot{U}_l(r)$ guarantee continuity with the plane waves coming from outside on the surface of the MT sphere in the non-relativistic situation.The wave functions thus augmented become the basis functions (LAPW) of the FP-LAPW method:

$$\phi(r)=\begin{cases}\frac{1}{\Omega^{1/2}}\sum_G C_G e^{i(G+K)r} r>R_\alpha \\ \sum_{lm}[A_{lm}U_l(r)+B_{lm}U_l(r)]Y_{lm}(r) r<R_\alpha\end{cases} \qquad \text{(II.51)}$$

Where the coefficients B_{lm} have a similar nature to the coefficients A_{lm} and are related to the function $\dot{U}_l(r)$.as with the APW approach, the LAPW functions are just plane waves in the interstitial zones.

The LAPW functions are more suitable for use inside spherical objects than the APW functions.in fact, a linear combination will more accurately recreate the radial function than the APW functions made up of a single radial function if $E_l$differs little from the band energy E.

As a result, the function U_l may be extended as a function of the energy E_l and its derivativ. $\dot{U}_l(r)$.

$$U_l(E,r) = U_l(E_l,r) + (E - E_l)\dot{U}_l(E,r) + 0((E - E_l)^2) \qquad \text{(II.52)}$$

where: $0((E - E_l)^2)$represents the energy squared error.

Thus, the LAPW approach assures that the wave function at the MT sphere's surface is continuous. However, this process results in less accurate computations than the APW approach, which reproduces wave functions extremely well. In contrast, the FP-LAPW method causes errors in wave functions of the order of $(E\text{-}E_l)^2$ and band energies of the order of $(E\text{-}E_l)^4$. despite this order of inaccuracy, the LAPW functions provide a solid foundation that makes it possible to acquire all the valence bands throughout a wide energy range with just one E_l.

The energy window may typically be split into two portions when this is not possible, which is a huge simplification compared to the APW approach.generally, if U_l is equal to zero at the sphere's surface, its derivative $\dot{U}_l$will be nonzero.therefore, the problem of continuity on the surface of the MT sphere will not arise in the LAPW method.

A version of the LAPW approach using N radial functions and their (N-1) derivatives was put out by Takeda and Kubler **[41]**.Each radial function having its own E_{li} parameter so that the error related to the linearization is avoided. We find the standard LAPW method for N=2 and E_{l1} close to E_{l2}, while for N>2 the errors can be reduced.Unfortunately, compared to the standard FP-LAPW technique, the inclusion of high-order derivatives to guarantee convergence necessitates a substantially longer calculation time.Singh **[42]**modified this approach by adding local orbitals to the base without increasing the plane wave cut-off energy.

II.2.3.1. Representation of charge density and potential

The twofold representation of the wave functions, charge and potential, provides the foundation for the LAPW method's solution of the Kohn-Sham equations.Symmetry is utilised in order to decrease the number of factors that must be stored, which simplifies the synthesis of the load and the Hamiltonian matrix.

The symmetries used are:

- Inside the spheres, the density has the symmetry of the site.

- The density in the interstitial region has the symmetry of the space group.

The densities inside the atoms, connected by symmetry operations, are identical.

II. 2.4 WIEN2K code

In this work, we used the FP-LAPW method, implemented in the Wien2k code **[34][43]**.

During a self-consistent computation, many programs include:

NN: software that provides the separations between the nearest neighbors and aids in calculating the sphere's atomic radius.

SGROUP: determines the space group of the structure defined in the case.struct file.

LSTART: An application that creates atomic densities and defines how various orbitals are handled in the band structure computation, such as core states with or without local orbitals.

SYMMETRY: It determines the local rotation matrices, the point group of each particular atomic site, the LM expansion for the lattice harmonics, and the space group symmetry operations.

KGEN: It creates a Brillouin zone mesh, k.

DSTART: It generates a starting density for the SCF (Self Consistent Field) cycle by the super position of the atomic densities generated in **LSTART**.

After then, until the convergence requirement is confirmed, a self-consistent cycle is begun and repeated.The following steps are included in this cycle:

LAPW0: Generates the potential from the electron density.

LAPW1: Calculates valence bands, eigenvalues and eigenvectors.

LAPW2: Calculation of valence densities for eigenvectors.

LCORE: Calculates core states and densities.

MIXER: Mixes the input and output densities.

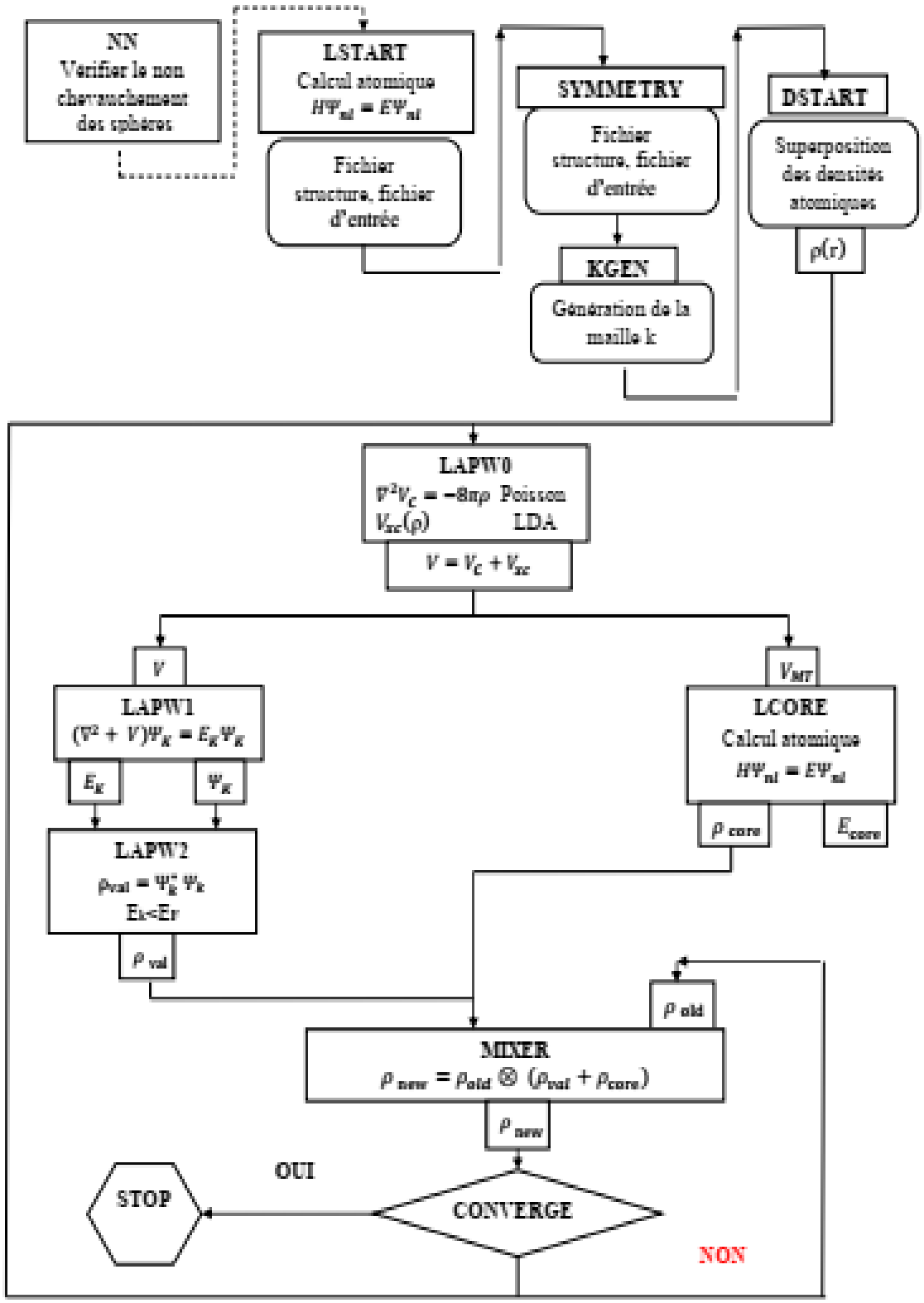

Figure.II.4: The structure of the WIEN2k program**[44]**.

References

1. Umul, Y.Z., On the reality of the Bohmian potential. Optik, 2020. **224**: p. 165729.
2. Born, M. and W. Heisenberg, Zur quantentheorie der molekeln. Original Scientific Papers Wissenschaftliche Originalarbeiten, 1985: p. 216-246.
3. Born, M. and R. Oppenheimer, On the quantum theory of molecules, in Quantum Chemistry: Classic Scientific Papers2000, World Scientific. p. 1-24.
4. Slater, J.C., Quantum theory of atomic structure, 1960.
5. Allan, G. and M. Lannoo, Trends in the cohesive properties of sp bonded elements. Journal de Physique, 1983. **44**(12): p. 1355-1363.
6. Basdevant, J.-L. and J. Dalibard, Problèmes quantiques2004: Editions Ecole Polytechnique.
7. BOUAKKAZ, A., Etude des propriétés structurales, électroniques, et élastiques des chalcogénures alcalino-terreux: CaX, CdX et $Ca_{0.75}Cd_{0.25}X$ (X: S, Se, Te). 2020.
8. Slater, J.C., Molecular energy levels and valence bonds. Physical Review, 1931. **38**(6): p. 1109.
9. BEDINA, R., Calcul de la polarisation instantanée et les constantes piézoélectriques des monocristaux PZT en utilisant la phase de Berry, 2016, Université Mohamed BOUDIAF de M'Sila.
10. Slater, J., Energy band calculations by the augmented plane wave method, in Advances in quantum chemistry1964, Elsevier. p. 35-58.
11. Lea, M. and N. March, Quantum-mechanical wigner electron crystallization with and without magnetic fields. International Journal of Quantum Chemistry, 1989. **36**(S23): p. 717-729.
12. Slater, J.C., A simplification of the Hartree-Fock method. Physical review, 1951. **81**(3): p. 385.
13. Hohenberg, P. and W. Kohn, Inhomogeneous electron gas. Physical review, 1964. **136**(3B): p. B864.
14. Cottenier, S., Density Functional Theory and the family of (L) APW-methods: a step-by-step introduction. Instituut voor Kern-en Stralingsfysica, KU Leuven, Belgium, 2002. **4**(0): p. 41.
15. Hohenberg, P. and W. Kohn, Density functional theory (DFT). Phys. Rev, 1964. **136**(1964): p. B864.

16. Slater, J.C., Quantum Theory of Molecular and Solids. The self-Consistent Field for Molecular and solids, 1974. **4**.
17. Moruzzi, V., JF Janak and AR Williams. Calculated Electronic Properties of Metals, 1978: p. 48.
18. Kohn, W. and L.J. Sham, Self-consistent equations including exchange and correlation effects. Physical review, 1965. **140**(4A): p. A1133.
19. Zunger, A. and A. Freeman, Ground-and excited-state properties of LiF in the local-density formalism. Physical Review B, 1977. **16**(6): p. 2901.
20. Ceperley, D.M. and B.J. Alder, Ground state of the electron gas by a stochastic method. Physical review letters, 1980. **45**(7): p. 566.
21. Perdew, J.P., et al., Atoms, molecules, solids, and surfaces: Applications of the generalized gradient approximation for exchange and correlation. Physical review B, 1992. **46**(11): p. 6671.
22. Perdew, J.P., et al., Erratum: Atoms, molecules, solids, and surfaces: Applications of the generalized gradient approximation for exchange and correlation. Physical Review B, 1993. **48**(7): p. 4978.
23. Furness, J.W., et al., Accurate and numerically efficient r2SCAN meta-generalized gradient approximation. The journal of physical chemistry letters, 2020. **11**(19): p. 8208-8215.
24. Perdew, J.P., K. Burke, and M. Ernzerhof, Generalized gradient approximation made simple. Physical review letters, 1996. **77**(18): p. 3865.
25. Benamra, S. and H. Chebabhi, Etude des propriétés optoélectroniques du ternaire antiperovskites Ca_3PN: application photovoltaïque, 2020,UNIVERSITE MOHAMED BOUDIAF-M'SILA.
26. Anisimov, V.I., J. Zaanen, and O.K. Andersen, Band theory and Mott insulators: Hubbard U instead of Stoner I. Physical Review B, 1991. **44**(3): p. 943.
27. Kohanoff, J., Electronic structure calculations for solids and molecules: theory and computational methods2006: Cambridge university press.
28. POPULAIRE, E., Mlle BAHNES Aicha, These de Doctorat, 2018, Université de Mostaganem.
29. Dreizler, R., J. da Provindencia, Density Functional Methods in, 1985, Physics.

30. Trickey, S.B., Short Course on Density Functional Theory and Applications X. References and Omitted Topics. Phys. Rev. A, 2006. **73**(012513): p. 1-12.

31. ASFOUR, I., Étude des propriétés physique des alliages Heusler et Half-Heusler, 2018.

32. Ching, W.-y., Electronic and Optical Properties of Lithium1974: Louisiana State University and Agricultural & Mechanical College.

33. HELLAL, T., Etude premier principes du ferromagnétisme dans les alliages à base de terres rares et métaux de transition, 2019.

34. Slater, J.C., Wave functions in a periodic potential. Physical Review, 1937. **51**(10): p. 846.

35. Loucks, T.L., Augmented plane wave method: a guide to performing electronic structure calculations1967: WA Benjamin.

36. Sami, H. and N. Oulimar, Effet du dopage sur les propriétés physiques d'un heusler a base du cobalt «Co_2ZrGe», 2022.

37. HELLAL, T., Etude premier principes du ferromagnétisme dans les alliages à base de terres rares et métaux de transition, 2019.

38. Koelling, D. and A. MacDonald, Relativistic effects in solids. Relativistic Effects in Atoms, Molecules, and Solids, 1983: p. 227-304.

39. Koelling, D. and G. Arbman, Use of energy derivative of the radial solution in an augmented plane wave method: application to copper. Journal of Physics F: Metal Physics, 1975. **5**(11): p. 2041.

40. Andersen, O.K., Linear methods in band theory. Physical Review B, 1975. **12**(8): p. 3060.

41. Takeda, T. and J. Kubler, Linear augmented plane wave method for self-consistent calculations. Journal of Physics F: Metal Physics, 1979. **9**(4): p. 661.

42. Singh, D., Ground-state properties of lanthanum: Treatment of extended-core states. Physical Review B, 1991. **43**(8): p. 6388.

43. Yamaguchi, A., et al., Probing directionality of local electronic structure by momentum-selected STEM-EELS. Applied Physics Letters, 2018. **113**(5): p. 053101.

44. Blaha, P., et al., wien2k. An augmented plane wave+ local orbitals program for calculating crystal properties, 2001. **60**: p. 1-302.

CHAPITRE III : RESULTATS AND DISCUSSION

III. 1. Introduction

Heusler materials have shown a groundbreaking role in material research because of their wide applicability in modern technologies and multi-dimensional properties.Heusler alloys were once thought to be intermetallic alloys, however, their atomic order feature makes them more appropriately characterized as intermetallic compounds. The Heuslers' general formula is X_2YZ, where X and Y are transition metals and Z is a periodic table element from Group III, IV, or V.In certain situations, however, Y is substituted with a rare earth metal or an alkaline Earthmetal **[1]**.

Among these compounds, let us quote the Manganese-based Heuslers: Mn_2YSn (Y= Mo,Nb, Zr)and Mn_2YSn (Y= Ru,Rh,Pd) among these compounds, let us quote the Manganese-based Heuslers: Mn_2YSn (Y= Mo, Nb, Zr) and Mn_2YSn (Y= Ru, Rh, Pd) This study is carried out by an employing state of an art first-principles computational approach named “full potential (FP) linearized (L) augmented plane wave plus local orbital (APW+lo)” as designed with “density functional theory (DFT)”and executed in WIEN2k computational code.to examine the structural, electrical, and magnetic characteristics of the entire Heusler compounds.

III.2.Computational method

By using the FP (LAPW) technique framed inside DFT and implemented in the form of the WIEN2k computational code **[2]**, the electronic structure computations of Mn_2YSn (Y=Ru, Rh, and Pd) and Mn_2YSn (Y=Mo, Nb, Zr) are carried out.

The space is split up using this approach into an interstitial region (IR) and non-overlapping muffin tin (MT) spheres centred at the atomic sites. Plane waves make up the foundation set in the IR region. The one particle Schrödinger equation's radial solutions (at fixed energies) and their energy derivatives compounded by spherical harmonics are used to define the basis sets inside the MT spheres.For the computation of the structural characteristics, the generalised gradient approximation (PBE-GGA) was used to address the exchange-correlation potential **[3]**.

The PBE-GGA+U technique **[4]**, in contrast, is used to more accurately compute the electronic and magnetic characteristics. U is the Hubbard-Coulomb energy term.

The values of the Hubbard term U for Mn, Ru, Rh and Pd atoms are taken as 3.0, 2.0,1.92 and 2.0 eV, from **[5-8]** respectively.

Calculations were done using the formula $R_{MT}K_{MAX}=8$, where K_{MAX} is the maximum basis set wave-vector value and R_{MT} is the radius of a muffin tin for each atom in the unit cell. In the interstitial area, $G_{max}=12a.u^{-1}$ was taken into consideration for the Fourier expansion of the plane-wave basis set, while $l_{max}=10$ was employed for the maximum value of the angular momentum. In order to satisfy the energy convergence condition and still be able to distinguish between the core and valence parts, the cut-off energy value of -6.0 Ry was chosen. However, for self-consistent computations, up to 10^{-4} Ryd of energy value was taken into account.

The electronics configurations for atoms in Mn_2YSn (Y= Mo, Nb, Zr) are: **Mn**: [Ar]$4s^2$ $3d^5$,**Mo** :[Kr]$4s^1$ $4d^5$,**Nb** :[Kr]$5s^1 4d^4$,**Zr** :[Kr]$5s^2 4d^2$,**Sn** : [Kr]$5s^2$ $4d^{10}5p^2$.

The electronic configuration for Mn_2YSn (Y=Ru, Rh, and Pd) is: **Mn**:[Ar]$4s^2 3d^5$; **Ru**:[Kr]$5s^1 4d^7$; **Rh**:[Kr]$5s^1 4d^8$;**Pd**:[Kr]$4d^{10}$; **Sn:**[Kr]$5s^2 4d^{10}5p^2$.

III.3. Results and discussion

III.3.1.Mn_2YSn (Y=Mo,Nb,Zr)

III.3.1.1 Structural Properties

The geometrical findings of the Mn_2YSn (Y= Mo, Nb, Zr) Heusler alloys, as well as the lattice parameters and bulk modulus, are presented in this subsection. The full-Heusler alloys have a general stoichiometric composition of X_2YZ, where X and Y are separate transition elements and Z is the main group element.Their highly organised structure significantly influences the Heusler compounds' electrical and magnetic properties.In Mn_2YSn with (Y= Mo, Nb, Zr), there are two possible atomic arrangements.

The first is $L2_1$ ("regular cubic phase" prototype Cu_2MnAl), where the two Mn atoms occupy A(0,0,0) and C(1/2, 1/2, 1/2) positions, while the Y, Sn atoms occupy B(1/4,1/4,1/4) and D(3/4, 3/4, 3/4).The order of the atoms occupying the four positions of the unit cell in the Cu_2MnAl type $L2_1$ structure is X-Y-X-Z. The second one is called XA ("inverted cubic phase" prototype Hg_2CuAl), in which the two Mn atoms occupy places A(0,0,0) and B (1/4,1/4,1/4), respectively, while y, Sn atoms occupy positions C (1/2,1/2,1/2), and D (3/4,3/4,3/4). The atoms are arranged in the following order: X-X-Y-Z.

The inter-exchange between the C-site and the B-site atoms is a key distinction between these two structures.Due to the fact that both structures have a general FCC-like symmetry and may be difficult to differentiate by X-ray diffraction, careful consideration must be given to the structural analysis **[9, 10]**.To determine the ground state properties of Mn_2YSn (Y=Mo, Nb, Zr), the calculation results of total energy versus the lattice constant for both structures Hg_2CuTi and Cu_2MnAl are plotted in **Figure.III.1**.

The variation of total energy with the volume is fitted to Murnaghan equation of state **[11]** to obtain the equilibrium lattice constant a (A°), bulk modulus B (GPa), derivative of bulk the modulus B´.

$$E=E_0(V)+\frac{BV}{B'(B'-1)}\left[B\left(1-\frac{V0}{V}\right)+\left(\frac{V0}{V}\right)^{B'}-1\right] \qquad \text{(III.1)}$$

Where E_0 the minimum energy at T= 0 K, B is the bulk modulus, B´ is the bulk modulus derivative and V_0 is the equilibrium volume.

Clearly, for Mn_2YSn (Y= Mo, Nb, Zr) compounds, the regular cubic phase (prototype Cu_2MnAl) Heusler structure is more stable than the inverted cubic phase (prototype Hg_2CuAl).

The results are shown in **Table.III.1**, where it is shown that the computed lattice constant of Mn_2YSn (Y= Mo, Nb, and Zr) is in good agreement with previously published theoretically optimised lattice constants from other studies.The number of electrons on an atom's site preference is a major factor, according to Luo and colleagues **[12]**, in both the X and Y atoms. The A and C positions are preferred by elements with more electrons, whereas the B

sites are often occupied by atoms with less electrons. The Cu2MnAl structure will be seen in the case of Mn_2YSn (Y= Mo, Nb, Zr), since the nuclear charge of X (Mn atom) is greater than that of Y (Y= Mo, Nb, Zr).Similar results are found by Kervan and al **[13]**for Mn_2NbAl, and Anjami and al **[14]**for Mn_2ZrX (X= Ge, Si).

Based on formation energy (E_f), we address the phase stability of Mn_2YSn (Y= Mo, Nb, Zr). Using this, one may determine whether certain alloys can be made experimentally. Here, the formation energy Ef is estimated by summing the total energies of the constituent elements and comparing them to the total energies of the Mn_2YSn (Y= Mo, Nb, Zr) Heusler alloys.

The formation energy of the Mn_2YSn (Y= Mo, Nb, Zr) materials are computed following the expression given below:

$$\Delta E_f = E_{Mn_2YSn}^{total} - \left[2E_{Mn}^{bulk} + E_Y^{bulk} + E_{Sn}^{bulk}\right] \quad \text{(III.2)}$$

Where $E_{Mn_2YSn}^{total}$ total is the total energy estimated using first principles for the Mn_2YSn (Y= Mo, Nb, Zr) complete Heusler alloys, and E_{Mn}^{bulk},E_Y^{bulk}, E_{Sn}^{bulk} are the total energies per atom for the corresponding elements of Mn, Y, and Sn in their bulk forms. The entire Heusler alloys Mn_2YSn (Y= Mo, Nb, Zr) are chemically stable, and these substances may be manufactured experimentally, according to the negative values of the formation energy. The computed results of the ΔE_f for the Cu_2MnAl type structures are found more negative than of the Hg_2CuTi type structures, endorsing that Cu_2MnAl type structures are more stable as compared to the Hg_2CuTi type ones.

Table.III.1:Calculated equilibrium lattice constant a (Å), the bulk modulus B (GPa), the minimum energy (Ry) and the formation energy E_f (Ry) of Mn_2YSN (Y= Mo, Nb, Zr Heusler compounds.

		a (A°)	B (GPa)	B´	Energy (Ry)	E_f (Ry)
Mn_2MoSn	Hg_2CuTi	6.2825	133.9353	5.2946	- 25091.956309	-1.257851
	Cu_2MnAl	6.1033	264.5693	6.9898	-25091.976771	-1.278313
Mn_2NbSn	Hg_2CuTi	6.3946	138.8278	4.0864	- 24633.748350	-1.296929
	Cu_2MnAl	6.1872	195.5253	4.4311	-24633.803953	-1.322501
Mn_2ZrSn	Hg_2CuTi	6.5743	98.2694	4.2436	-24191.251440	- 1.149113
	Cu_2MnAl	6.3195	162.0852	4.0633	-24191. 311742	-1.192513

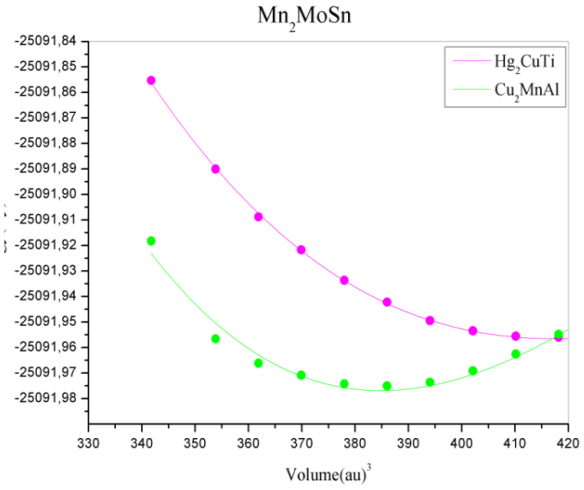

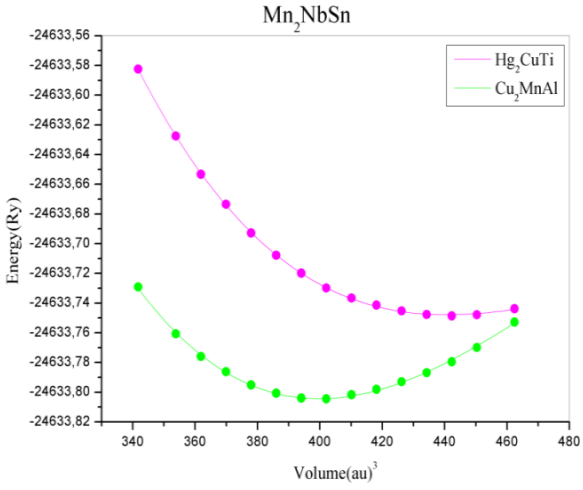

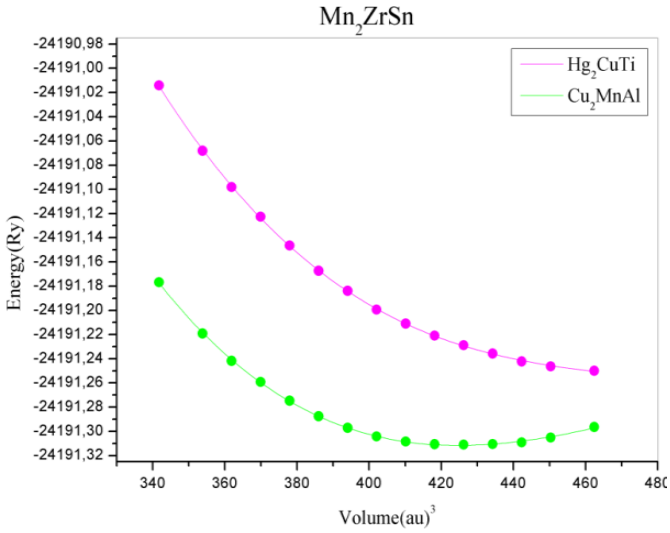

Figure.III.1: Total energy versus lattice constant for both structure Hg_2CuTi and Cu_2MnAl for Mn_2YSn (Y= Mo, Nb, Zr).

III.3.1.2 Electronic properties

The density of states is a basic quantum mechanics function that measures the density of eigenstates at a given energy level . It is mostly easily calculated when the system is large and its dispersion relation is spherically symmetric with respect to the quantum numbers.

In the opposite spin state, E_f cuts through the bands, whereas the gap is present in half-metallic Heusler alloys in one state. The Fermi level's location is mostly determined by the d-

band. The explanation of spin-polarized electronic band structures heavily relies on transition metals' d-states; in one spin state, the density of states peaks around E_F, whereas in another, the density of states is zero around E_F **[15]**.

The conduction electrons are thus 100% spin-polarized, and it is useful to define the electron spin polarization at the Fermi energy of a material where the spin polarization at E_f is given by eq.

$$P = \frac{N\uparrow(E_f) - N\downarrow(E_f)}{N\uparrow(E_f) + N\downarrow(E_f)} \qquad \text{(III.3)}$$

Where $\boldsymbol{N}\uparrow\left(\boldsymbol{E_f}\right)$ and $\boldsymbol{N}\downarrow\left(\boldsymbol{E_f}\right)$are the spin depended densities of states at E_F .the arrows ↑ and ↓ assign states of the opposite spins, that are the majority and minority states, respectively.

in order to fully comprehend the electron structures of Mn_2YSn (Y= Mo, Nb, Zr). We give the energy bands along high symmetry directions in the Brillouin zone (Bz), the total density of states (TDOS) and partial density of states (PDOS) plots for Mn2YSn (Y= Mo, Nb, Zr) in **Figure.III.2** To show the contributions from different atomic states close to E_F, PDOS plots are presented. For easier comparison, we treat the spin-up channel as positive and the spin-down channel as negative.

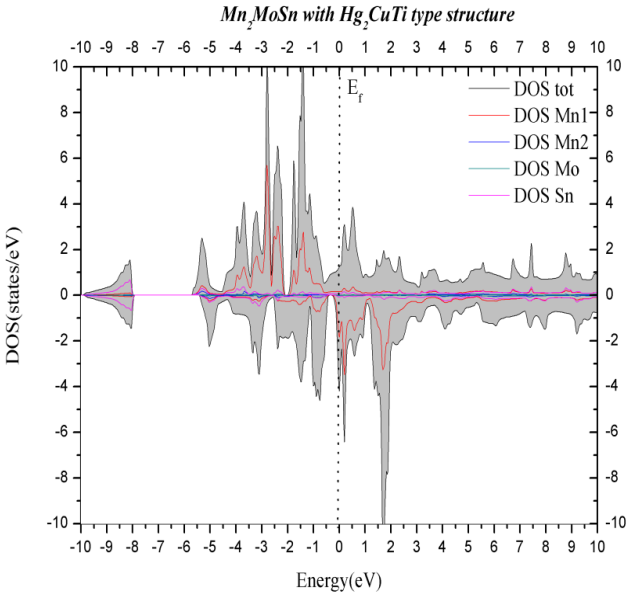
Mn2MoSn with Hg2CuTi type structure
DOS tot
DOS Mn1
DOS Mn2
DOS Mo
DOS Sn
Ef
DOS(states/eV)
Energy(eV)

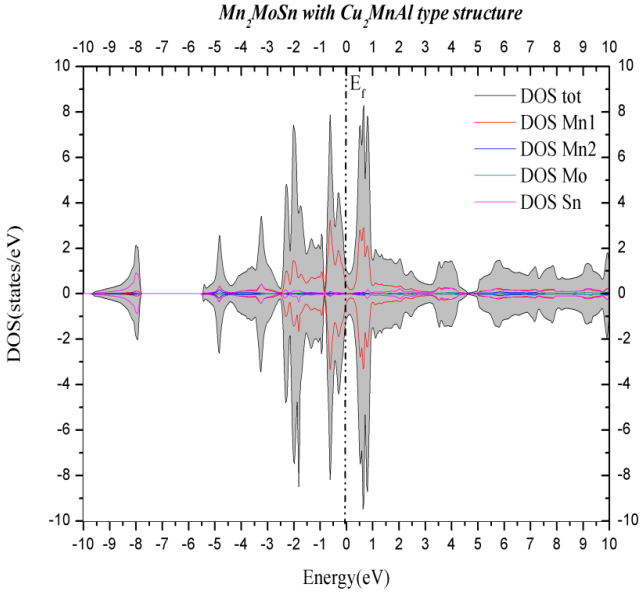
Mn2MoSn with Cu2MnAl type structure
DOS tot
DOS Mn1
DOS Mn2
DOS Mo
DOS Sn
Ef
DOS(states/eV)
Energy(eV)

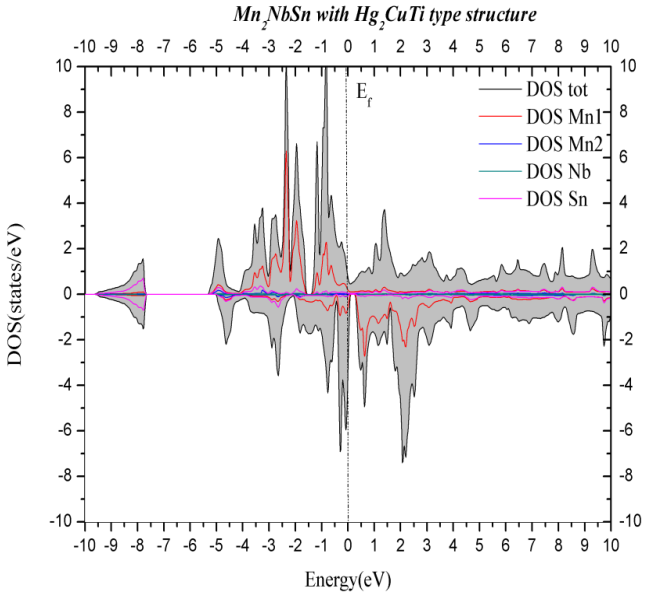
Mn2NbSn with Hg2CuTi type structure
DOS tot
DOS Mn1
DOS Mn2
DOS Nb
DOS Sn
Ef
DOS(states/eV)
Energy(eV)

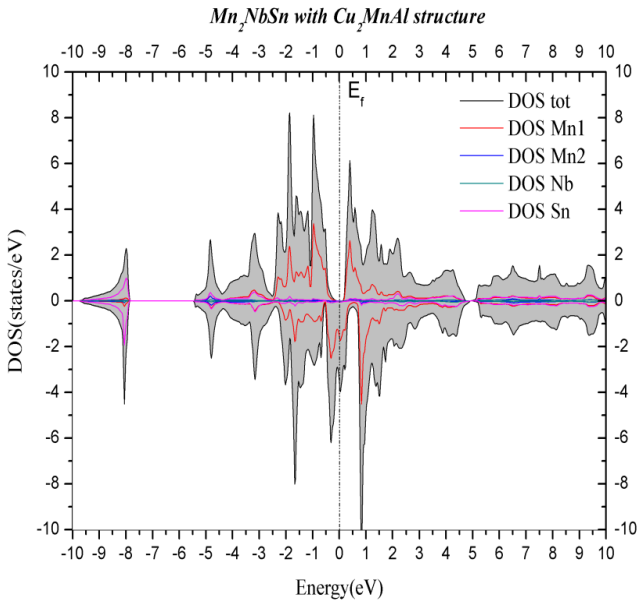
Mn2NbSn with Cu2MnAl structure
DOS tot
DOS Mn1
DOS Mn2
DOS Nb
DOS Sn
Ef
DOS(states/eV)
Energy(eV)

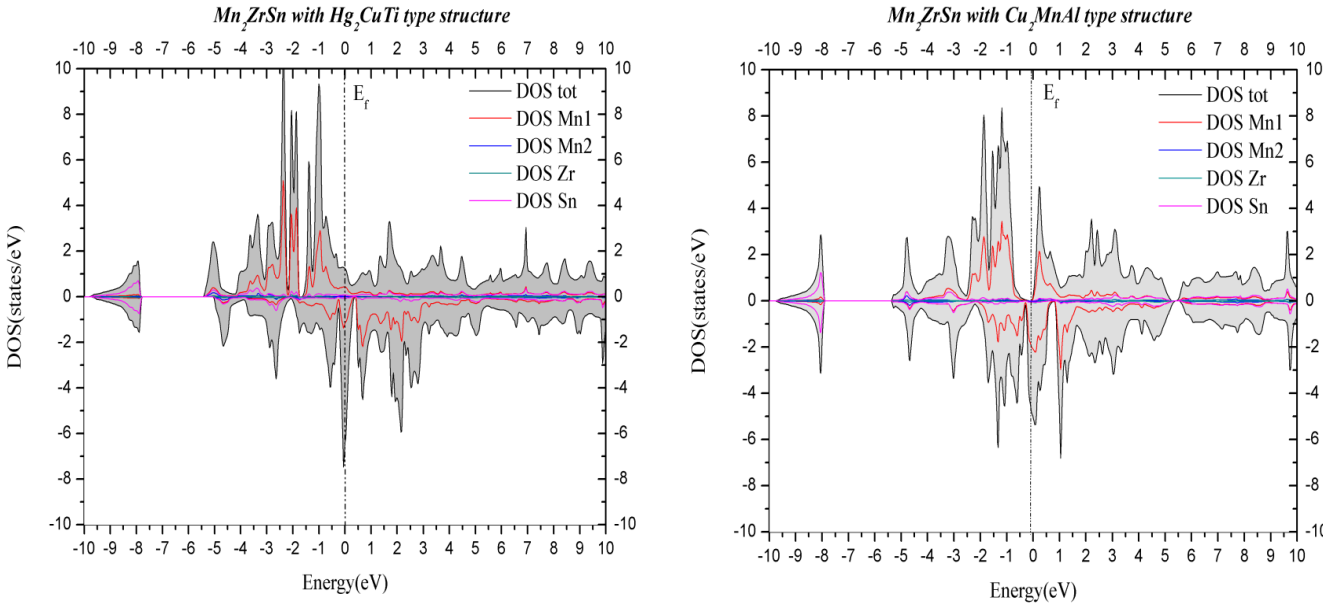

Figure.III.2: Total and partial density of states for Mn_2YSn (Y= Mo, Nb, Zr) for both structure Hg_2CuTi and Cu_2MnAl.

Figure.III.2 shows the estimated spin-polarized total densities of states (DOS) and atom-projected DOS of the Mn_2MoSn compound at their optimized equilibrium lattice constants for the Cu_2MnAl type structure and the Hg_2CuTi type structure.We can see from the Cu_2MnAl structure that the spin up and spin down are symmetric and that the band structures are the same, which explains why this alloy is not magnetic. Mn_2MoSn exhibits metallic properties for the Hg_2CuTi type structure at the junction of the band structure and Fermi level in spin up and spin dn.

In the Mn_2ZrSn, the majority spin channel (spin up) has a gap at the Fermi level, which gives it semiconductor behaviour, while the minority spin channel (spin dn) intersects the Fermi level and has a metallic character.As represented in **Figure.III.3**, the energy gap Eg, in the majority spin channel, the indirect band gaps at around F_f along the Γ-X symmetry is 0.42062 eV. This gap indicates that compounds are half-metallic and produce 100% spin polarisation at E_f.

In **Figure.III.2**, the calculated spin-polarized (DOS), total densities of states, and atom-projected DOS of the Mn_2NbSn Heusler alloy are shown at their optimized equilibrium lattice constants for the structures Hg_2CuTi and Cu_2MnAl.

The form of total DOS and atom projected DOS of the Mn_2NbSn Heusler alloys for two different structures are very different. For the Cu_2MnAl type structure there is a gap in majority spin (spin-up state), the Fermi level just falls within the gap in the spin-up band indicating

semiconductor behaviour and it crosses energy bands in minority spin state which makes Mn_2NbSn

Heusler alloys with Cu_2MnAl type structure a Half metallic (HM) magnetic compounds at the equilibrium lattice constant.

The Fermi level crosses energy bands for both majority and minority spin in the Hg_2CuTi-type structure, demonstrating metallic behaviour for this structure.

The valence band maximum and conduction band minimum are located at -0.06572 and 0.23442, respectively, in the majority spin band gap. This energy gap in spin-up stat leads to 100% spin polarisation at the Fermi level, resulting in half-metallic behaviour at the equilibrium state of the Cu_2MnAl type structure.

For Mn_2MoSn the band in both structure Cu_2MnAl and Hg_2CuTi, and for the spin up and the spin down, it is evident that the structure has metallic intersections at the Fermi level, indicating a strong metallic nature of the spin-up and spin-down electrons.

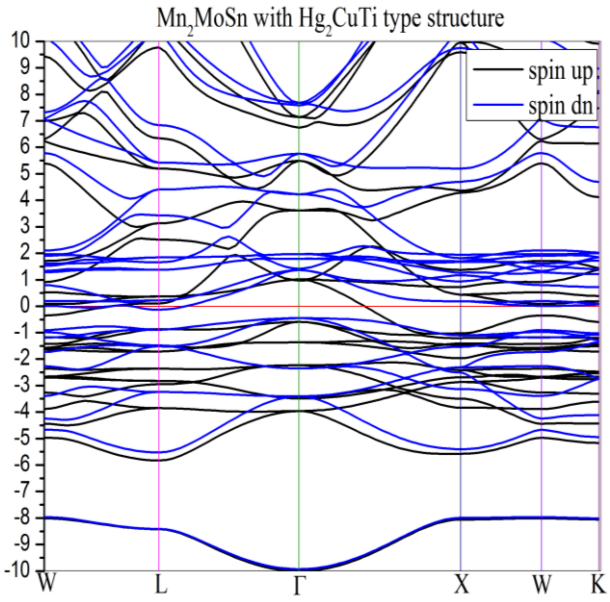
Mn2MoSn with Hg2CuTi type structure
spin up
spin dn
W
L
Γ
X
W
K

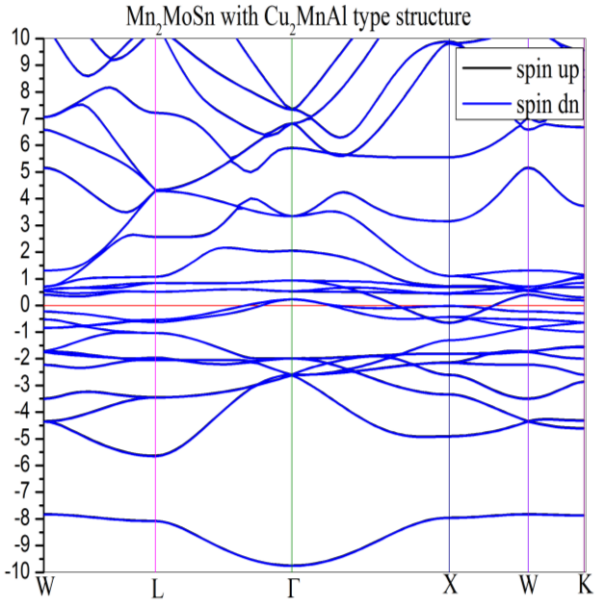
Mn2MoSn with Cu2MnAl type structure
spin up
spin dn
W
L
Γ
X
W
K

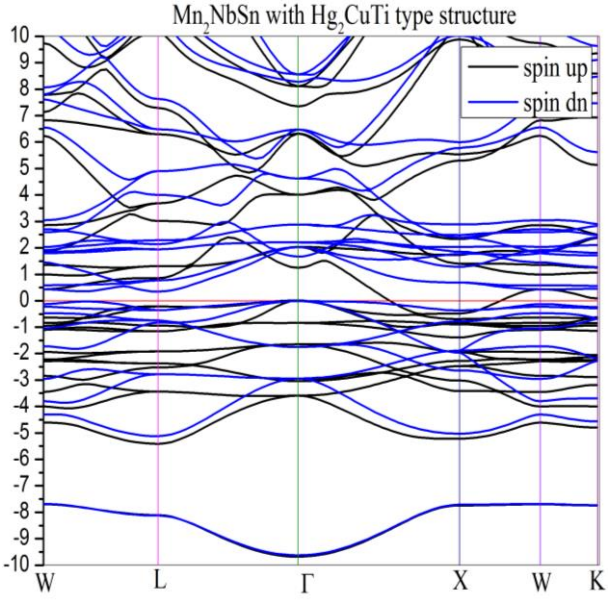
Mn2NbSn with Hg2CuTi type structure
spin up
spin dn
W
L
Γ
X
W
K

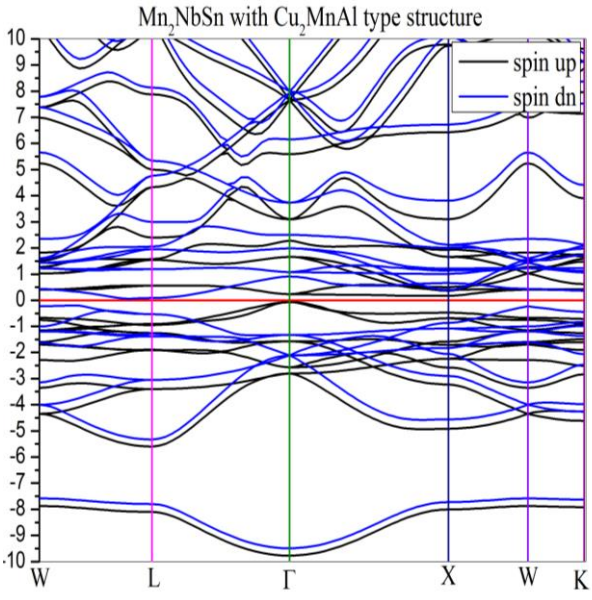
Mn2NbSn with Cu2MnAl type structure
spin up
spin dn
W
L
Γ
X
W
K

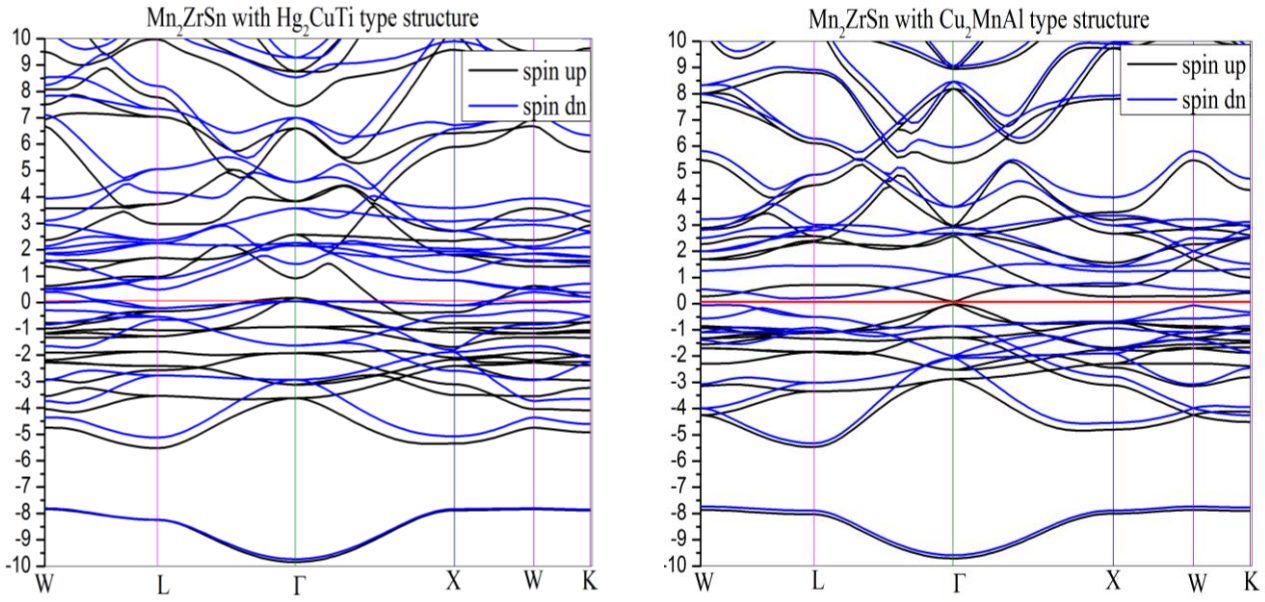

Figure.III.3: Band structure for Mn_2YSn (Y= Mo, Nb, Zr) for both structure Hg_2CuTi and Cu_2MnAl

III.3.1.3 Magnetic properties

By using GGA, the equilibrium lattice parameter, the total magnetic moment (MT) of Mn_2YSn (Y= Mo, Nb, Zr) full-Heusler alloys, the atomic moment of each ion, and the magnetic moment in interstitial zones are computed. The resulting results are shown in **Table.III.2**.

Table.III.2: The calculated magnetic moments values (µB) of the of Mn_2YSN (Y= Mo, Nb, Zr) Heusler compounds

		M_{Mn1}	M_{Mn2}	M_Y	M_{Sn}	$M_{interstitial}$	M_{total} (Mt)
Mn_2MoSn	Hg_2CuTi	3.473	2.770	- 0.815	- 0.029	-0.136	5.262
	Cu_2MnAl	0.004	0.000	- 0.010	- 0.003	-0.062	0.000
Mn_2NbSn	Hg_2CuTi	3.423	2.539	- 0.585	- 0.052	-0.153	5.170
	Cu_2MnAl	0.761	0.761	- 0.331	- 0.032	-0.165	1.000
Mn_2ZrSn	Hg_2CuTi	3.163	2.937	- 0.182	- 0.048	-0.061	5.931
	Cu_2MnAl	1.262	1.262	- 0.283	- 0.045	-0.190	2.000

With a Cu_2MnAl type structure, it can be seen that they are integral values, 1 μ_B for Mn_2NbSn and 2μ_B for Mn_2ZrSn and that the contributions to the total magnetic moments Mt are primarily attributed to the Mn atom. The magnetic moments of the Y (Y = Mo, Nb, and Zr) and Sn atoms can thus be disregarded.

The unequal magnetic moments on the Mn1 and Mn2 atoms, for Hg_2CuTi type structure, result from different atomic environments.

There is antiferromagnetic interaction with the Mn atom, as evidenced by the negative magnetic moments on the Y (Y= Mo, Nb, Zr), and Sn atoms.

With a Cu_2MnAl structure, Mn_2MoSn's total magnetic moment is equal to zero, confirming the compound's non-magnetic behaviour.

The magnetic properties can be directly connected to the electronic structure by the Slater-Pauling rule: $M_t = Z_t - 24$, the M_t is total spin magnetic moments in the unit cell, and Z_t is the total number of valence electrons. Z_t is equal to 24 for Mn_2MoSn ((7x2) + 6+4 =24), equal to 23 for Mn_2NbSn ((7x2) + 5+4 =23) and it equal to 22 for Mn_2ZrSn ((7x2) + 4+4 =22).

The minority band in full-Heusler alloys has 12 electrons per unit cell. The alloy is nonmagnetic as a result of the equal distribution of the 24 valence electrons in both spin directions.

If the alloy has more than 24 valence electrons, spin polarization will occur and the exchange

interaction will shift the majority states to lower energies.

The additional electrons will fill in only the majority of spins, which results in an integral spin moment **[16]**.

However, for Half metallic full-Heusler alloys with less than 24 electrons per unit cell, such as our case study, the energy gap is in the majority spin band and not in the minority spin band. A similar result was found by Anjami and al**[17]**.

III.3.2.Mn2YSn (Y=Ru,Rh,Pd)

III.3.2.1. Structural Properties

Compounds made by Heusler, X_2YZ, have a highly organised cubic structure **[18, 19]**.A primitive cell typically has four distinct positions: A (0, 0, 0), B (0.25, 0.25, 0.25), C (0.5, 0.5, 0.5), and D (0.75, 0.75, 0.75), in that order. The major group element Z is chosen to occupy the D position, while the transition metal elements X and Y occupy places A, B, and C.

Different X and Y occupancy locations will result in different structures, such as Cu_2MnAl ($L2_1$) or Hg_2CuTi (XA) structures (The crystal structure of Mn_2PdSn as the prototype is displayed in **Figure.III.4**).In the former, two X atoms are found in locations A and C, while Y and Z atoms occupy places B and D, respectively **[20, 21]**; in the latter, two X atoms are found in positions A and B, while Y and Z atoms are found in positions C and D, respectively**[20, 22]**.

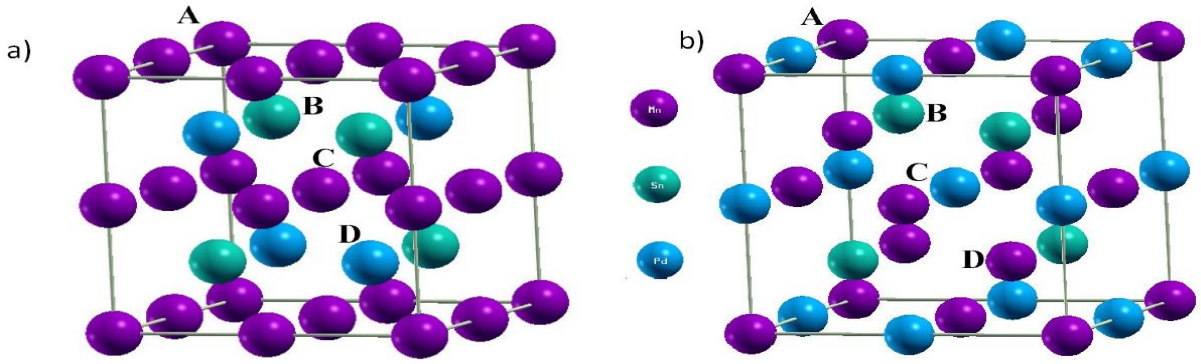

Figure.III.4: Crystal structure of Mn_2YSn (Y= Ru, Rh, Pd): a) Cu_2MnAl ($L2_1$) and b) Hg_2CuTi (Xa)**[30]**.

The competition between the Cu_2MnAl and Hg_2CuTi structures in the investigated Mn_2YSn (Y=Ru, Rh, and Pd) compounds was next studied.

Figure.III.5 shows the total energy of the investigated compounds at the ground state with various structures against the unit cell volume ($L2_1$ and XA).

It is evident that the total energy of Hg_2CuTi is lower than Cu_2MnAl for Mn_2YSn compounds (Y=Ru, Rh, and Pd), indicating that the most stable ordered structure for these systems is Hg_2CuTi (XA), which is in excellent accord with previous studies on these compounds**[23, 24]**. It is because, according to Luo and al**[12]**.

A and C sites are selected by elements with more electrons, whereas the B sites are favoured by those with fewer electrons. This is because the quantity of electrons in the X and Y atoms has a significant influence on their site selection.As the nuclear charge of X (Mn) atoms is lesser as compared to Y (Ru, Rh, and Pd), the Hg_2CuTi type structure of Mn_2YSn (Y=Ru, Rh, and Pd) is observed to be the stable, one similar to many other materials such as Mn_2RuSn**[25]**, Mn_2RuGe, Mn_2RuSn **[23]**, Mn_2RhAl, Mn_2YIn (Y=Ni, Pd and Pt) **[13, 26]**Mn_2NiSn**[27]**.

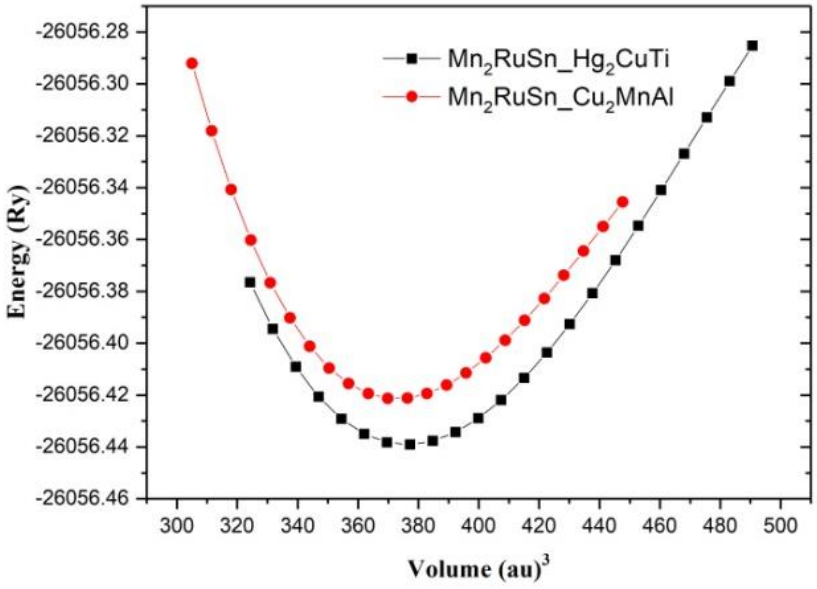
Mn2RuSn_Hg2CuTi
Mn2RuSn_Cu2MnAl
Energy (Ry)
Volume (au)3
-26056.28
-26056.30
-26056.32
-26056.34
-26056.36
-26056.38
-26056.40
-26056.42
-26056.44
-26056.46
300 320 340 360 380 400 420 440 460 480 500

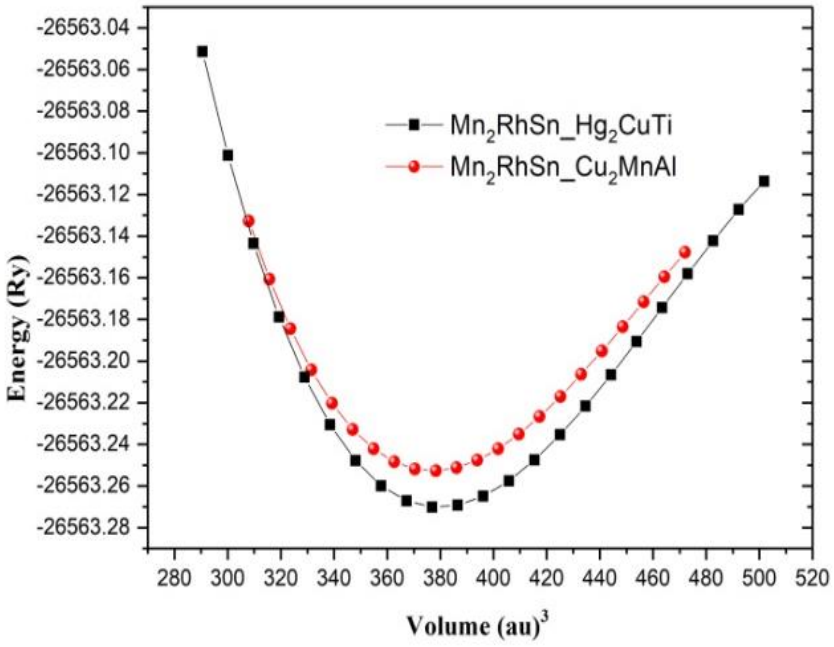
Mn2RhSn_Hg2CuTi
Mn2RhSn_Cu2MnAl
Energy (Ry)
Volume (au)3
-26563.04
-26563.06
-26563.08
-26563.10
-26563.12
-26563.14
-26563.16
-26563.18
-26563.20
-26563.22
-26563.24
-26563.26
-26563.28
280 300 320 340 360 380 400 420 440 460 480 500 520

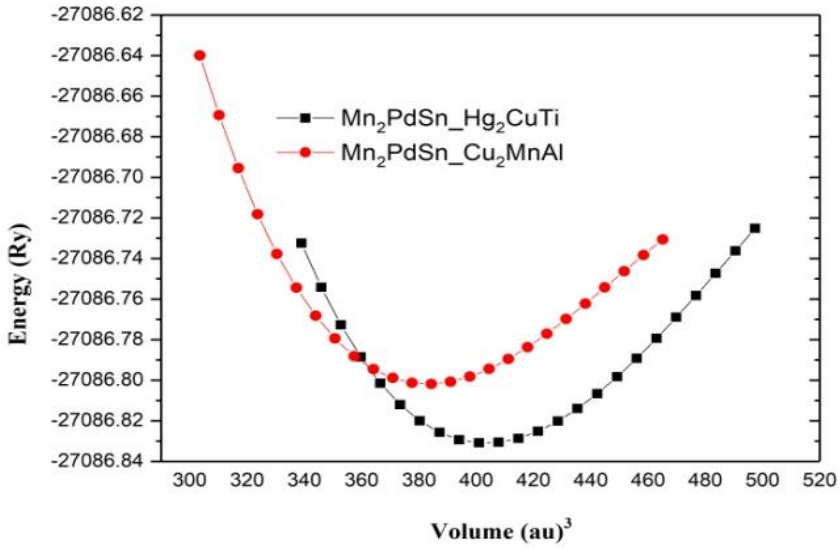

Figure.III.5: Total energy as a function of unit cell volume for the Mn_2YSn (Y=Ru, Rh, and Pd) compounds in the Cu_2MnAl and Hg_2CuTi-type structures using the GGA-PBE approximation.

.

In **Figure.III.6**, we further give a comparison of the total energy of the nom magnetic state (NM) and the two magnetic states [ferromagnetic (FM) and antiferromagnetic (AFM)] of the stable Hg_2CuTi-type structure of Mn_2YSn (Y=Ru, Rh, and Pd) compounds. As shown in **Figure.III.6**, the energy of Mn_2YSn (Y=Ru, Rh, and Pd) compounds in the FM states with using GGA+ U is lower highlighting that these compounds tend to exhibit the FM magnetic states.

to Calculating the ground state structural characteristics of Mn_2YSn (Y= Ru, Rh, and Pd) compounds, such as the equilibrium lattice constant a, the bulk modulus B, the bulk modulus pressure derivative B', and the energy E, Both the Cu_2MnAl ($L2_1$) and the Hg_2CuTi (XA) structures' calculated total energies plotted against unit cell volume is fitted by the Murnaghan equation of state **[28]**, which is represented by the (III.1) relation .

Where B, V, B', E_0, and V_0 note the bulk modulus, volume, first derivative of the bulk modulus, minimum energy at T=0 K, and the equilibrium volume, respectively.

Table.III.3lists the computed findings for the three compounds' lattice parameters, bulk moduli, derivatives of their pressures, and minimum energy (Ry).

The stability of these compounds in the Hg_2CuTi-type structure with the ferromagnetic state is confirmed by the higher negative energy.The obtained lattice constants are in fairly good agreement with previously reported theoretical investigations.As it can be seen from **Table.III.3**, the a_0 values of the series of Mn_2YSn increase in the following sequence: a_0 (Mn_2RuSn) < a_0 (Mn_2RhSn) < a_0 (Mn_2PdSn).This finding may be simply explained by the rise in the size of the X element in Mn_2YSn compounds since Mn and Sn atoms are identical in all three compounds. Meanwhile, the B values decrease in the following sequence: B (Mn_2RuSn) >B (Mn_2RhSn) >B (Mn_2PdSn) >B, i.e.according to the well-known connection between B and the lattice constants: $B \propto V_0^{-1}$ whereV_0 is the unit cell volume, in reverse order to "a." This straightforward relationship between "a" larger lattice constant and a smaller bulk modulus.

Table.III.3:Computed results of lattice constant a (Å), bulk modulus B (GPa), its derivative pressure, the minimum energy (Ry) and the formation energy E_f (Ry) for Mn_2RuSn, Mn_2RhSn and Mn_2PdSn Heusler compounds

		a(Å)	B(GPa)	B´	E(Ry)	E_f(Ry)
Mn_2RuSn	Hg_2CuTi					
	AFM	6.16	130.33	6.32	-26056. 526276	
	FM	6.30	112.71	4.68	-26056. 576045	
		6.21 [25]				
		6.25 [23]				
	GGA+U	6.09	206.20	4.48	-26057. 468437	-1.24
	Cu_2MnAl					
	F M	6.30	143.66	4.87	-26056. 558177	
		6.27 [23]				
	GGA+U	6.56	89.72	4.79	-26057. 432544	-1.21
Mn_2RhSn	Hg_2CuTi					
	AFM	6.28	126.15	5.24	-26563. 440450	
	FM	6.32	131,65	5,26	-26563. 461340	
	GGA+U	6.41	127.55	4.04	-26566.954625	-1.10
	Cu_2MnAl					
	F M	6.35	118.87	5.14	-26563. 422655	
	GGA+U	6.56	110.90	3.79	-26566. 324149	-1.05
Mn_2PdSn	Hg_2CuTi					
	AFM	6.38	97.92	5.03	-27086. 89064	
	FM	6.37	138.66	4.84	-27086. 974857	
		6.35 [13]				
	GGA+U	6.53	95.08	4.35	-27088. 503522	-0. 97
	Cu_2MnAl					
	F M	6.43	96.15	4.86	-27086. 960158	
	GGA+U	6.10	179.29	5.49	-27088. 428592	-0. 96

We investigate the phase stability of Mn_2YSn (Y=Ru, Rh, and Pd) based on the energy of formation (E_f). This can also be used to determine whether it is possible to make the investigated alloys in a laboratory.The total sum of the energy of the constituent atoms of the various elements involved in compound production is compared to the total energies of the Mn_2YSn (Y=Ru, Rh, and Pd) Heusler compounds.The energy of formation of Mn_2YSn (Y= Ru, Rh, and Pd) materials are calculated using the (III.2) relation.

where $E^{total}_{Mn_2YSn}$ is the equilibrium total energy for both types of crystal structures (Hg_2CuTi and Cu_2MnAl), E^{bulk}_{Mn},E^{bulk}_{Y}, E^{bulk}_{Sn} correspond to total energy per atom respectively for Mn, Sn and Y (Y= Ru, Rh, and Pd) element in their bulk form. These alloys can be made experimentally since the values of the formation energy for the Mn_2YSn (Y=Ru, Rh, and Pd) compounds mentioned in Table 1 are found to be negative, showing their chemical stability.

When compared to Cu_2MnAl type structures, the computed formation energy E_f values for Hg_2CuTi type structures are found to be more negative, suggesting that Hg_2CuTi type structures are more stable.

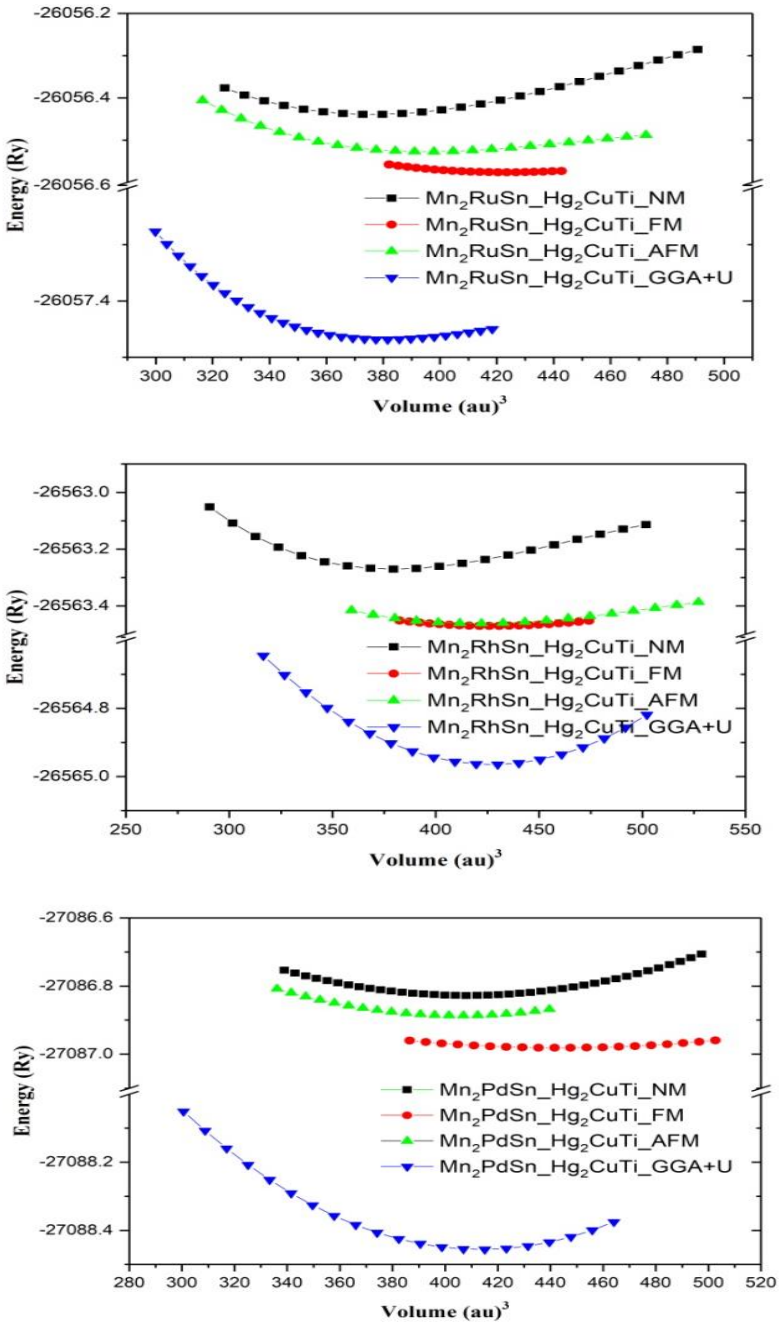

Figure.III.6: Total energy as a function of unit cell volume for the Mn_2YSn (Y=Ru, Rh, and Pd) compounds in the Hg_2CuTi-type structure for AFM, FM and NM states, using the GGA+U.

III.3.2.2. Electronic properties

Using the estimated values of the lattice parameters, partial and total densities of states (PDOS and TDOS) for both Hg_2CuTi and Cu_2MnAl-type crystal structures are calculated in order to identify the electronic characteristics of the complete Heusler (Mn_2RuSn, Mn_2RhSn, and Mn_2PdSn).The Spin-polarized band structures and the densities of states (DOS) of the considered compounds for spin-up and spin-down states are displayed in **Figure.III.7 and Figure.III.8**, respectively.

Spin-up and spin-down DOS are represented by positive and negative values, respectively. It is clear from these figures that these compounds have a metallic character. The metallic character of these compounds may be clearly shown by paying close attention to small charts near the Fermi level. It should be highlighted that 3d transition metal (Mn) atoms have a significant role in the band structure in the energy range from -6 to 6 eV as well as in the Fermi level for the Heusler compounds Mn_2RuSn, Mn_2RhSn, and Mn_2PdSn.

On the other hand, a technique for determining the majority and minority close to the Fermi energy level is known as spin polarisation or SP. The SP relation for Heusler alloys is as follows (III.3).

where$\rho \uparrow (Ef) \rho \downarrow (Ef)$ represent, respectively,the density of the majority and minority states at the Fermi level (E_F).If the electron spin polarisation (SP) value is 100%, the Heusler compounds or alloys are considered to be really half-metallic. This is possible when the DOS at E_F for one of the channels is zero and non-zero for the other channel.

Ling Yang et al**[25]**provide the computed findings for TDOS for Mn2RuSn with varied levels of atomic disorder.Moreover, they discovered a tiny number of minority states in the gap and a low spin polarisation ratio, indicating that the Mn2RuSn is still not an ideal half-metal at equilibrium lattice, according to Ling Yang et al **[25]**.

however, suggests that a little lattice contraction can stabilise half-metallicity in Mn2RuSn according to Ref **[23]**.

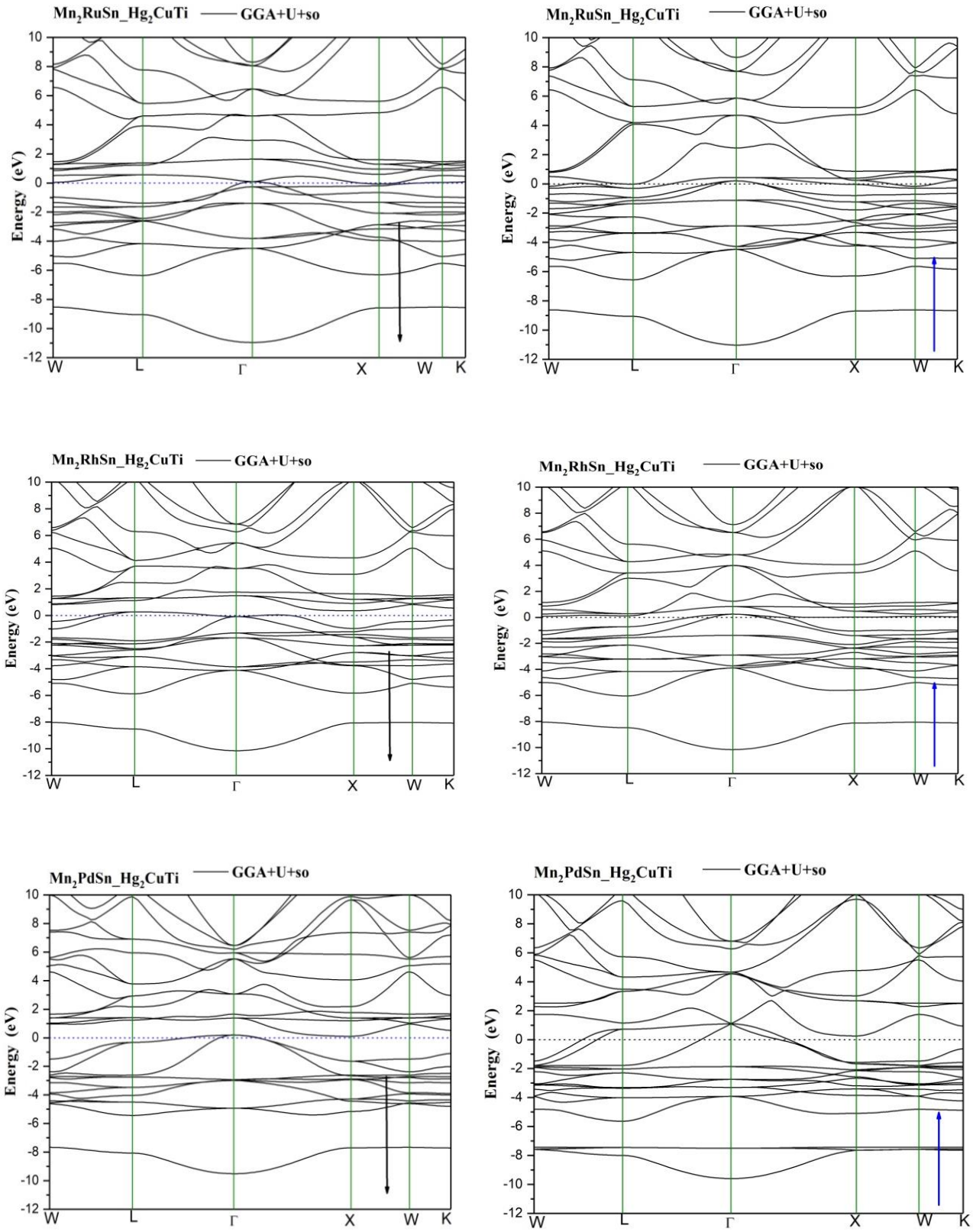

Figure.III.7: The Spin polarized band structure of of Mn_2YSn (Y=Ru, Rh, and Pd) alloys

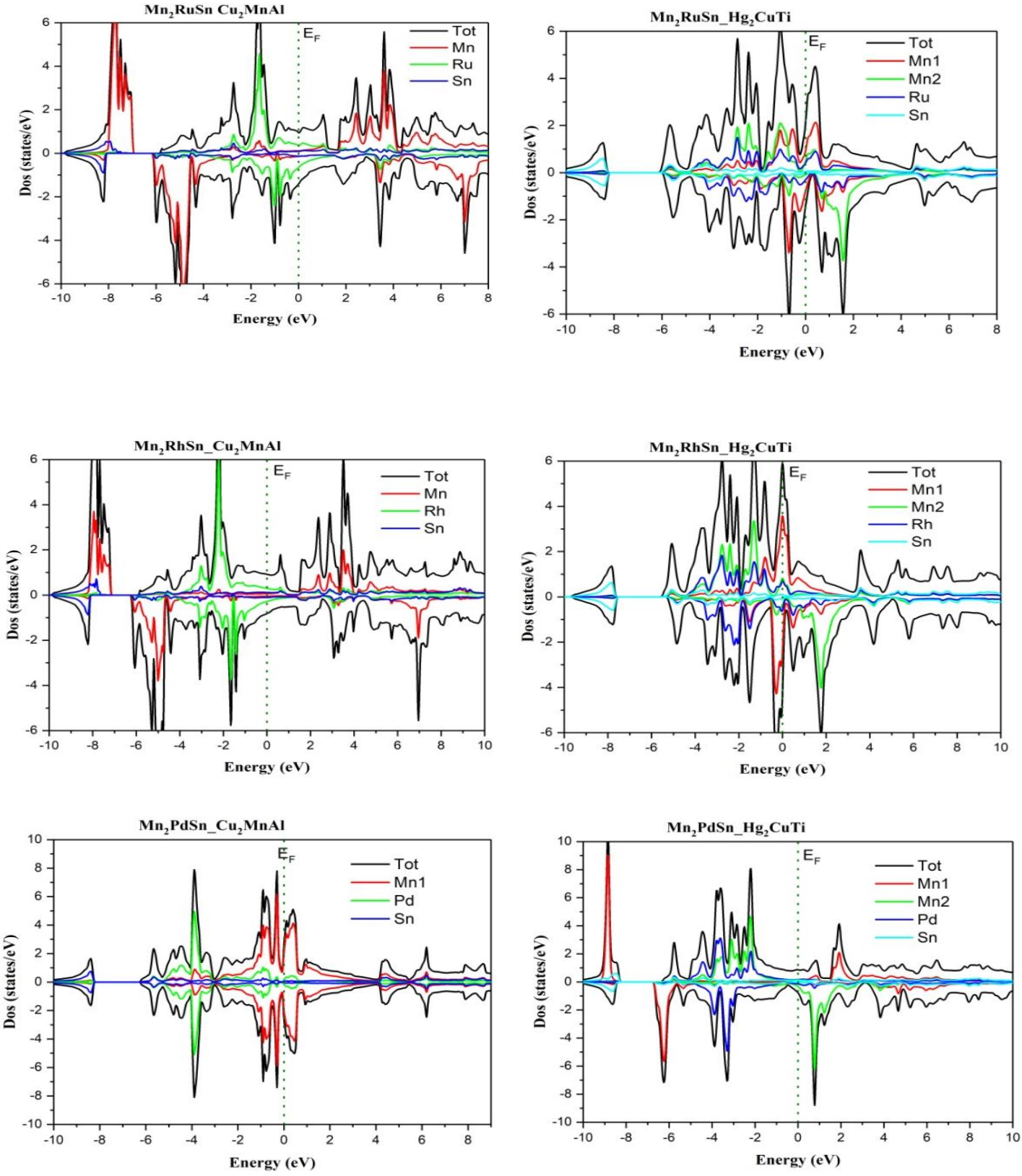

Figure.III.8: Computed results of SP-TDOS and SP-PDOS for Mn_2YSn (Y=Ru, Rh, and Pd) with both Cu_2MnAl and Hg_2CuTi types structures

III.3.2.3. Magnetic properties

The total and partial magnetic moment for both (Hg_2CuTi and Cu_2MnAl) configurations of Mn_2RuSn, Mn_2RhSn, and Mn_2PdSn were measured in order to understand the magnetic behaviour of the compounds under consideration. The estimated equilibrium lattice constants at the level of the PBE-GGA and GGA+U methods are used to calculate Heusler compounds, and the results are listed in **Table.III.4**.

Table.III.4:Computed results of atomic resolved, total and interstitial magnetic moment (in μB) per unit cell of Mn_2YSn(Y=Ru,Rh,Pd)

Compound	Phase	M_{tot}	M_{Mn1}	M_{Mn2}	M_y	M_{Sn}	M_{int}
Mn_2RuSn	Hg_2CuTi (FM)						
	GGA	7.14564	3.41643	3.41949	0.27656	-0.06333	0.0465
	GGA+U	2.33380	-0.18683	2.42697	0.04448	-0.01399	0.06318
Mn_2RhSn	Hg_2CuTi (FM)						
	GGA	7.41157	3.40885	3.58783	0.41643	-0.07263	0.07108
	GGA+U	3.47694	-0.27589	3.31491	0.27987	-0.02762	0.18568
Mn_2PdSn	Hg_2CuTi (FM)						
	GGA	6.33069	2.71351	3.41314	0.20341	-0.06890	0.06952
	GGA+U	3.54842	-0.66074	3.60234	0.20534	0.0629	0.33848

The magnetic behavior of the Heusler compounds Mn_2YSn (Y=Ru, Rh, and Pd) is noticed by the non-symmetrical density of states as in **Figure.III.5**.Moreover, it can be observed from the tabular data that none of the three compounds' total magnetic moments can be obtained in integral form, further confirming that these alloys are not half metallic.Furthermore, using both GGA and GGA+U, the calculated magnetic moments of the compounds under consideration for the ferromagnetic states in the stable Hg_2CuTi-type structure reveal that Mn atoms a majority contribute to the total magnetic moment, with Y atoms making a minor contribution.The Sn atoms' contribution is essentially ignored.

III.3.2.4. Pressure dependence structural electronic and magnetic properties Mn2YSn(Y=Ru,Rh,Pd)

Since the properties of solids are closely connected to the interatomic distances, the pressure effect on materials is an important field.When pressure is applied, the atoms' arrangements change, changing the materials' physical characteristics[29].

The hydrostatic pressure is described by following Murnaghan equation of states:

$$P = \frac{B_0}{B'_0}\left[\left(\frac{V_0}{V}\right)^{B'_0} - 1\right] \qquad \text{(III.4)}$$

where P, V_0 and V denote pressure, volume at pressure zero and certain pressure respectively. B_0 and B_0' bulk modulus and its pressure derivative respectively.

The lattice constant results are evaluated as a function of pressure by the following relation:

$$a(P) = a_0\left[1 + P\left(\frac{B'_0}{B}\right)\right]^{-\frac{1}{3B'_0}} \qquad \text{(III.5)}$$

Where a_0 is the equilibrium lattice parameter of the unit cell

The stability of Mn_2YSn Heusler compounds for both Hg_2CuTi and Cu_2MnAl-type structures under hydrostatic pressure is further investigated in the sections that follow by calculating the magnetic moment.

The effect of pressure on the lattice constant values for Mn2YSn (Y= Ru, Rh, and Pd) in the pressure range of 10 GPa to 50 GPa can be shown in Fig. 6. (The findings are shown in Table 1 for P=0 GPa.

The effect of pressure on the lattice constant values*a* (Å) for Mn_2YSn (Y= Ru, Rh, and Pd) in the pressure range of 10 GPa to 50 GPa can be shown in **Figure.III.9**. (The findings are shown in **Table.III.3** for P=0 GPa.).

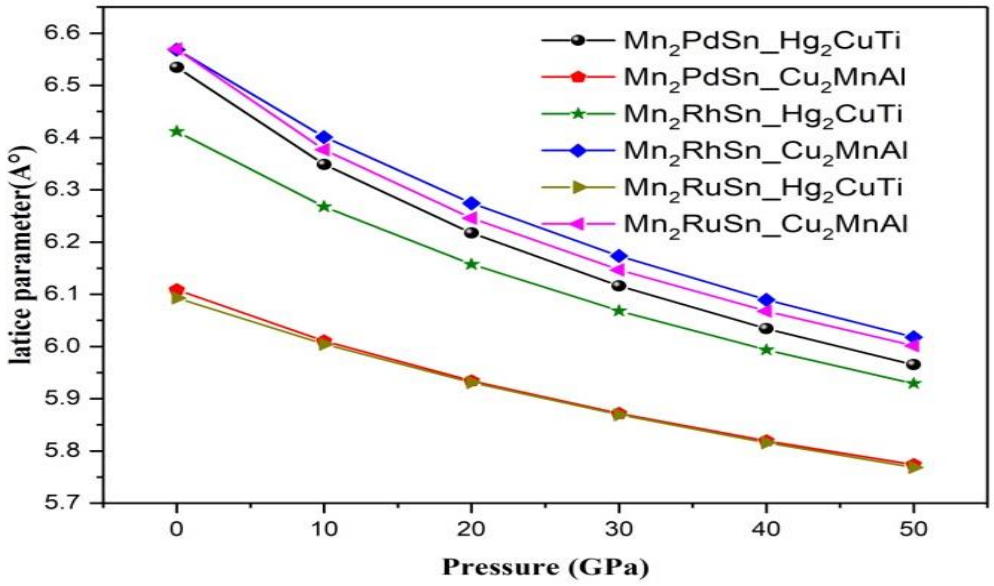

Figure.III.9: Lattice parameter as a function of pressure

The lattice parameter values decrease as pressure increases from 10 GPa to 50 GPa, as seen in **Figure.III.9**.

To more understand the nature of the pressure effect, the evaluated PDOS and TDOS of Mn_2RuSn and Mn_2RhSn with Hg_2CuTi-type structures at pressures of 10 GPa are presented in **Figure.III.10**.where the Fermi level is positioned at 0 eV.

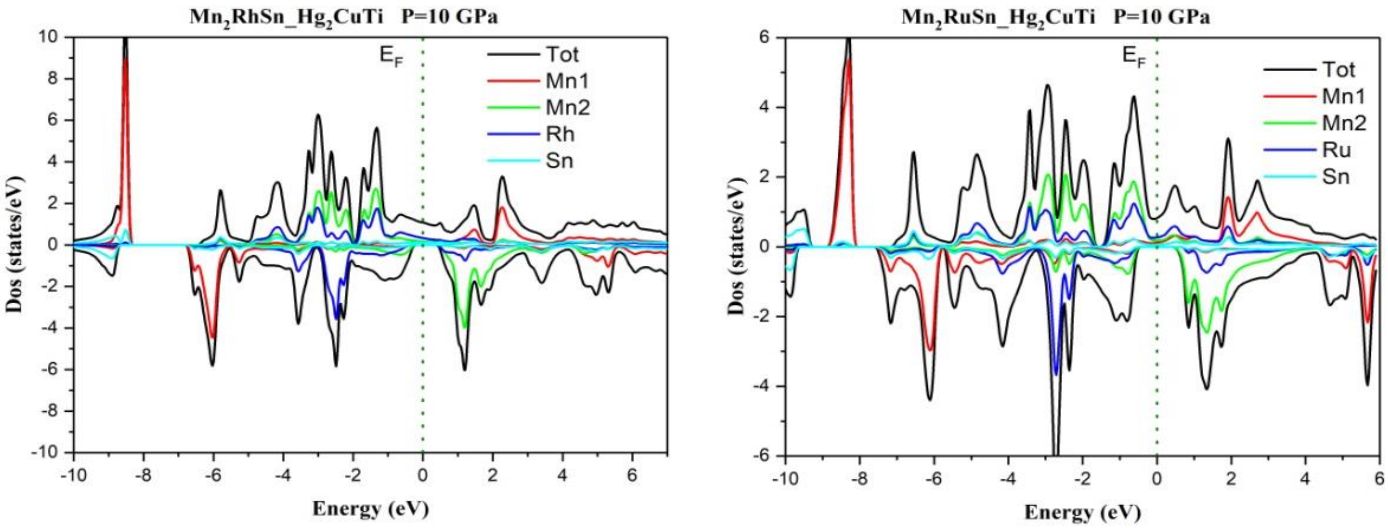

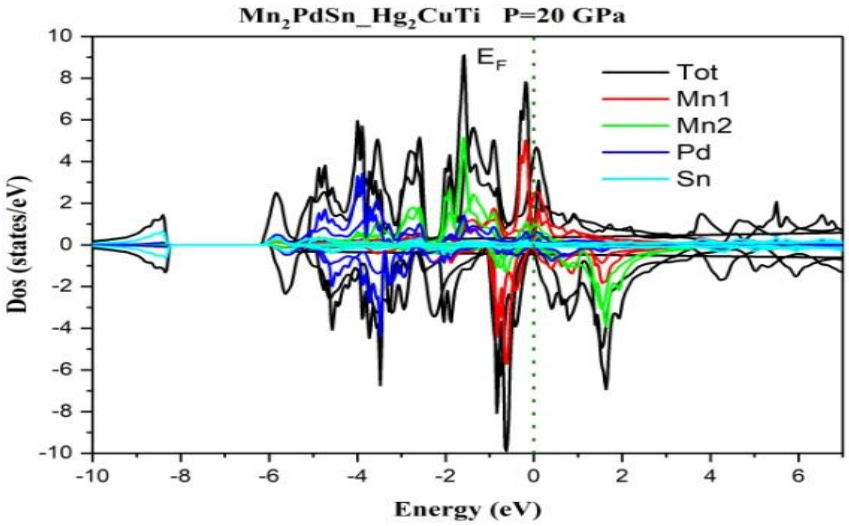

Figure.III.10: TDOS and PDOS under the pressure of 10GPa for Mn_2RuSn and Mn_2RhSn and under pressure of 20 GPA for Mn_2PdSn with Hg_2CuTi type structure.

For the Hg_2CuTi type structure of Mn_2RuSn Heusler compound,Electronic density of states provides a better understanding of the pressure effect. **Figure.III.10** shows the PDOS and TDOS at transition pressure (10 GPa) from metallic to half-metallic.The TDOS shows that although the majority spin states represent metallic character, the minority spin states show a band gap between the valence and conduction bands.Mn_2RuSn Heusler alloy behaviour for Hg_2CuTi structure supports that metallic nature for majority spin states and semiconductor nature for minority spin states, confirming the half metallic character of the title alloy at a pressure of 10GPa.

For Mn_2RhSn Heusler compound in Hg_2CuTi-type structure , TDOS clearly demonstrates that the majority spin states support the metallic, While the minority states indicate out a gap for Hg_2CuTi at 10GPa, which suggests that the Mn_2RhSn Heusler compound becomes a half-metallic under applied pressure.At the pressure of 20 GPa, the Mn_2PdSn compound becomes half metal. The overlapping of Mn 3d and Y 4d (Y=Ru,Rh,Pd) states in the building of electronic energy bands is the most notable aspect of the partial DOS, implying hybridization between the Mn and Y (Y=Ru,Rh,Pd) states during compound synthesis.

On the other hand, the obtained results of the total spin magnetic moments under pressure are tabulated in **Table.III.5**. For all the three compounds (Mn_2RuSn, Mn_2RhSn, and Mn_2PdSn), the impact of the

pressure is remarkable. **Table.III.5** shows a slight decrease in the values of the magnetic moment under pressure effect.

Table.III.5 : Total magnetic moment as a function of the pressure of Mn2YSn (Y= Ru, Rh, and Pd) compounds in Hg2CuTi-type structure.

	P(GPa)	Total Magnetic Moment (μ_B) GGA+U
Mn_2RuSn	**10**	**2.001**
	20	**1.985**
	30	**1.972**
	40	**1.97**
	50	**1.97**
Mn_2RhSn	**10**	**2.999**
	20	**2.98**
	30	**2.97**
	40	**2.965**
	50	**2.952**
Mn_2PdSn	**10**	**3.18**
	20	**3.06**
	30	**2.89**
	40	**2.85**
	50	**2.852**

For the Hg_2CuTi type structure of Mn_2RuSn Heusler compound, the total magnetic moment is found to be decreased by applying pressure and has an integer value equal to 2.001 μ_B of the magnetic moment at a pressure of 10 GPa, meaning that the material becomes half metal compound. For Mn_2RhSn Heusler compound in Hg_2CuTi-type structure the magnetic moment decrease as a function of the pressure and pass through an integral value of about 2.99$\mu_B$under the pressure of 10GPa for Hg_2CuTi type structure. At this value of pressure the compound changes it character. This result is also verified from DOS plots.

References

1. ZENASNI, H., Etude théorique des propriétés magnétiques, électroniques et structurales des alliages Heusler, 2013.

2. Lejaeghere, K., et al., Reproducibility in density functional theory calculations of solids. Science, 2016. **351**(6280): p. aad3000.

3. Perdew, J.P., K. Burke, and M. Ernzerhof, Generalized gradient approximation made simple. Physical review letters, 1996. **77**(18): p. 3865.

4. Anisimov, V.I., et al., Density-functional theory and NiO photoemission spectra. Physical Review B, 1993. **48**(23): p. 16929.

5. Dahani, A., et al., DFT+ U Analysis of Structural, Electronic, and Magnetic Properties of Mn–As–Sb Ternary Systems. Journal of Superconductivity and Novel Magnetism, 2014. **27**: p. 2263-2275.

6. Krishnaveni, S. and M. Sundareswari, Band gap engineering in ruthenium-based Heusler alloys for thermoelectric applications. International Journal of Energy Research, 2018. **42**(2): p. 764-775.

7. Benkhelifa, F., A. Lekhal, and S. Méçabih, GGA and GGA+ U Description of Structural, Magnetic, and Elastic Properties of Rh_2MnZ (Z= Ge, Sn, and Pb). Journal of superconductivity and novel magnetism, 2013. **26**: p. 2573-2583.

8. Hamri, B., et al., Electronic structure and mechanical properties of X_2MnSn (X= Cu, Ni, Pd) under hydrostatic pressure: GGA+ U calculations. Computational Condensed Matter, 2015. **3**: p. 14-20.

9. Wei, X.-P., et al., Electronic structure and magnetism in full-Heusler compound Mn2ZnGe. Journal of magnetism and magnetic materials, 2011. **323**(12): p. 1606-1610.

10. Dahmane, F., et al., First-principle study of the electronic, magnetic and structural characteristics of the $Mn_2CoAs_{1-x}Al_x$ (x= 0, 0.25, 0.50, 0.75) Heusler alloys. Chinese Journal of Physics, 2018. **56**(4): p. 1764-1771.

11. Hong, F., et al., Pressure-induced isostructural transition in a distorted perovskite via octahedron reconfiguration. Applied Physics Letters, 2016. **109**(24): p. 241904.

12. Luo, H., et al., Prediction of half-metallic properties for the Heusler alloys Mn_2CrZ (Z= Al, Ga, Si, Ge, Sb): A first-principles study. Journal of Magnetism and Magnetic Materials, 2008. **320**(3-4): p. 421-428.

13. Kervan, N., et al., Half-metallic ferrimagnetism in the Mn_2NbAl full-Heusler compound: a first-principles study. Journal of Superconductivity and Novel Magnetism, 2016. **29**: p. 187-192.

14. Yu, S., et al., Large magnetoresistance in single-crystalline $Ni_{50}Mn_{50-x}In_x$ alloys (x= 14–16) upon martensitic transformation. Applied Physics Letters, 2006. **89**(16): p. 162503.

15. Rauf, S., et al., The first principle study of magnetic properties of Mn_2WSn, Fe_2YSn (Y= Ti, V), Co_2YSn (Y= Ti, Zr, Hf, V, Mn) and Ni_2YSn (Y= Ti, Zr, Hf, V, Mn) heusler alloys. Journal of Physics and Chemistry of Solids, 2015. **76**: p. 153-169.

16. Luo, H., et al., Half-metallic properties for the Mn_2Fe Z (Z= Al, Ga, Si, Ge, Sb) Heusler alloys: a first-principles study. Journal of Applied Physics, 2008. **103**(8): p. 083908.

17. Anjami, A., et al., Ab-initio study of mechanical, half-metallic and optical properties of Mn_2ZrX (X= Ge, Si) compounds. Results in physics, 2017. **7**: p. 3522-3529.

18. Han, Y., et al., 171 Scandium-based full Heusler compounds: A comprehensive study of competition between XA and $L2_1$ atomic ordering. Results in Physics, 2019. **12**: p. 435-446.

19. Wu, M., et al., Phase transition and electronic structures of all-d-metal Heusler-type X_2MnTi compounds (X= Pd, Pt, Ag, Au, Cu, and Ni). Frontiers in Chemistry, 2020. **8**: p. 546947.

20. Amari, D., et al., A comparative study between Hg_2CuTi and Cu_2MnAl type structures for Zr_2CoZ (Z= Al, Ga, In) Heusler alloys. Chinese Journal of Physics, 2019. **60**: p. 450-461.

21. Zenasni, H., H. Faraoun, and C. Esling, First-principle prediction of half-metallic ferrimagnetism in Mn-based full-Heusler alloys with highly ordered structure. Journal of magnetism and magnetic materials, 2013. **333**: p. 162-168.

22. Song, T., et al., The effect of pressure on the structural, electronic, magnetic, and thermodynamic properties of the Mn_2RuGe inverse Heusler alloy. Journal of Magnetism and Magnetic Materials, 2017. **428**: p. 287-292.

23. Chen, J., et al., Site preference and electronic structure of Mn_2RuSn: a theoretical study. Journal of magnetism and magnetic materials, 2014. **365**: p. 132-137.

24. Feng, L., et al., Principles, Possible Martensitic Transformation in Heusler Alloy Mn_2PdSn from First Principle. J. Magn. Magn. Mater., 2016. **419**: p. 543.

25. Yang, L., et al., Investigation of the site preference in Mn_2RuSn using KKR-CPA-LDA calculation. Journal of Magnetism and Magnetic Materials, 2015. **382**: p. 247-251.

26. Luo, H., et al., Martensitic transformation in Heusler alloys Mn_2YIn (Y= Ni, Pd and Pt): Theoretical and experimental investigation. Journal of Magnetism and Magnetic Materials, 2015. **395**: p. 190-195.

27. Duan, Y.-N., et al., Possible martensitic transformation and ferrimagnetic properties in Heusler alloy Mn_2NiSn. Journal of Magnetism and Magnetic Materials, 2015. **386**: p. 102-106.

28. Murnaghan, F.D., The compressibility of media under extreme pressures. Proceedings of the National Academy of Sciences, 1944. **30**(9): p. 244-247.

29. Ackland, G.J., High-pressure phases of group IV and III-V semiconductors. Reports on Progress in Physics, 2001. **64**(4): p. 483.

30. Kokalj, A., XCrySDen—a new program for displaying crystalline structures and electron densities. Journal of Molecular Graphics and Modelling, 1999. **17**(3-4): p. 176-179.

GENERAL CONCLUSION

Conclusion

On Mn_2YSn (Y= Mo, Nb, and Zr), first-principles FP-LAPW calculations were done. We conclude that the Cu_2MnAl type structure is more stable than the Hg_2CuTi type based on the findings. It is concluded that spin polarized band structure and densities of states of the Mn_2ZrSn and Mn_2NbSn present 100% spin polarization around Fermi level and are half metallic ferromagnets.

With spin up and spin down symmetric (DOS), identical band structures (up and dn), and a magnetic moment of 0 μβ, the Mn_2MoSn combination with Cu_2MnAl exhibits nonmagnetic behaviour.

The structural, electronic, and magnetic characteristics of the Heusler compounds Mn_2YSn (Y=Ru, Rh, and Pd) in both types of structures (Hg_2CuTi and Cu_2MnAl) are investigated using first-principles DFT-based methodology. The calculations were performed at zero pressure and under pressure effect. To do so, the PBE-GGA, GGA+U approach of exchange-correlation energy/potential functional were used. In addition to GGA+U, the spin-orbit coopling (SO) is also used for the calculation of electronic and magnetic properties. Our computed results were found to be in good agreement with the available experimental measurements and theoretical data. The obtained results showed that all the investigated materials behave as metal at zero pressure.

Half metallicity was seen for Mn_2RuSn and Mn_2RhSn in a Hg_2CuTi-type structure, however at a higher pressure of 10GPa. At 20 GPa, half metallicity for Mn_2PdSn's Hg_2CuTi-type structure was also noted.

Condensed Matter Physics, 2021, Vol. 24, No 1, 13703: 1–9
DOI: 10.5488/CMP.24.13703
http://www.icmp.lviv.ua/journal

CONDENSED MATTER PHYSICS

Prediction of electronic and half metallic properties of Mn_2YSn (Y = Mo, Nb, Zr) Heusler alloys

S. Zeffane[1,2], M. Sayah[1,2], F. Dahmane[1,3], M. Mokhtari[1,2], L. Zekri[2], R. Khenata[3], N. Zekri[2]

[1] Département de SM, Institut des Sciences et des Technologies, Centre Universitaire de Tissemsilt, 38000 Tissemsilt, Algérie

[2] Université des Sciences et de la Technologie d'Oran Mohamed Boudiaf, USTO-MB, LEPM, BP 1505, El M' Naouar, 31000 Oran, Algeria

[3] Laboratoire de Physique Quantique et de Modélisation Mathématique (LPQ3M), Département de Technologie, Université de Mascara, 29000 Mascara, Algérie

Received April 23, 2020, in final form September 5, 2020

We investigate the structural, electronic and magnetic properties of the full Heusler compounds Mn_2YSn (Y = Mo, Nb, Zr) by first- principles density functional theory using the generalized gradient approximation. It is found that the calculated lattice constants are in good agreement with the theoretical values. We observe that the Cu_2MnAl-type structure is more stable than the Hg_2CuTi type. The calculated total magnetic moments of Mn_2NbSn and Mn_2ZrSn are 1 μ_B and 2 μ_B at the equilibrium lattice constant of 6.18 Å and 6.31 Å, respectively, for the Cu_2MnAl-type structure. Mn_2MoSn have a metallic character in both Hg_2CuTi and Cu_2MnAl type structures. The total spin magnetic moment obeys the Slater-Pauling rule. Half-metal exhibits 100% spin polarization at the Fermi level. Thus, these alloys are promising magnetic candidates in spintronic devices

Key words: *Heusler, half metallic, magnetic moment, spintronic*

1. Introduction

To ameliorate the performance of spintronic devices is indispensable for the advance of modern technology [1]. Half-metallic ferromagnets (HMFs) are interesting spin-polarized materials and, thus these are ideal for the application in spintronic devices [2]. Half-metal magnets have got broad attentions. They are utilized in the manufacturing of electronic gadgets because of their wide band gap in minority spins, magnetic random access memory effect, high data processing rate and low consumption of electric power and gradually increasing density [3, 4]

Numerous half-metallic ferromagnets have been predicted and verified experimentally since NiMnSn was predicted in1983 by De Groot et al. [5]. Ferromagnetic materials display diverse electronic properties in the spin up and down bands, with metallic properties in one spin band and insulator or semiconductor properties in another, thus leading to 100% spin polarization at the Fermi level [6] [7] [8]. Heusler alloys are a class of inter-metallic compounds, simple structures and unique properties [9]. In 1903, a German scientist Heusler found that the atoms in the alloy Cu_2MnAl were non-magnetic (NM), but the alloys showed an adjustable magnetism through heat treatment and chemical components. During the past few decades, Heusler alloys have been favorable candidates for multifunctional materials because of their numerous excellent properties, such as: Magnetocaloric effect [10] [11], giant magnetoresistance [12], magnetic field-drive shape memory effects [13], half-metallicity [14], Hall effects [15]. In addition, some Heusler compounds exhibit excellent thermoelectric properties [16, 17].

Furthermore, a very interesting class of Heusler alloys that has received considerable theoretical studies is the HM, Mn_2YZ. These materials are much more favorable than their ferromagnetic coun-

terparts in magneto-electronic applications [18]. One important application of Mn_2YZ Heusler alloys is spintronic materials. Many Mn_2-based Heusler alloys have been reported to be half-metals or spin gapless semiconductors (SGSs) such as Mn_2CoAl inverse Heusler alloy under pressure [19], Mn_2CoZ (Z = Al, Ga, In, Si, Ge, Sn, Sb) [20], Mn_2VZ (Z = Al, Ga, In, Si, Ge, Sn) [21], Mn_2CoAl [22].

In this paper, we present an investigation on the structural, electronic, magnetic properties and halfmetallic behavior of Mn_2YSn (Y= Mo, Nb, Zr). This paper is structured as follows: in section 2, we briefly describe the computational method used in this work, Results and discussions of our study are present in section 3. Finally, a summary of the work is given in section 4.

2. Computational method

In order to calculate the electronic, structure and magnetic properties, we employed the FP-LAPW method in the framework of the density functional theory (DFT) [23] as implemented in the WIEN2k code [24] .In this method, the space is divided into non-overlapping muffin-tin (MT) sphere separated by an interstitial region. The generalized approximation proposed by Perdew-Burke-Ernzerhof was used for the exchange correlation potential [25]. Spin polarized calculations were performed with both spin-up and spin-down states. The maximum value of angular momentum $L_{max} = 10$ for the wave function expansion inside the muffin tin sphere. The convergence of the basis was controlled by cut-off of $K_{max} = 8.0/R_{MT}$ where R_{MT} is the muffin tin sphere radius and K_{max} is the largest reciprocal lattice vector used in the plane wave expansion within the interstitial region. The cutoff energy, which defines the separation of valence and core states, was chosen as −6.0 Ry. A mesh of 64 special k-points was made in the irreducible wedge of the Brillouin zone. In the interstitial region, the charge density and the potential were expanded as a Fourier series with wave vectors up to $G_{max} = 12$ a.u.$^{-1}$. A convergence norm for self-consistent field calculations was chosen in such a way that the difference in the energy between two successive iterations did not exceed 10^{-4} Ry.

The radii R_{MT} of the muffin-tin are selected to be as large as possible under the condition that the spheres do not overlap. The electronics configurations for atoms in Mn_2YSn (Y = Mo, Nb, Zr) are: Mn: $[Ar]4s^2 3d^5$, Mo: $[Kr]4s^1 4d^5$, Nb: $[Kr]5s^1 4d^4$, Zr: $[Kr]5s^2 4d^2$, Sn: $[Kr]5s^2 4d^{10} 5p^2$.

3. Results and discussion

In this subsection, we present the results of the geometrical structure of the Mn_2YSn (Y = Mo, Nb, Zr) Heusler alloys as well as the lattice parameters and bulk modulus. The general stoichiometric composition of the full-Heusler alloys is X_2YZ, where X and Y are different transition elements, while Z refers to the main group element. The high ordered structure is a very important factor for the electronic, magnetic properties of Heusler compounds. There are two possible atomic orderings in Mn_2YSn with (Y = Mo, Nb, Zr): the first one is L21 ("regular cubic phase" prototype Cu_2MnAl) in which the two Mn atoms occupy A(0,0,0) and C(1/2, 1/2, 1/2) positions, and Y, Sn atoms occupy B (1/4,1/4,1/4) and D(3/4, 3/4, 3/4). In the case of the Cu_2MnAl type L21 structure, the sequence of the atoms occupying the four sites of the unit cell is X-Y-X-Z. The second one is XA ("inverted cubic phase" prototype Hg_2CuAl, in which the tow Mn atoms occupy A(0,0,0) and B (1/4,1/4,1/4) positions, and Y, Sn atoms occupy C (1/2,1/2,1/2) and D (3/4,3/4,3/4) positions, respectively, the sequence of the atoms is X-X-Y-Z. The important difference between these two structures is the inter-exchange between the C site atom and the B-site atom. Both structures may be indistinguishable by X-ray diffraction and much care should be taken in the structural analysis, because both have the general FCC like symmetry [26] [27]. To determine the ground state properties of Mn_2YSn (Y = Mo, Nb, Zr), the calculation results of total energy versus lattice constant for both Hg_2CuTi and Cu_2MnAl structures are plotted in figure 1. The variation of total energy with the volume is fitted to Murnaghan equation of state [28] to obtain the equilibrium lattice constant a Å, the bulk modulus B (GPa), the derivative of the bulk with respect to the modulus B'.

$$E(V) = E_0(V) + \frac{BV}{B'(B'-1)}\left[B\left(1-\frac{V_0}{V}\right) + \left(\frac{V_0}{V}\right)^{B'} - 1\right], \tag{3.1}$$

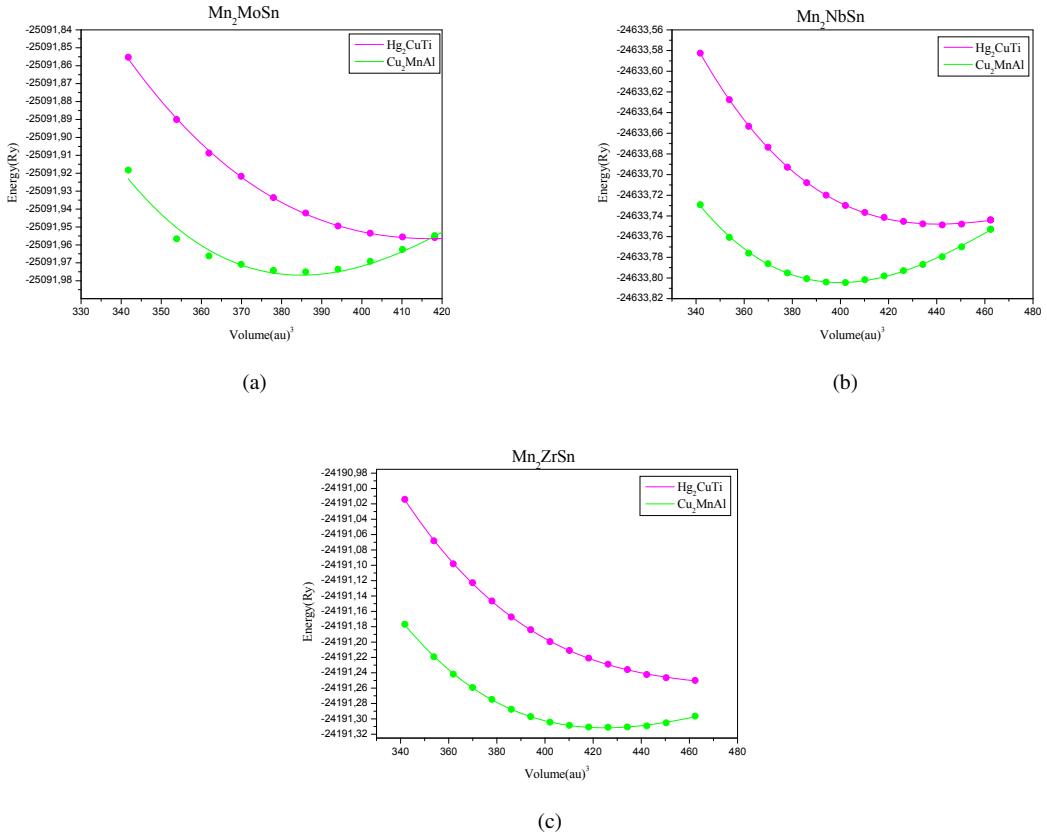

Figure 1. (Colour online) Total energy versus lattice constant for both structure Hg_2CuTi and for Mn_2YSN (Y = Mo, Nb, Zr).

where is E_0 the minimum energy at $T = 0$ K, B is the bulk modulus, B' is the bulk modulus derivative and V_0 is the equilibrium volume. Clearly, for Mn_2YSn (Y = Mo, Nb, Zr) compounds, the regular cubic phase (prototype Cu_2MnAl) Heusler structure is more stable than the inverted cubic phase (prototype Hg_2CuAl). The results are listed in table 1. The calculated lattice constant of Mn_2YSn (Y = Mo, Nb, Zr) is in good agreement with the previously theoretically optimized lattice constants reported by other researchers. According to Luo and al [29], the site preference of the X and Y atoms is strongly influenced by the number of their electrons. Those elements with more electrons prefer to occupy the A and C sites, and those with fewer electrons tend to occupy the B sites. In the case of Mn_2YSn (Y = Mo, Nb, Zr), we have the nuclear charge of X (Mn atom) larger than Y (Y = Mo, Nb, Zr), so the Cu_2MnAl structure will be observed. Similar results are found by Kervan and al [30] for Mn_2NbAl, and Anjami and al [14] for Mn_2ZrX (X = Ge, Si). We discuss the phase stability of Mn_2YSn (Y = Mo, Nb, Zr) based on the formation energy (ΔE_F). This can help to predict whether these alloys can be prepared experimentally. Here, the formation energy ΔE_F is calculated by comparing the total energies of the Mn_2YSN (Y = Mo, Nb, Zr) Heusler alloys with the sum of the total energies of the constituting elements. The formation energy of the Mn_2YSn (Y = Mo, Nb, Zr) materials is computed following the expression given below

$$\Delta E_F = E^{Total}_{Mn_2YSn} - \left[2E^{bulk}_{Mn} + E^{bulk}_{Y} + E^{bulk}_{Sn}\right], \tag{3.2}$$

where $E^{Total}_{Mn_2YSn}$ is the first-principles computed results of the total energy at equilibrium for the Mn_2YSn (Y = Mo, Nb, Zr) full Heusler alloys, and E^{bulk}_{Mn}, E^{bulk}_{Y}, E^{bulk}_{Sn} represent total energy per atom for Mn, Y, and Sn elements in the bulk form, respectively. The negative values of the formation energy specify that Mn_2YSn (Y = Mo, Nb, Zr) full Heusler alloys are chemically stable, and these materials can be

Table 1. Calculated equilibrium lattice constant a (Å), the bulk modulus B (GPa), the minimum energy (Ry) and the formation energy E_F (Ry) of Mn_2YSn (Y = Mo, Nb, Zr) Heusler compounds.

		a (Å)	B (GPa)	B'	Energy (Ry)	E_F (Ry)
Mn_2MoSn	Hg_2CuTi	6.2825	133.9353	5.2946	−25091.956309	−1.257851
	Cu_2MnAl	6.1033	264.5693	6.9898	−25091.976771	−1.278313
Mn_2NbSn	Hg_2CuTie	6.3946	138.8278	4.0864	−24633.748350	−1.296929
	Cu_2MnAl	6.1872	195.5253	4.4311	−24633.803953	−1.322501
Mn_2ZrSn	Hg_2CuTi	6.5743	98.2694	4.2436	−24191.251440	−1.149113
	Cu_2MnAl	6.3195	162.0852	4.0633	−24191.311742	−1.192513

synthesized experimentally. The computed results of the ΔE_f for the Cu_2MnAl type structures are found to be more negative than these of the Hg_2CuTi type structures, endorsing that Cu_2MnAl type structures are more stable compared to the Hg_2CuTi type ones.

The gap in half-metallic Heusler alloys exist in one state, whereas in the opposite spin state, E_f cuts though the bands. The d-band is mostly responsible for the position of the Fermi level lying in it. The role of transition metals d-states is very essential in the explanation of spin-polarized electronic band structures; the density of states of one spin state has a peak at E_f while in another spin state, the density of the state is zero around the E_f [31]. The conduction electrons are thus 100% spin-polarized, and it is useful to define the electron spin polarization at the Fermi energy of a material where the spin polarization at E_f is given by equation.

$$P = \frac{N_\uparrow(E_f) - N_\downarrow(E_f)}{N_\uparrow(E_f) + N_\downarrow(E_f)}, \tag{3.3}$$

where $N_\uparrow(E_f)$ and $N_\downarrow(E_f)$ are the spin dependent densities of states at E_F, the $\uparrow$ and $\downarrow$ assign states of the opposite spins, that are the majority and minority states, respectively. With the aim to profoundly understand the electron structures of Mn_2YSn (Y = Mo, Nb, Zr), we present the energy bands along high symmetry directions in the Brillouin zone, the total density of states (TDOS) and partial density of states (PDOS) plots for Mn_2YSn (Y = Mo, Nb, Zr) in figure 2. PDOS plots are plotted to see the contributions from various atomic states near E_F. We treat the spin-up channel as positive and the spin-down channel as negative for better comparison. The calculated spin-polarized total densities of states (DOS) and atom projected DOS of theMn_2MoSn compound for the Cu_2MnAl type structure and the Hg_2CuTi type structure are presented at their optimized equilibrium lattice constants in figure 2. We can see in Cu_2MnAl structure that the spin up and spin down are symmetric and the band structures are identical explaining the non-magnetic behavior of this alloy. For Hg_2CuTi type structure Mn_2MoSn is metallic with intersection of the band structure with Fermi level in spin up and spin down. For the Mn_2ZrSn, the minority spin channel (spin down) has intersection with Fermi level, so it has a metallic character, while the majority spin channel (spin up) has a gap at Fermi level. Consequently, it shows a semiconductor behavior. As presented in figure 3, the energy gap E_g, in the majority spin channel, the indirect band gaps at around Ef along the Γ-X symmetry, is 0.42062 eV. This gap implies the HM character of compounds and causes 100% spin polarization at Ef. The calculated spin-polarized (DOS), total densities of states and atom-projected DOS of the Mn_2NbSn Heusler alloy for both Hg_2CuTi and Cu_2MnAl structures are presented at their optimized equilibrium lattice constants in figure 2. The form of total DOS and atom projected DOS of the Mn_2NbSn Heusler alloys for two different structures is very different. For the Cu_2MnAl type structure, there is a gap in the majority spin (spin up state), the Fermi level just falls within the gap in the spin-up band indicating a semiconductor behavior and it crosses the energy bands in the minority spin state which makes Mn_2NbSn Heusler alloys with Cu_2MnAl type structure half-metallic (HM) magnetic compounds at the equilibrium lattice constant. In Hg_2CuTi type structure, the Fermi level crosses the energy bands for both majority and minority spin indicating the metallic behavior for this structure. In the majority spin band gap, the valence band maximum is situated at −0.06572 and the conduction band minimum is situated at 0.23442. This energy gap in spin up state leads to 100% spin polarization at the Fermi level, resulting in the half-metallic behavior at the

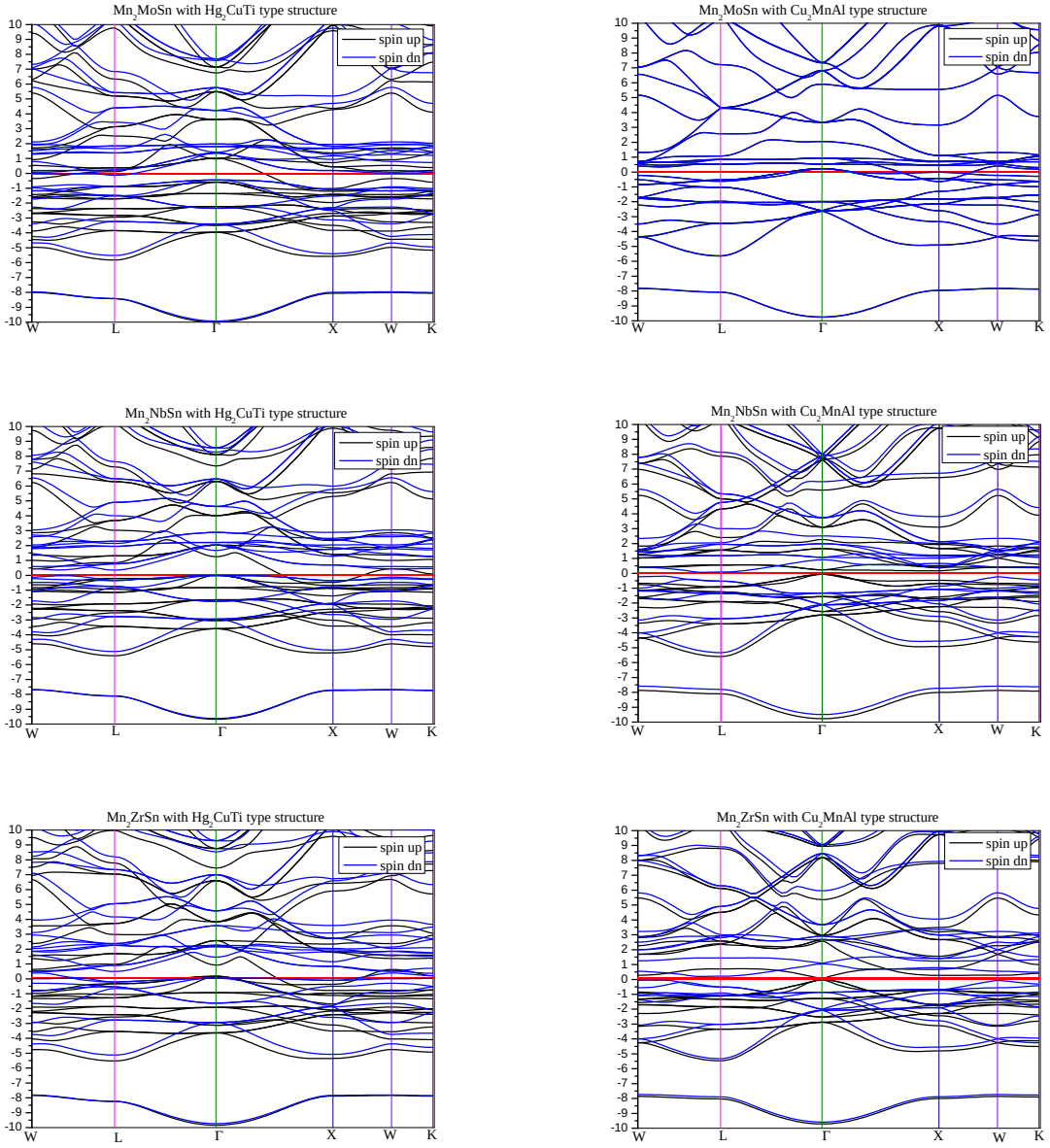

Figure 2. (Colour online) Band structure for Mn_2YSn (Y = Mo, Nb, Zr) for both structure Hg_2CuTi and Cu_2MnAl.

equilibrium state of the Cu_2MnAl type structure. For Mn_2MoSn, the band in both Cu_2MnAl and Hg_2CuTi structures, and for the spin up and the spin down, it is evident that the structure has metallic intersections at the Fermi level, indicating a strong metallic nature of the spin-up and spin-down electrons.

Total magnetic moment (MT) of Mn_2YSn (Y = Mo, Nb, Zr) full-Heusler alloys, the atomic moment of each ion and magnetic moment in interstitial zones are calculated at the equilibrium lattice parameter by GGA. The obtained results are presented in table 2. It can be seen that they are integral values, 1 μ_B for Mn_2NbSn and 2μ_B for Mn_2ZrSn with Cu_2MnAl type structure, and the contributions to the total magnetic moments Mt are mainly attributed to the Mn atom, the Y(Y = Mo, Nb, Zr) and Sn atomic magnetic moments can be neglected. The unequal magnetic moments on the Mn1 and Mn2 atoms, for Hg_2CuTi type structure, result from different atomic environments. The negative magnetic moments on

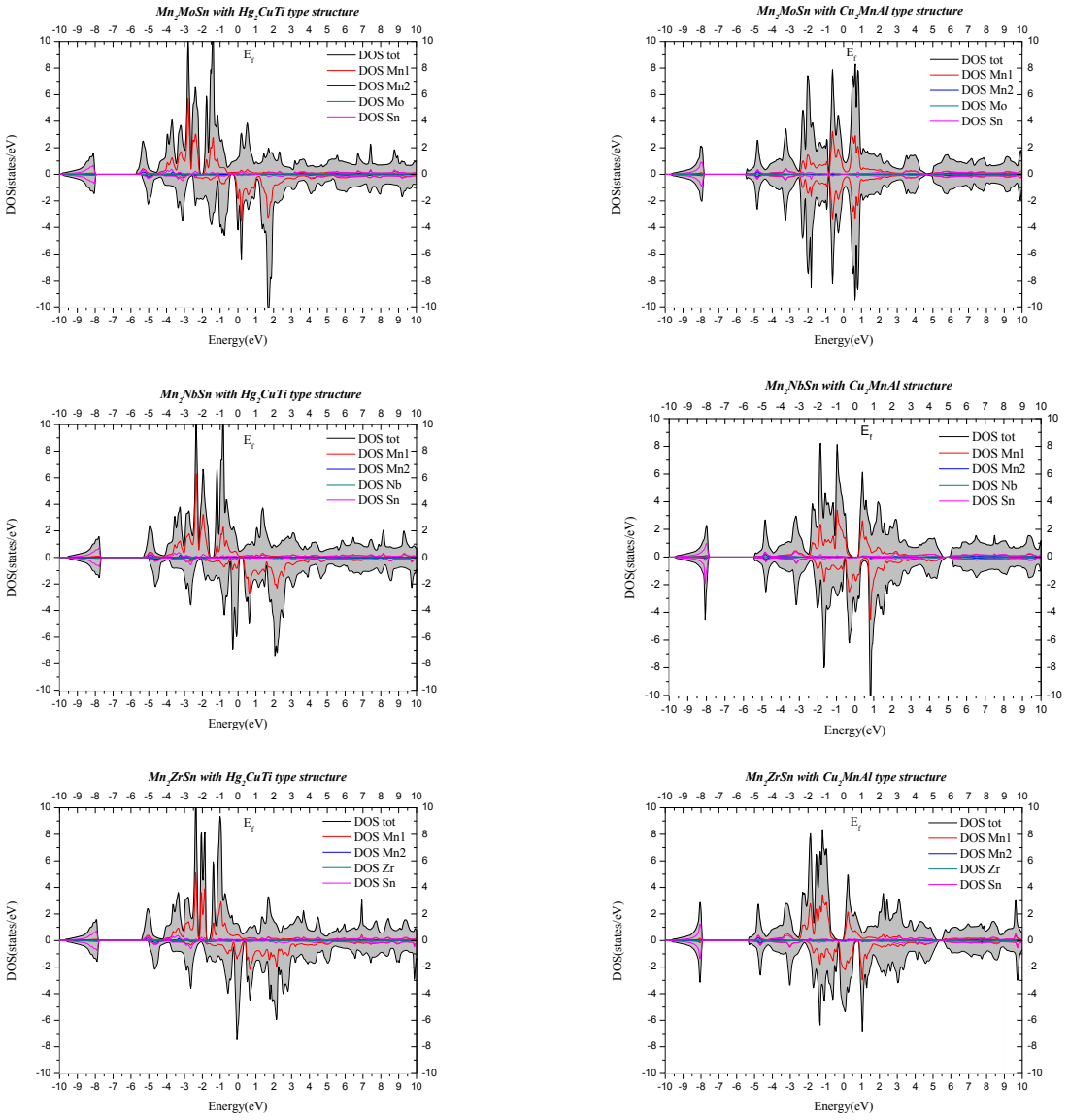

Figure 3. (Colour online) Total and partial density of states for Mn_2YSn (Y = Mo, Nb, Zr) for both structure Hg_2CuTi and Cu_2MnAl.

Table 2. The calculated values of magnetic moments (μ_B) of the of Mn_2YSn (Y = Mo, Nb, Zr) Heusler compounds.

		M_{Mn_1}	M_{Mn_2}	M_Y	M_{Sn}	$M_{interstitial}$	M_{total} (M_t)
Mn_2MoSn	Hg_2CuTi	3.473	2.770	−0.815	−0.029	−0.136	5.262
	Cu_2MnAl	0.004	0.000	−0.010	−0.003	−0.062	0.000
Mn_2NbSn	Hg_2CuTi	3.423	2.539	−0.585	−0.052	−0.153	5.170
	Cu_2MnAl	0.761	0.761	−0.331	−0.032	−0.165	1.000
Mn_2ZrSn	Hg_2CuTi	3.163	2.937	−0.182	−0.048	−0.061	5.931
	Cu_2MnAl	1.262	1.262	−0.283	−0.045	−0.190	2.000

the Y (Y= Mo, Nb, Zr), and Sn atoms show that there is antiferromagnetic coupling with the Mn atom. For Mn_2MoSn, the total magnetic moment is equal to zero (with Cu_2MnAl structure) which confirms the non-magnetic behavior for this compound. Magnetic properties can be directly connected to the electronic structure by the Slater-Pauling rule: $M_t = Z_t - 24$, the M_t is total spin magnetic moments in the unit cell, and Z_t is the total number of valence electrons. Z_t is equal to 24 for Mn_2MoSn $[(7 \times 2) + 6 + 4 = 24]$, equal to 23 for Mn_2NbSn $[(7 \times 2) + 5 + 4 = 23]$ and it is equal to 22 for Mn_2ZrSn $[(7 \times 2) + 4 + 4 = 22]$. In full-Heusler alloys, the minority band comprises 12 electrons per unit cell. Therefore, the 24 valence electrons are equally distributed into both spin directions, and the alloy is nonmagnetic. If the alloy has more than 24 valence electrons, spin polarization will occur and the exchange interaction will shift the majority states to lower energies. The additional electrons will fill in only the majority spins, which results in an integral spin moment [32]. However, for half-metallic full-Heusler alloys with less than 24 electrons per unit cell, such as our case study, the energy gap is in the majority spin band rather than in the minority spin band. A similar result was found by Anjami et al. [14].

4. Conclusion

First principles FP -LAPW calculations were performed on Mn_2YSn (Y = Mo, Nb, Zr). Based on the results, we predict that Cu_2MnAl type structure is more stable than the Hg_2CuTi type. It is concluded that the spin polarized band structure and densities of states of the Mn_2ZrSn and Mn_2NbSn present 100% spin polarization around Fermi level and are half-metallic ferromagnets. The calculated total magnetic moments are 1 μ_B and 2 μ_B for Mn_2NbSn and Mn_2ZrSn, respectively, for the Cu_2MnAl type structure, which is quite well proved with the Slater-Pauling rule.

The Mn_2MoSn compound with Cu_2MnAl presents a non-magnetic behavior with spin up and spin down symmetric (DOS), the band structures are identical (up and down) and the magnetic moment is equal to 0 μ_B.

5. Acknowledgement

This work was supported by DGRST-ALGERIA.

References

1. Paudel R., Zhou F., Liao M., Uhu J., J. Phys. Chem. Solids, 2020, **136**, 109190, doi:10.1016/j.jpcs.2019.109190.
2. Guha S., Kumar R., Kumar S., Pradhan L.K., Pandey R., Kar M., Physica B, 2020, **579**, 411805, doi:10.1016/j.physb.2019.411805.
3. Anjami A., Boochani A., Elahi S.M., Akbari H., Results Phys., 2017, **7**, 3522–3529, doi:10.1016/j.rinp.2017.09.008.
4. Kervan S., Kervan N., Curr. Appl. Phys., 2013, **13**, 80–83, doi:10.1016/j.cap.2012.06.018.
5. De Groot R.A., Mueller F.M., van Engen P.G., Buschow K.H.J., Phys. Rev. Lett., 1983, **50**, 2024–2027, doi:10.1103/PhysRevLett.50.2024.
6. Dahmane F., Tadjer A., Doumi B., Mesri D., Aourag H., Mater. Sci. Semicond. Process., 2014, **21**, 66–73, doi:10.1016/j.mssp.2014.01.037.
7. Dahmane F., Mesri D., Tadjer A., Khenata R., Benalia S., Djoudi L., Doumi B., Boumia L., Aourag H., Mod. Phys. Lett. B, 2016, **30**, 1550265, doi:10.1142/S0217984915502656.
8. Mokhtari M., Dahmane F., Benabdellah G., Zekri L., Benalia S., Zekri N., Condens. Matter Phys., 2018, **21**, 43705,doi:10.5488/CMP.21.43705.
9. Zhou Y., Zhang J., Huang Yu., Wei X.M., J. Phys. Chem. Solids, 2020, **138**, 109246, doi:10.1016/j.jpcs.2019.109246.
10. Wu Y., Wang J., Zhang J., Ma Y., Intermetallics, 2017, **89**, 100–104, doi:10.1016/j.intermet.2017.05.021.
11. Liu J., Gottschall T., Skokov K.P., Moore J.D., Gutfleisch O., Nat. Mater., 2012, **11**, 620–626, doi:10.1038/nmat3334.
12. Yu S.Y., Liu Z.H., Liu G.D., Chen J.L., Cao Z.X., Wub G.H., Appl. Phys. Lett., 2006, **89**, 162503, doi:10.1063/1.2362581.

13. Kainuma R., Imano Y., Ito W., Sutou Y., Morito H., Okamoto S., Kitakami O., Oikawa K., Fujita A., Kanomata T., Ishida K., Nature, 2006, **439**, 957–60, doi:10.1038/nature04493.
14. Anjami A., Boochani A., Elahi S.M., Akbari H., Results Phys., 2017, **7**, 3522–3529, doi:10.1016/j.rinp.2017.09.008.
15. Dubenko I., Pathak A.K., Stadler S., Ali N., Kovarskii Ya., Prudnikov V.N., Perov N.S., Granovsky A.B., Phys. Rev. B, 2009 , **80**, 092408, doi:10.1103/PhysRevB.80.092408.
16. Gavera R., Hirian R., Isnard O., Pop V., Benea D., Solid State Commun., 2020, **309**, 113812, doi:10.1016/j.ssc.2020.113812.
17. Mokhtari M., Amari D., Dahmane F., Benabdellah G., Zekri L., Zekri N., Spin, 2020, **10**, 2050005, doi:10.1142/S2010324720500058.
18. Abada A., Amara K., Hiadsi S., Amrani B., J. Magn. Magn. Mater., 2015, **388**, 59–67, doi:10.1016/j.jmmm.2015.04.023.
19. Chen X., Zhong M., Feng Y., Zhou Y., H.-K. Yuan, Chen H., Phys. Status Solidi B, 2015, **252**, No. 12, 2830–2839, doi:10.1002/pssb.201552389.
20. Liu G.D., Dai X.F., Liu H.Y., Chen J.L., Li Y.X., Xiao Gang, Wu G.H., Phys. Rev. B, 2008, **77**, 014424, doi:10.1103/PhysRevB.77.014424.
21. Ozdogan K., Galanakis I., Sasioglu E., Aktas B., J. Phys.: Condens. Matter, 2006, **18** 2905–2914, doi:10.1088/0953-8984/18/10/013.
22. Ouardi S., Fecher G.H., Felser C., Kübler J., Phys. Rev. Lett. 2013, **110**, 100401, doi:10.1103/PhysRevLett.110.100401.
23. Kohn W., Sham L.J., Phys. Rev. A, 1965, **140**, 1133–1138, doi:10.1103/PhysRev.140.A1133.
24. Blaha P., Schwary K., Madsen G.K.H., Kvasnicka D., Luitz J., An Augmented Plan Wave Plus Local Orbitals Program for Calculating Crzstal Properties, Vienna University of Technologz, Vienna, 2001.
25. Perdew J.P., Burke K., Ernzerhof M., Phys. Rev. Lett., 1996, **77**, 3865–3868, doi:10.1103/PhysRevLett.77.3865.
26. Wei X.-P., Hu X., Liu B., Deng H., Yang M.-K., Deng J.-B., J. Magn. Magn. Mater., 2011, **323**, 1606–1610, doi:10.1016/j.jmmm.2010.12.044.
27. Dahmane F., Semari F., Doumi B., Bin Omran S., Parkash D., Khenata R., Chin. J. Phys., 2018, **56**, 1764–1771, doi:10.1016/j.cjph.2018.05.005.
28. Murnaghan F.D., Proc. Natl. Acad. Sci. U.S.A., 1947, **30**, **244**, doi:10.1073/pnas.30.9.244.
29. Luo H., Zhu Z., Liu G., Xu S., Wu G., Liu H., Qu J., Li Y., J. Magn. Magn. Mater., 2008, **320**, 421–428, doi:10.1016/j.jmmm.2007.06.021.
30. Kervan N., Kervan S., Canko O., Atis M., Taskin F., J. Supercond. Novel Magn., 2016, **29**, 87–192, doi:10.1007/s10948-015-3228-x.
31. Rauf S., Arif S., Haneef M., Amin B., J. Phys. Chem. Solids., 2015, **76**, 153–169, doi:10.1016/j.jpcs.2014.07.021.
32. Luo H.Y., Zhang H.W., Zhu Z.Y., Ma L., Xu S.F., Wu G.H., Zhu X.X., Jiang C.B., Xua H.B., J. Appl. Phys., 2008, **103**, 083908, doi:10.1063/1.2903057.

Прогнозування електронних та напівметалевих властивостей сплавів Гейслера Mn_2YSn (Y = Mo, Nb, Zr)

С. Зеффане[1,2], М. Саях[1,2], Ф.Дахман[1,3], М. Мохтарі[1,2], Л. Зекрі[2], Р. Хената[3], Н. Зекрі[2]

[1] Інститут природничих наук і технологій, університетський центр Тіссемсілту, 38000 Тіссемсілт, Алжир

[2] Інститут природничих наук і технологій ім. Мохамеда Будіафа м. Оран, USTO-MB, LEPM, BP 1505, 31000 Оран, Алжир

[3] Лабораторія квантової фізики і математичного моделювання (LPQ3M), відділ технологій, університет Маскари, 29000 Маскара, Алжир

Ми досліджуємо структурні, електронні та магнітні властивості сполук Гейслера M_2YSn (Y = Mo, Nb, Zr) з використанням першопринципної теорії функціоналу густини та узагальненого градієнтного наближення. Встановлено, що розраховані константи гратки добре узгоджуються з теоретичними значеннями. Ми спостерігаємо, що структура типу Cu_2MnAl є більш стійкою, ніж структура типу Hg_2CuTi. Розраховані сумарні магнітні моменти Mn_2NbSn та Mn_2ZrSn дорівнюють 1 μ_B і 2 μ_B при рівноважній сталій гратки 6,18 Å і 6,31 Å, відповідно, для структури типу Cu_2MnAl. Mn_2MoSn має металевий характер як у структурах типу Hg_2CuTi, так і в Cu_2MnAl. Повний спіновий магнітний момент підпорядковується правилу Слейтера-Полінга. Напівметал демонструє 100% спінової поляризації на рівні Фермі. Таким чином, ці сплави є перспективними магнітними кандидатами в спінтронних пристроях.

Ключові слова: *Гейслер, напівметалевий, магнітний момент, спінтронний*

Journal of Electronic Materials
https://doi.org/10.1007/s11664-022-09945-5

ORIGINAL RESEARCH ARTICLE

Electronic and Magnetic Properties of Mn_2YSn (Y = Ru, Rh, and Pd) Heusler Alloys Under Hydrostatic Pressure

S. Zeffane[1,2] · A. Haddou[3] · M. Mokhtari[1,2] · D. Amari[4,5] · F. Dahmane[1,6] · R. Khenata[6] · R. Ahmed[7,8] · S. Bin Omran[9] · Abdeazim M. Mebed[10] · Muhammad Mushtaq[11]

Received: 23 April 2022 / Accepted: 8 September 2022

Abstract
Heusler materials have shown a ground-breaking role in material research because of their widespread applicability in modern technologies and multi-dimensional properties. In this study, the pressure effects on the structural, electronic, and magnetic properties of Mn_2YAN (Y = Ru, Rh, and Pd) Heusler alloys are investigated. This study is carried out by employing a state-of-the-art first-principles computational approach called "full potential (FP) linearized (L) augmented plane wave plus local orbital (APW + lo)" as designed using density functional theory (DFT), and executed in WIEN2k computational code. The computed results for the lattice constants have been found to be in fairly good agreement with previously reported results in the literature. The results show that the Mn_2RuSn, Mn_2RhSn, and Mn_2PdSn compounds are stable in the Hg_2CuTi-type structure. Furthermore, under the pressure effect, the Mn_2RuSn, Mn_2RhSn, and Mn_2PdSn compounds become half-metals at about 10 GPa, 10 GPa, and 20 GPa, respectively.

Keywords Heusler materials · first-principles calculations · pressure effects · half-metallic ferromagnetics

Introduction

The full-Heusler compounds/alloys are among a group of materials called Heusler alloys; they got this name from its first discoverer.[1] Half-metallic (HM) materials are known, as these materials behave differently in both spin bands (spin-up, spin-down), the one spin band showing metallic behavior, while the other spin band presents a semiconductor behavior.[2,3] Given this feature, these materials are promising in various fields, in particular, spintronics applications.[4–6] Moreover, Heusler materials have been shown their diverse properties for spin-up and spin-down channels. Showing an

✉ F. Dahmane
fethallah05@gmail.com

✉ R. Khenata
rabah_khenata@univ-mascara.dz

1 Département de Sciences de la Matière, Université de Tissemsilt, 38000 Tissemsilt, Algérie

2 Laboratoire d'Etudes Physique des Matériaux, Département de Physique Énergétique, Université des Sciences et de Technologie, USTO-MB, BP 1505, El M'naour, Oran, Algérie

3 Department of Physics, Faculty of Exact Sciences, University of Sidi Bel Abbes-Algeria, 22000, Sidi Bel Abbès, Algeria

4 Material and Energies Research Laboratory, Tamanghasset University, 11000 Tamanghasset, Algeria

5 Material Sciences Department, Faculty of Sciences and Technologies, Tamanghasset University, 11000 Tamanghasset, Algeria

6 Laboratoire de Physique Quantique et de Modélisation Mathématique (LPQ3M), Département de Technologie, Université de Mascara, 29000 Mascara, Algérie

7 Centre for High Energy Physics, University of the Punjab, Quaid-e-Azam Campus, Lahore 54590, Pakistan

8 Department of Physics, Faculty of Science, University Teknologi Malaysia, 8130 Johor Bahru, Johor, Malaysia

9 Department of Physics and Astronomy, College of Science, King Saud University, P.O.Box 2455, Riyadh 11451, Saudi Arabia

10 Department of Physics, College of Science, Jouf University, P.O. Box 2014, Sakaka, Al-Jouf, Saudi Arabia

11 Department of Physics, University of Poonch Rawalakot, Rawalakot 12350, Pakistan

Published online: 06 October 2022

insulator/semiconductor character in one spin channel and metallic in the other channel has led to Heusler materials being completely spin-polarized at the Fermi level.[7–9] These materials have attracted considerable attraction from the research community since F. Heusler exposed the ferromagnetic character of the Cu_2MnAl, although no one constituent of this ternary compound had a ferromagnetic nature.[1] Since that time, many Mn-based Heusler materials have been investigated, including the materials previously cited in the literature.[10–20] Recently, research on Heusler compounds/alloys has been extended to include all the Mn_2RhZ systems (Z = Ga, Al, In, Ge, Si, Sb, and Sn),[21] Mn_2RuZ (Z = Si, Sn, Ge, Sb),[22–26] Mn_2PdZ(Z = In, Sn),[27] Mn_2PtCo,[28] and Mn_2YZ(Y = Ni, Cu, and Zn; Z = Ga, Ge, and As).[29] Hoat et al.[30] studied the structural, half-metallic, and elastic properties of Mn_2CoX (X = P and As) full-Heusler alloys. The site preference, electronic structure, and magnetism of the Mn_2RuSn Heusler alloy have been investigated by Chen and coauthors using the pseudo-potential method with a plane-wave basis set.[23] This study reveals that the Hg_2CuTi-type (XA) structure is energetically favored in Mn_2RuSn, with a predicted tetragonal martensitic transformation for this alloy. The tetragonal distortion, electronic structure, and magnetic properties of Mn_2PdSn have been studied by Feng and coauthors using the pseudo-potential method.[31] This study indicates that the energy difference between the tetragonal and cubic phases for Mn_2PdSn is about 41.62 meV/f.u., and that the corresponding c/a ratio of the tetragonal phase is 1.23, suggesting that a martensitic transformation is very likely to occur in Mn_2PdSn with decreasing temperature. The enhancement of the Curie temperature in tetragonal Mn_2RhSn and Mn_2RuSn alloys is due to the Co substitution.[32,33] Additionally, numerous studies can be found in the literature for Mn_2YAN (Y = Rh, Ru and Pd) Heusler compounds, but very few of them are focused on the pressure effect on the properties of the title compound.[34–37]

To investigate the pressure effect on the physical properties of Heusler materials is crucial for further exposing their potential for future technologies and commercial applications. Moreover, what will be the response of these characteristics under pressure? The structure of crystalline materials mostly changes with pressure and corresponding properties, and the structure properties relationship is the main theme of material research. In this study, we perform a computational systematic study to see the effect of the standard site preference rule on the Mn_2-based Heusler materials. Moreover, the competition between the Hg_2CuTi-type (XA) and Cu_2MnAl (L21) structures of these compounds is investigated. This work has been carried out using density functional theory (DFT) methodology implemented in the WIEN2k code. This study includes the pressure effect on the structural, electronic, and magnetic properties, as well as the metallic behavior, of Mn_2YSn (Y = Ru, Rh, and Pd). The paper is arranged as the follows; Sect. 2 deals with computational details, while Sect. 3 describes the important results of the calculations and the corresponding discussion. Finally, conclusions are drawn.

Computational Details

The electronic structure calculations of Mn_2YAN (Y = Ru, Rh, and Pd) were performed by employing the FP-L (APW + lo) approach framed within DFT, and executed in the form of WIEN2k computational code.[38] In this method, the space is divided into an interstitial region (IR) and non-overlapping muffin tin (MT) spheres centered at the atomic sites. In the IR region, the basis set consists of plane waves. Inside the MT spheres, the basis set is described by radial solutions of the one-particle Schrödinger equation (at fixed energy) and their energy derivatives multiplied by spherical harmonics. The exchange–correlation potential was treated with the generalized gradient approximation (PBE-GGA) for the calculation of the structural properties,[39] while the PBE-GGA + U approach[40] (where U is the Hubbard Coulomb energy term) has been applied for better computation of the electronic and magnetic properties. The spin–orbit coupling has also been included for the calculation of the electronic and magnetic properties. The values of the of Hubbard term U for Mn, Ru, Rh and Pd atoms have been taken as 3.0 eV, 2.0 eV,1.92 eV, and 2.0 eV, from Refs. 41, 42, 43, and 44, respectively.

To perform the calculations, $R_{MT}K_{MAX} = 8$ was used where K_{MAX} represents the largest value of the basis set wave-vector and R_{MT} describes the muffin tin radii for each atom in the unit cell. The $l_{max} = 10$ was used for the maximum value of the angular momentum, while, in the interstitial region, $G_{max} = 12$ a.u.$^{-1}$ was considered for the Fourier expansion of the plane-wave basis set. To separate a core and a valence part, the cut-off energy value was taken to be equal to − 6.0 Ry; however, to meet the energy convergence criterion, an up to10^{-4} Ryd energy value was considered for self-consistent calculations, which are considered to be converged when the total energy of the system is stable within 10^{-5} Ryd. The electronic configuration for Mn_2YAN (Y = Ru, Rh, and Pd) is: Mn:[Ar]$4s^2 3d^5$; Ru:[Kr]$5s^1 4d^7$; Rh:[Kr]$5s^1 4d^8$;Pd:[Kr]$4d^{10}$; Sn:[Kr]$5s^2 4d^{10} 5p^2$.

Results and Discussion

Structural Properties

Heusler compounds, X_2YZ, enjoy a highly ordered cubic structure.[45,46] There are generally four different positions in a primitive cell, namely, A (0, 0, 0), B (0.25, 0.25, 0.25),

C (0.5, 0.5, 0.5), and D (0.75, 0.75, 0.75). The transition metal elements X and Y occupy the A, B, and C positions, and the main group element Z is preferred to occupy the D position. Different occupation positions of the X and Y atoms will lead to different structures, namely, Cu_2MnAl (L21) or Hg_2CuTi-type (XA) structures (the crystal structure of Mn_2PdSn as prototype is displayed in Fig. 1). In the former, two X atoms occupy the A and C positions, and the Y and Z atoms enter the B and D positions, respectively,[47,48] while, in the latter, two X atoms occupy the A and B positions, and the Y and Z atoms are located at the C and D positions, respectively.[47,49] Next, we studied the competition between the Hg_2CuTi-type structure and the Cu_2MnAl structure of Mn_2YSn (Y = Ru, Rh, and Pd) compounds. In Fig. 2, the total energy versus the unit cell volume of the compounds in the ground state with different structures (L21 and XA) is determined. One can clearly seen that, for the Mn_2YAN (Y = Ru, Rh, and Pd) compounds, the total energy of Hg_2CuTi is lower than the Cu_2MnAl one, reflecting that the most stable ordered structure for these systems is the Hg_2CuTi (XA), which is in good agreement with previous studies on these compounds.[23,31] This is because, according to Luo et al.,[20] the number of electrons in the X and Y atoms has a considerable impact on their site selection, hence the A and C sites are preferred by elements with more electrons, whereas the B sites are preferred by those with fewer electrons. As the nuclear charge of the X (Mn) atoms is smaller compared to the Y (Ru, Rh, and Pd), the Hg_2CuTi-type structure of Mn_2YAN (Y = Ru, Rh, and Pd) is observed to be the stable one, similar to many other materials, such as Mn_2RuSn,[50] Mn_2RuGe,[51] Mn_2RuSn,[23] Mn_2RhAl, Mn_2YIn (Y = Ni, Pd and Pt), and[52,53] Mn_2NiSn.[54] In Fig. 3, we further give a comparison of the total energy of the non-magnetic state (NM) and the two magnetic states [ferromagnetic (FM) and antiferromagnetic (AFM)] of the stable Hg_2CuTi-type structure of the Mn_2YSn (Y = Ru, Rh, and Pd) compounds. As shown in Fig. 3, the energy of the Mn_2YAN (Y = Ru, Rh, and Pd) compounds in the FM state using GGA + U is lower, highlighting that these compounds tend to exhibit FM magnetic states.

In order to calculate the ground state structural parameters, such as the equilibrium lattice constant a, the bulk modulus B, the bulk modulus pressure derivative B' and the energy E of Mn_2YAN (Y = Ru, Rh and Pd) compounds, the computed total energies versus unit cell volume of both the Cu_2MnAl (L21) or Hg_2CuTi (XA) structures have been fitted by the Murnaghan equation of state[55] given by the following relationship:

$$E = E_0(V) + \frac{BV}{(B'(B'-1))}\left[B\left(1-\frac{V_0}{V}\right)+\left(\frac{V_0}{V}\right)^{(B')}-1\right] \quad (1)$$

where B, V, B', E_0, and V_0 denote the bulk modulus, volume, first derivative of the bulk modulus, minimum energy at $T = 0$ K, and the equilibrium volume, respectively.

The computed results for the lattice parameters, bulk moduli, their pressure derivatives, and the minimum energy (Ry), under zero pressure of all three compounds are tabulated in Table 1. The more negative energy confirms the stability of these compounds in the Hg_2CuTi-type structure with the ferromagnetic state. The obtained lattice constants are in fairly good agreement with previously reported theoretical investigations. As can be seen from Table I, the a_0 values of the series of Mn_2YAN increase in the following sequence: a_0 (Mn_2RuSn) < a_0 (Mn_2RhSn) < a_0 (Mn_2PdSn). As the Mn and Sn atoms are the same in the three compounds, this result can be easily explained by the increase of the size of the X element in the Mn_2YAN compounds. Meanwhile, the B values decrease in the following sequence:

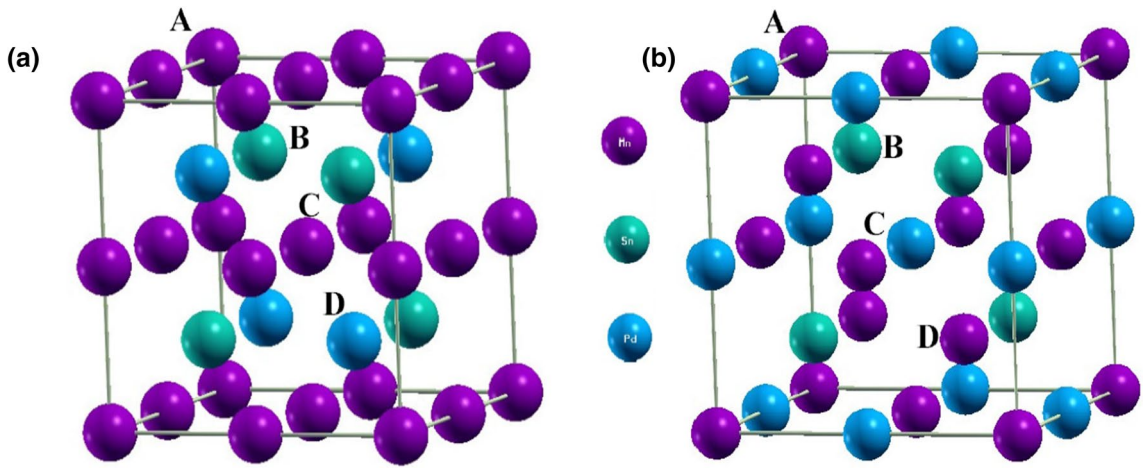

Fig. 1 Crystal structure of Mn_2YAN (Y = Ru, Rh, Pd): (a) Cu_2MnAl (L21) and (b) Hg_2CuTi (Xa).

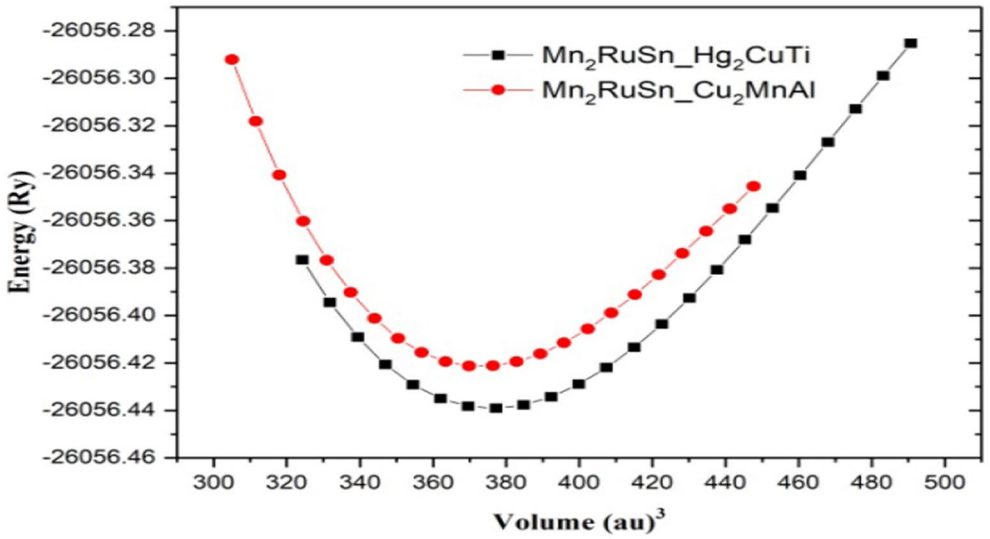
Mn2RuSn_Hg2CuTi
Mn2RuSn_Cu2MnAl
Energy (Ry)
Volume (au)3

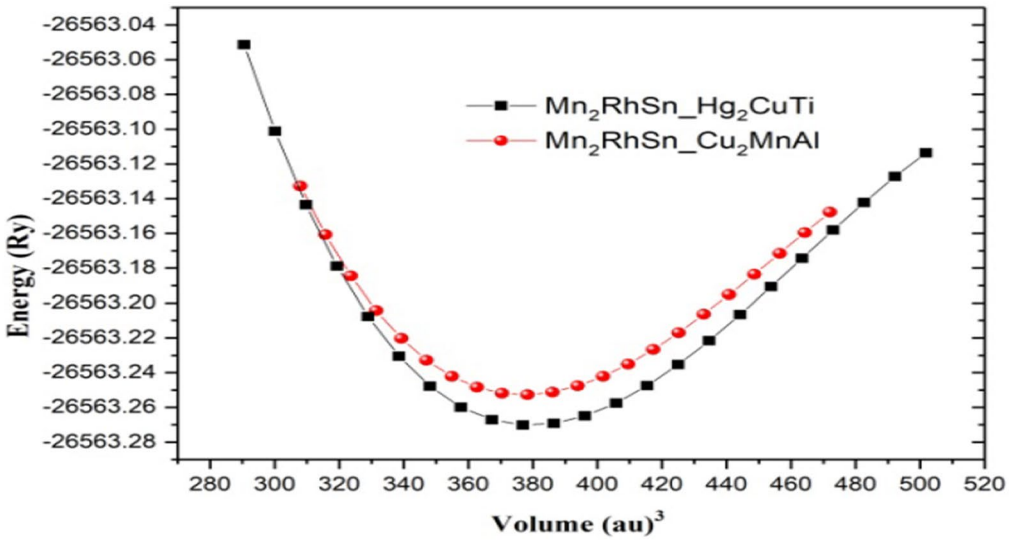
Mn2RhSn_Hg2CuTi
Mn2RhSn_Cu2MnAl
Energy (Ry)
Volume (au)3

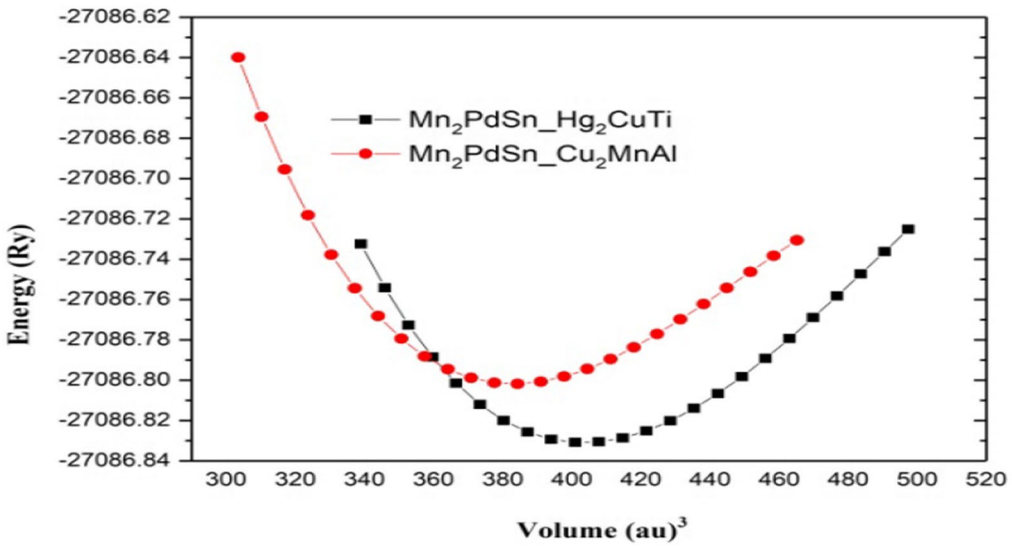
Mn2PdSn_Hg2CuTi
Mn2PdSn_Cu2MnAl
Energy (Ry)
Volume (au)3

◂**Fig. 2** Total energy as a function of unit cell volume for the Mn_2YAN (Y = Ru, Rh, and Pd) compounds in the Cu_2MnAl and Hg_2CuTi-type structures using the GGA-PBE approximation.

B (Mn_2RuSn) > B (Mn_2RhSn) > B (Mn_2PdSn) > B, i.e., in inverse sequence to a, in agreement with the well-known relationship between B and the lattice constants:$B \propto V_0^{-1}$, where V_0 is the unit cell volume. This simple trend, a, of the larger lattice constant leads to a smaller bulk modulus.

Based on the energy of formation (EF), the phase stability of Mn_2YAN (Y = Ru, Rh, and Pd) has been explored. This can be used further in determining whether the studied alloys are possible to be prepared in the laboratory. The total energies of the Mn_2YAN (Y = Ru, Rh, and Pd) Heusler compounds are compared to the total sum of the energies of the constituent atoms of different elements involved in the formation of compounds. The EF of Mn_2YAN (Y = Ru, Rh, and Pd) materials are calculated using the following relationship:

$$\Delta E_f = E^{\text{total}}_{Mn_2YSn} - \left[2E^{\text{bulk}}_{Mn} + E^{\text{bulk}}_{Y} + E^{\text{bulk}}_{Sn}\right] \quad (2)$$

where $E^{\text{total}}_{Mn_2YSn}$ is the equilibrium total energy for both types of crystal structure (Hg_2CuTi and Cu_2MnAl), E^{bulk}_{Mn},E^{bulk}_{Y}, and E^{bulk}_{Sn} correspond to total energy per atom, respectively, for the Mn, Sn, and Y (Y = Ru, Rh, and Pd) elements in their bulk form. Values of the EF for Mn_2YAN (Y = Ru, Rh, and Pd) compounds quoted in Table I are negative, indicating their chemical stability, hence these alloys can be prepared experimentally. The calculated EF values for the Hg_2CuTi type structures are more negative compared to the Cu_2MnAl-type structures, implying that Hg_2CuTi-type structures are more stable than Cu_2MnAl-type structures.

Electronic Properties

To determine the electronic properties of the full-Heusler (Mn_2RuSn, Mn_2RhSn, and Mn_2PdSn), partial and total densities of states (PDOS and TDOS) for both Hg_2CuTi and Cu_2MnAl-type crystal structures have been calculated using the computed values of the lattice parameters. The spin-polarized (SP) band structures and the densities of states (DOS) of the considered compounds for spin-up and spin-down states are displayed in Figs. 4 and 5, respectively. The positive and negative numbers correspond to spin-up and spin-down DOS, respectively. From these figures, it can be observed that these compounds exhibit a metallic nature. By giving close attention to the small charts near to the Fermi level, the metallic character of these compounds is clearly revealed. It can be further noted that the largest contribution to the band structure in energy range from − 6 to 6 eV is governed by 3d transition metal (Mn) atoms, also showing a key role around the Fermi level for the Mn_2RuSn, Mn_2RhSn, and Mn_2PdSn Heusler compounds.

SP, on the other hand, can be defined as a mechanism for distinguishing between the minority and the majority near the Fermi energy level. The SP relationship for Heusler alloys is as follows:

$$\text{SP} = \frac{\rho\uparrow(Ef) - \rho\downarrow(Ef)}{\rho\uparrow(Ef) + \rho\downarrow(Ef)} \quad (3)$$

where $\rho\uparrow(Ef)\rho\downarrow(Ef)$ denotes at the Fermi energy level (E_F) the density of the majority and the minority states, respectively. The Heusler compounds/alloys are said to be truly half-metallic if the SP value is 100%. This is attained when the DOS at E_F for one of the channels is zero while the other one is non-zero.

The computed results for the TDOS for Mn_2RuSn with various degrees of atomic disorder were presented by Yang et al.,[50] and they found a tiny number of minority states in the gap and a low SP ratio, so, according to Yang et al.,[50] the Mn_2RuSn is still not an ideal half-metal at equilibrium lattice. However, according to Ref. 23, half-metallicity in Mn_2RuSn can be stabilized by a slight lattice contraction; this is realized in Pressure-Dependent Structural Electronic and Magnetic Properties of Mn_2YAN (Y = Ru, Rh, Pd) Section

Magnetic Properties

To understand the magnetic behavior of the compounds under investigation, the total and partial magnetic moments for both the Hg_2CuTi and Cu_2MnAl configurations of the Mn_2RuSn, Mn_2RhSn, and Mn_2PdSn Heusler compounds were computed using the computed results of the equilibrium lattice constants at the level of PBE-GGA and GGA + U approaches, and are tabulated in Table II. The magnetic behavior of the Heusler compounds, Mn_2YSn (Y = Ru, Rh, and Pd), is noticed by the non-symmetrical DOS, as shown in Fig. 5. It can also be seen from the tabulated data that the total magnetic moments are not found in integral form for all three compounds, confirming that these alloys are not half-metallic. Moreover, the computed magnetic moments of the compounds for the ferromagnetic states in the stable Hg_2CuTi-type structure, using both GGA and GGA + U, show that the Mn atoms majorly contribute to the total magnetic moment for a minor contribution of Y atoms. The contribution of the Sn atoms is almost neglected.

Pressure-Dependent Structural Electronic and Magnetic Properties of Mn2YAN (Y = Ru, Rh, Pd)

The pressure effect on the materials is a very important area, since the properties of solids are directly related to the

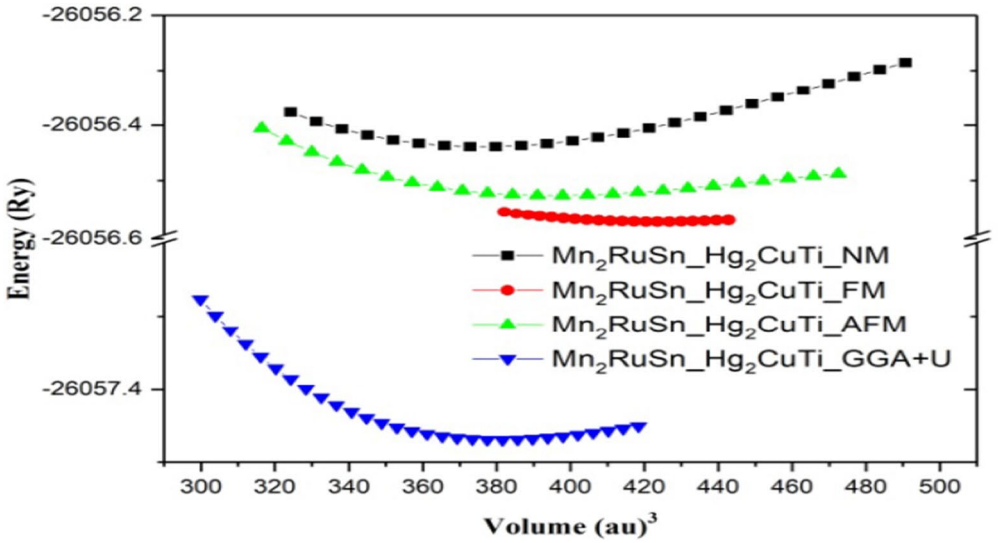
-26056.2
-26056.4
-26056.6
-26057.4
Energy (Ry)
300 320 340 360 380 400 420 440 460 480 500
Volume (au)³
Mn2RuSn_Hg2CuTi_NM
Mn2RuSn_Hg2CuTi_FM
Mn2RuSn_Hg2CuTi_AFM
Mn2RuSn_Hg2CuTi_GGA+U

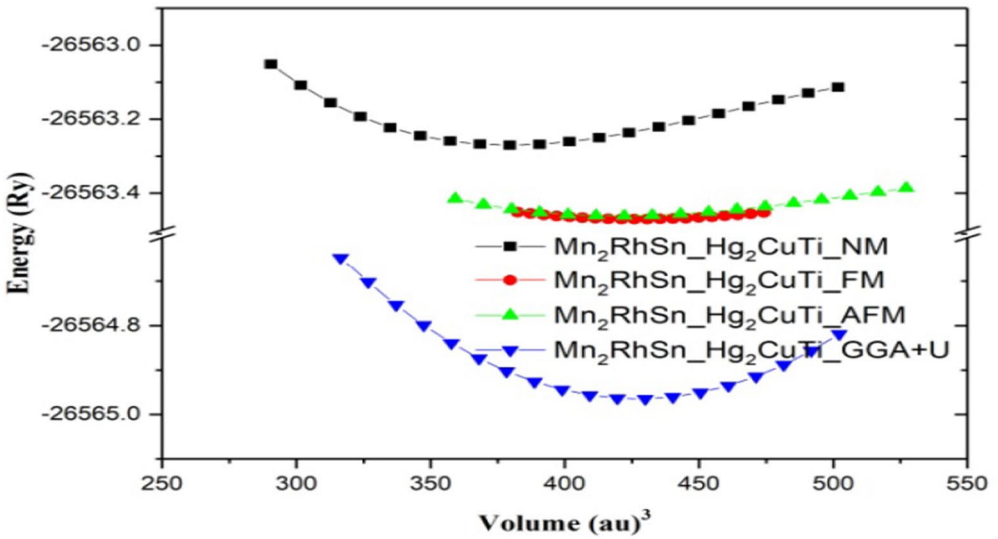
-26563.0
-26563.2
-26563.4
-26564.8
-26565.0
Energy (Ry)
250 300 350 400 450 500 550
Volume (au)³
Mn2RhSn_Hg2CuTi_NM
Mn2RhSn_Hg2CuTi_FM
Mn2RhSn_Hg2CuTi_AFM
Mn2RhSn_Hg2CuTi_GGA+U

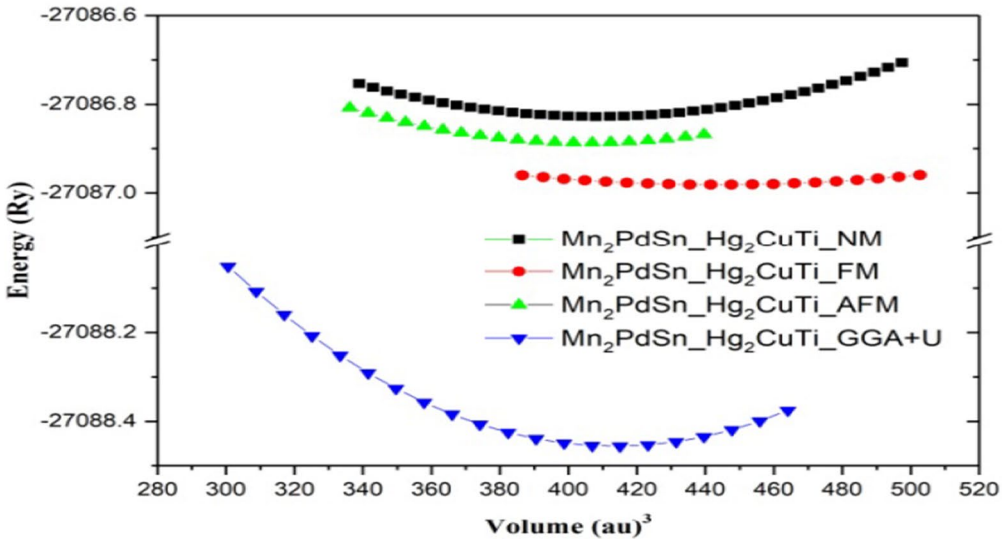
-27086.6
-27086.8
-27087.0
-27088.2
-27088.4
Energy (Ry)
280 300 320 340 360 380 400 420 440 460 480 500 520
Volume (au)³
Mn2PdSn_Hg2CuTi_NM
Mn2PdSn_Hg2CuTi_FM
Mn2PdSn_Hg2CuTi_AFM
Mn2PdSn_Hg2CuTi_GGA+U

◂**Fig. 3** Total energy as a function of unit cell volume for the Mn_2YAN (Y = Ru, Rh, and Pd) compounds in the Hg_2CuTi-type structure for the AFM, FM, and NM states, using the GGA + U.

interatomic distances. Under an applied pressure, the arrangement of the atoms is changed, leading to a change in the physical properties of the materials.[57] Hydrostatic pressure is described by the following Murnaghan equation of states:

$$P = \frac{B_0}{B_0'}\left[\left(\frac{V_0}{V}\right)^{B_0'} - 1\right] \tag{4}$$

where P, V_0 , and V denote the pressure, volume at pressure zero, and certain pressure, respectively. B_0 and B_0' are the bulk modulus and its pressure derivative, respectively.

The lattice constant results are evaluated as a function of pressure by the following relationship:

$$a(P) = a_0\left[1 + P\left(\frac{B_0'}{B}\right)\right]^{-\frac{1}{3B_0'}} \tag{5}$$

where a_0 is the equilibrium lattice parameter of the unit cell.

In the following, we also investigate the stability of the Mn_2YAN (Y = Ru, Rh and Pd) Heusler compounds for both Hg_2CuTi- and Cu_2MnAl-type structures under hydrostatic pressure via calculating the magnetic moments.

From Fig. 6, the impact of the pressure on the lattice constant values a (Å) for Mn_2YAN (Y = Ru, Rh, and Pd) in the range of pressure from 10 to 50 GPa can be seen. For $P = 0$ GPa, the results are listed in Table I. We can see from Fig. 6 that the lattice parameter values decrease with the pressure increasing from 10 to 50 GPa.

The evaluated PDOS and TDOS of Mn_2RuSn and Mn_2RhSn with Hg_2CuTi-type structures at pressures of 10 GPa are shown in Fig. 7 to better understand the nature of the pressure effect, where the Fermi level is positioned at 0 eV, while the obtained results of the total spin magnetic moments under pressure are tabulated in Table III. For all three compounds (Mn_2RuSn, Mn_2RhSn, and Mn_2PdSn), the impact of the pressure is remarkable. Table III shows a slight decrease in the values of the magnetic moments under pressure.

For the Hg_2CuTi type-structure of the Mn_2RuSn Heusler compound, the total magnetic moment is found to be decreased by applying pressure, and has an integer value equal to 2.001 μ_B of the magnetic moment at a pressure of 10 GPa, meaning that the material becomes a half-metal compound.

Table I Computed results of lattice constant a (Å), bulk modulus B (GPa), its derivative pressure, the minimum energy (Ry) and the formation energy EF (Ry) for Mn_2RuSn, Mn_2RhSn, and Mn_2PdSn Heusler compounds

		a (Å)	B (GPa)	B'	E (Ry)	E_f(Ry)
Mn_2RuSn	Hg_2CuTi					
	AFM	6.16	130.33	6.32	− 26,056.526276	
	FM	6.30	112.71	4.68	− 26,056.576045	
		6.21[56]				
		6.25[23]				
	GGA + U	6.09	206.20	4.48	− 26,057.468437	− 1.24
	Cu_2MnAl					
	FM	6.30	143.66	4.87	− 26,056.558177	
		6.27[23]				
	GGA + U	6.56	89.72	4.79	− 26,057.432544	− 1.21
Mn_2RhSn	Hg_2CuTi					
	AFM	6.28	126.15	5.24	− 26,563.440450	
	FM	6.32	131,65	5,26	− 26,563.461340	
	GGA + U	6.41	127.55	4.04	− 26,566.954625	− 1.10
	Cu_2MnAl					
	FM	6.35	118.87	5.14	− 26,563.422655	
	GGA + U	6.56	110.90	3.79	− 26,566.324149	− 1.05
Mn_2PdSn	Hg_2CuTi					
	AFM	6.38	97.92	5.03	− 27,086.89064	
	FM	6.37	138.66	4.84	− 27,086.974857	
		6.35[27]				
	GGA + U	6.53	95.08	4.35	− 27,088.503522	− 0.97
	Cu_2MnAl					
	FM	6.43	96.15	4.86	− 27,086.960158	
	GGA + U	6.10	179.29	5.49	− 27,088.428592	− 0.96

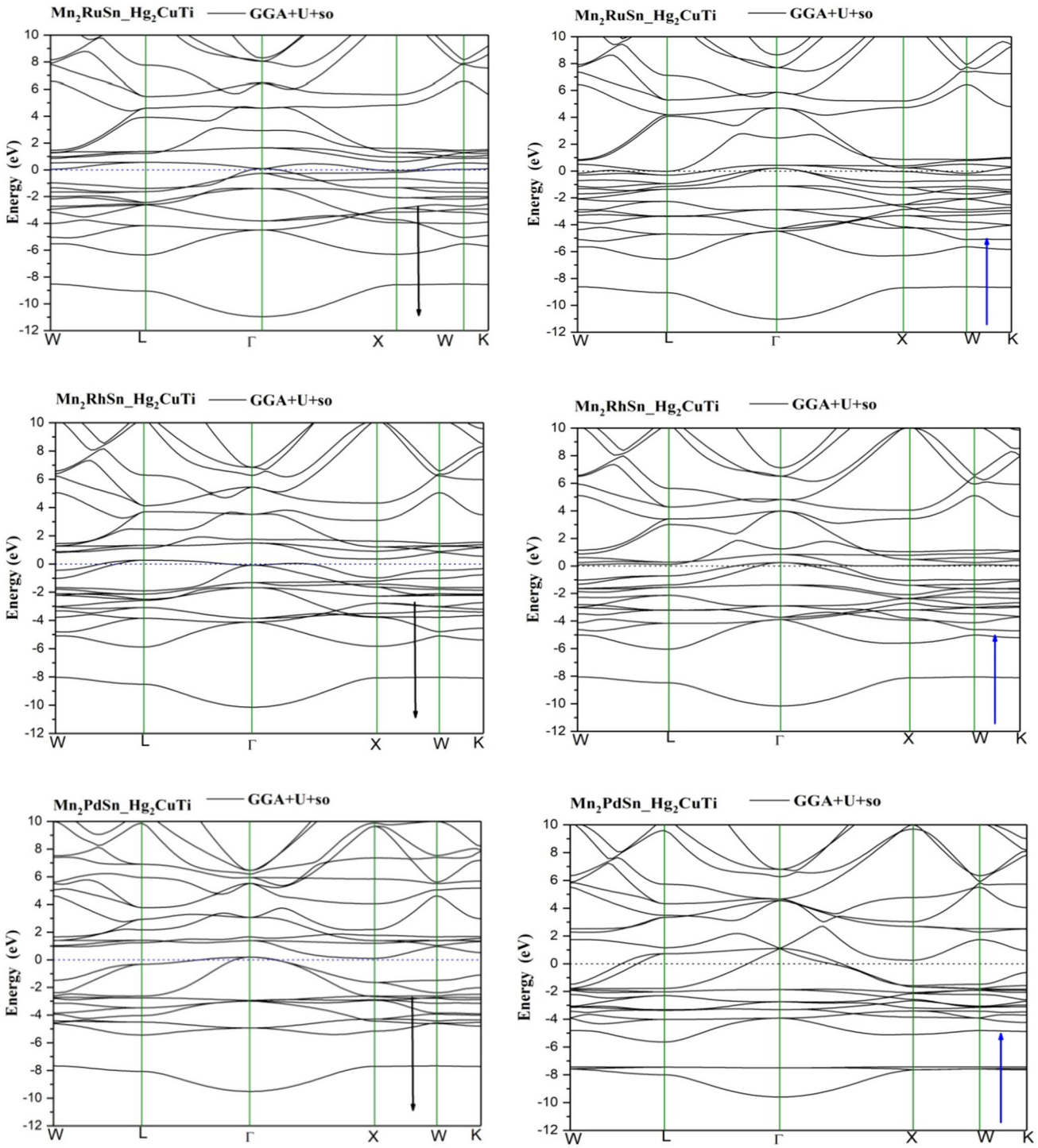

Fig. 4 Spin-polarized band structure of the Mn_2YAN (Y = Ru, Rh, and Pd) alloys.

The pressure effect is better understood by the electronic DOS. The PDOS and TDOS at the transition pressure (10 GPa) from metallic to half-metallic is presented in Fig. 7. The TDOS illustrates that the minority spin states display a band gap between the valence and conduction bands, whereas the majority spin states depict a metallic nature. For the Hg_2CuTi structure, the Mn_2RuSn Heusler alloy behavior indicates a semiconductor nature for the minority spin states and a metallic nature for the majority spin states, confirming the half-metallic character of the title alloy at a pressure of 10GPa. For the Mn_2RhSn Heusler compound in a Hg_2CuTi-type structure, the magnetic

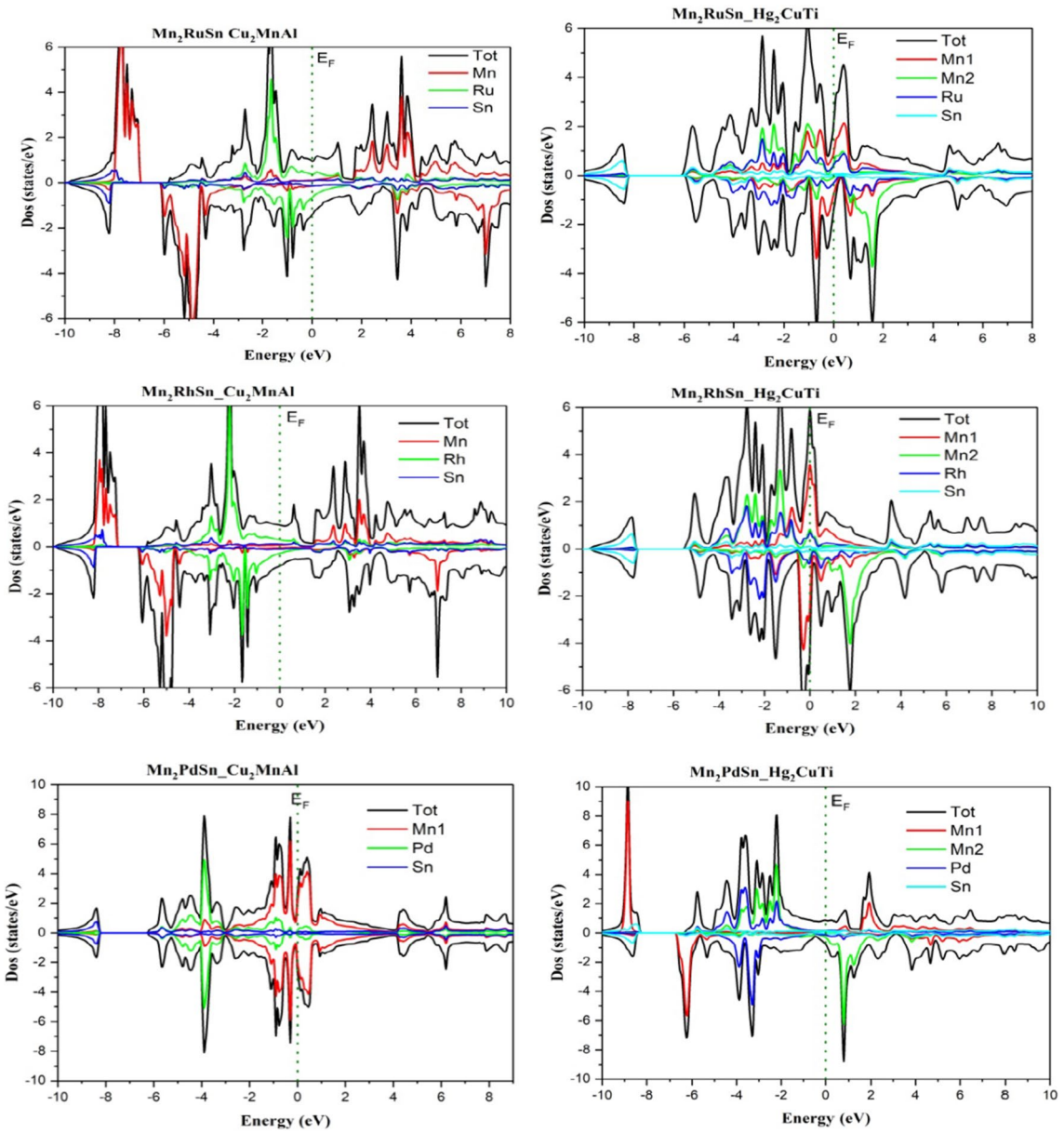

Fig. 5 Computed results of SP-TDOS and SP-PDOS for Mn_2YAN (Y = Ru, Rh, and Pd) with both Cu_2MnAl- and Hg_2CuTi-type structures.

Table II Computed results of atomic resolved and total and interstitial magnetic moments (in μ_B) per unit cell of Mn_2YAN(Y = Ru, Rh, Pd)

Compound	Phase	M_{tot}	M_{Mn1}	M_{Mn2}	M_y	M_{Sn}	M_{int}
Mn_2RuSn	Hg_2CuTi (FM) GGA	7.14564	3.41643	3.41949	0.27656	− 0.06333	0.0465
	GGA + U	2.33380	− 0.18683	2.42697	0.04448	− 0.01399	0.06318
Mn_2RhSn	Hg_2CuTi (FM) GGA	7.41157	3.40885	3.58783	0.41643	− 0.07263	0.07108
	GGA + U	3.47694	− 0.27589	3.31491	0.27987	− 0.02762	0.18568
Mn_2PdSn	Hg_2CuTi (FM) GGA	6.33069	2.71351	3.41314	0.20341	− 0.06890	0.06952
	GGA + U	3.54842	− 0.66074	3.60234	0.20534	0.0629	0.33848

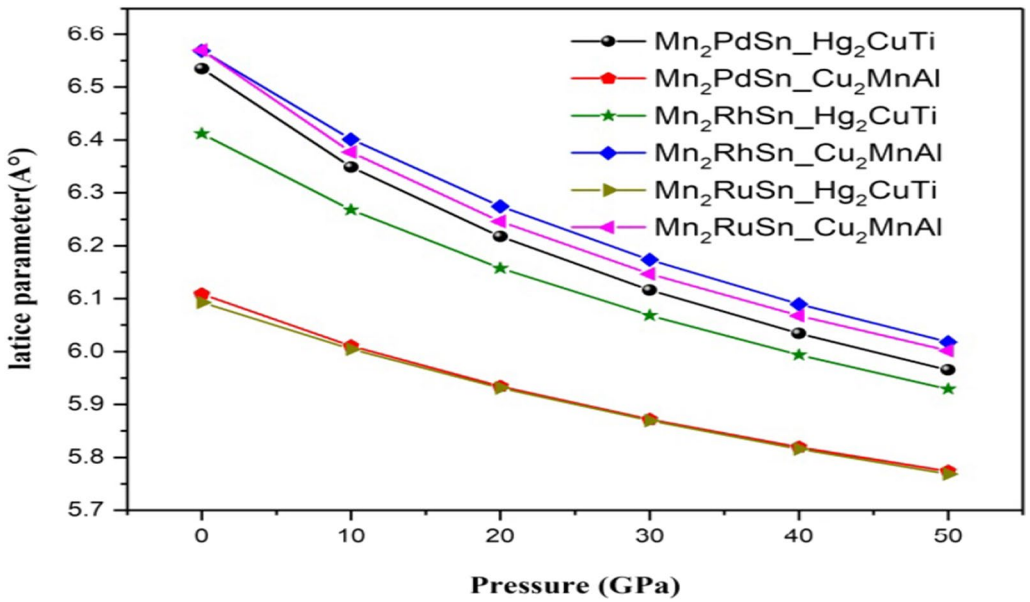

Fig. 6 Lattice parameters as a function of pressure.

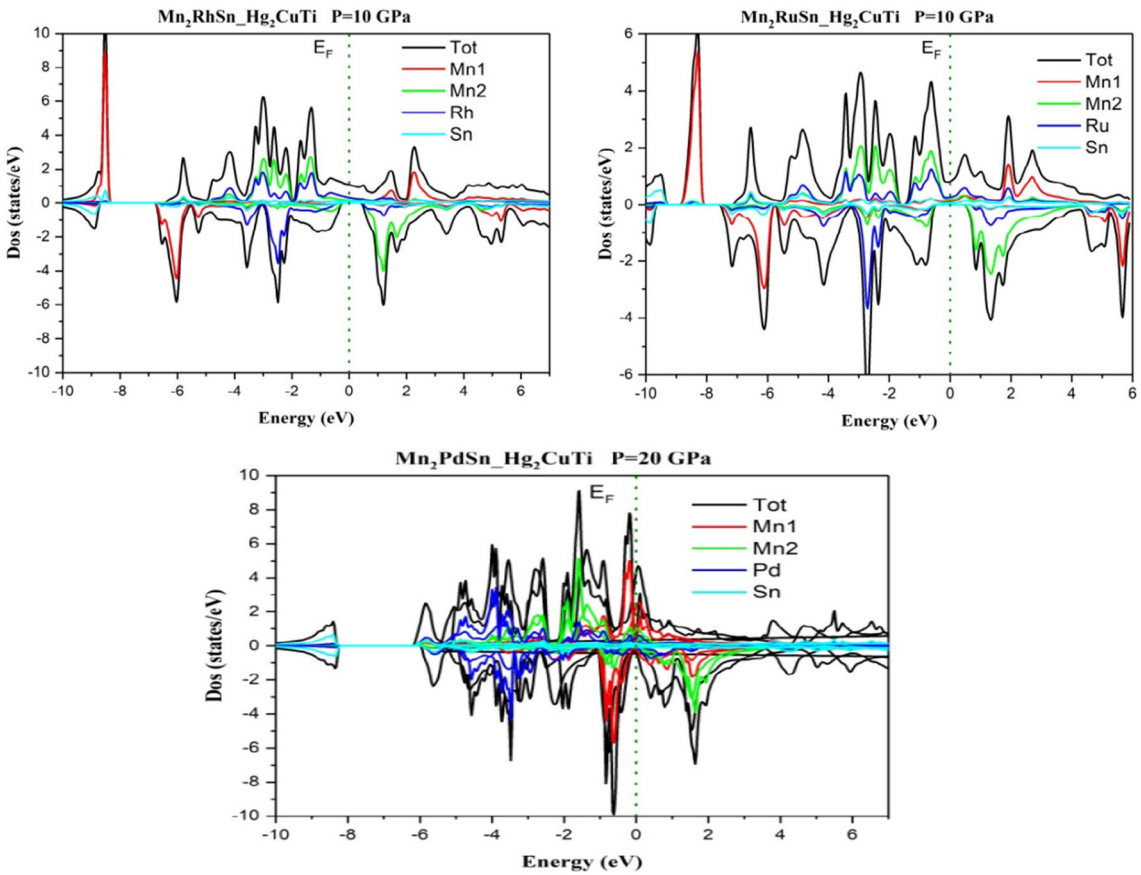

Fig. 7 TDOS and PDOS under a pressure of 10GPa for Mn_2RuSn and Mn_2RhSn, and under a pressure of 20 GPA for Mn_2PdSn with Hg_2CuTi-type structure.

Table III Total magnetic moment as a function of the pressure of Mn_2YAN (Y = Ru, Rh, and Pd) compounds in a Hg_2CuTi-type structure

	P (GPa)	Total magnetic moment (μ_B) GGA + U
Mn_2RuSn	10	2.001
	20	1.985
	30	1.972
	40	1.97
	50	1.97
Mn_2RhSn	10	2.999
	20	2.98
	30	2.97
	40	2.965
	50	2.952
Mn_2PdSn	10	3.18
	20	3.06
	30	2.89
	40	2.85
	50	2.852

moment decreases as a function of the pressure ,and passes through an integral value of about 2.99 under the pressure of 10GPa for the Hg_2CuTi-type structure. At this value of pressure, the compound changes in character. This result is also verified from the DOS plots. The TDOS clearly shows that the majority spin states endorse the metallic states, whereas the minority states highlight a gap for Hg_2CuTi at 10GPa, which means that the Mn_2RhSn Heusler compound becomes half-metallic under applied pressure. At a pressure of 20 GPa, the Mn_2PdSn compound becomes half-metal. The overlapping of the Mn 3d and Y 4d (Y = Ru, Rh, Pd) states in the building of electronic energy bands is the most notable aspect of the partial DOS, implying hybridization between the Mn and Y (Y = Ru, Rh, Pd) states during compound synthesis.

Conclusions

By employing first-principles DFT-based methodology, the structural, electronic, and magnetic properties of the Heusler ternary compounds, Mn_2YAN (Y = Ru, Rh and Pd) have been examined in both types of structure (Hg_2CuTi and Cu_2MnAl). The calculations were performed at zero pressure and under pressure. To do so, the PBE-GGA and GGA + U approaches of exchange–correlation energy/potential functional were used. In addition to GGA + U, spin–orbit coupling was also used for the calculation of the electronic and magnetic properties. Our computed results were found to be in good agreement with the available experimental measurements and theoretical data. The obtained results show that all the investigated materials behave as metal at zero pressure. However, at an elevated pressure 10GPa, half-metallicity was noted for Mn_2RuSn and Mn_2RhSn in a Hg_2CuTi-type structure, while for Mn_2PdSn, half-metallicity was also observed at 20 GPa for its Hg_2CuTi-type structure.

Acknowledgments The author Bin-Omran acknowledges Researchers Supporting Project Number (RSP-2021/82), King Saud University, Riyadh, Saudi Arabia.

Conflict of interests The authors declare that they have no conflict of interest.

References

1. F. Heusler, W. Starck, and E. Haupt, Magnetisch-chemische studien. *Verh. Dtsch. Phys. Ges.* 5, 219 (1903).
2. H. Itoh and J. Inoue, Spin Polarization at the Interface and Tunnel Magnetoresistance. *J. Magn. Magn. Mater.* 226, 930 (2001).
3. I. Žutić, J. Fabian, and S.D. Sarma, Spintronics: Fundamentals and Applications. *Rev. Mod. Phys.* 76, 323 (2004).
4. S. Qi, J. Shen, and C.H. Zhang, First-Principles Study on the Structural, Electronic and Magnetic Properties of the Ti_2VZ (Z= Si, Ge, Sn) Full-Heusler Compounds. *Mater. Chem. Phys.* 164, 177 (2015).
5. J. Li, H. Liu, Z. Zhang, S. Zhang, and X. Xu, Obtaining Half-Metallic Ferrimagnetism and Antiferromagnetism by Doping Mn and Fe for DO_3-type Heusler Compound Cr_3Si. *J. Alloys Compd.* 597, 8 (2014).
6. C. Felser, G.H. Fecher, and B. Balke, Spintronics: A Challenge for Materials Science and Solid-State Chemistry. *Angew. Chem. Int. Ed.* 46, 668 (2007).
7. S. Amari, F. Dahmane, S. Bin Omran, B. Doumi et al., Theoretical Investigation of the Structural, Magnetic and Band Structure Characteristics of $Co_2FeGe_{1-x}Si_x$ (x = 0, 0.5, 1) full-Heusler alloys. *J. Korean Phys. Soc.* 69, 1462 (2016).
8. F. Dahmane, A. Tadjer, B. Doumi, and H. Aourag, First-Principle Calculations of Structural, Electronic, and Magnetic Properties of Cubic $Al_{1-x}TM_xN$ (TM= V, Cr, Mn, Fe). *J. Supercond. Nov. Magn.* 27, 2647 (2014).
9. A. Zerouali, A. Mokaddem, B. Doumi, F. Dahmane, M. Elkeurti, A. Sayede et al., First-Principle Calculations of Electronic and Ferromagnetic Properties of $Al_{1-x}V_xSb$. *J. Comput. Electron.* 15, 1255 (2016).
10. R. Weht and W.E. Pickett, Half-Metallic Ferrimagnetism in Mn_2VAl. *Phys. Rev. B* 60, 13006 (1999).
11. G. Liu, X. Dai, H. Liu, J. Chen, Y. Li, G. Xiao et al., Mn_2CoZ (Z= Al, Ga, Iin, Si, Ge, Sn, Sb) Compounds: Structural, Electronic, and Magnetic Properties. *Phys. Rev. B* 77, 014424 (2008).
12. S. Kervan and N. Kervan, Half-Metallic Properties of the $CuHg_2Ti$-Type Mn_2ZnSi Full-Heusler Compound. *Curr. Appl. Phys.* 13, 80 (2013).
13. X.P. Wei, J.B. Deng, S.B. Chu, G.Y. Mao, T. Lei, and X.R. Hu, Half-Metallic Ferrimagnetism in Full-Heusler Alloy Mn_2CuMg. *J. Magn. Magn. Mater.* 323, 185 (2011).
14. X. Dai, G. Liu, L. Chen, J. Chen, and G. Wu, Mn_2 CoSb Compound: Structural, Electronic, Transport and Magnetic Properties. *Solid State Commun.* 140, 533 (2006).

15. H. Luo, Z. Zhu, L. Ma, S. Xu, X. Zhu, C. Jiang et al., Effect of Site Preference of 3D Atoms on the Electronic Structure and Half-Metallicity of Heusler Alloy Mn_2YAl. *J. Phys. D Appl. Phys.* 41, 055010 (2008).
16. Y. Xin, H. Hao, Y. Ma, H. Luo, F. Meng, H. Liu et al., Competition of XA and L21B Ordering in Heusler Alloys Mn_2CoZ (Z= Al, Ga, Si, Ge and Sb) and Its Influence on Electronic Structure. *Intermetallics* 80, 10 (2017).
17. X.P. Wei, X.R. Hu, G.Y. Mao, S.B. Chu, T. Lei, L.B. Hu et al., Half-Metallic Ferrimagnetism in Mn_2CuGe. *J. Magn. Magn. Mater.* 322, 3204 (2010).
18. H. Luo, H. Zhang, Z. Zhu, L. Ma, S. Xu, G. Wu et al., Half-Metallic Properties for the Mn_2FeZ (Z= Al, Ga, Si, Ge, Sb) Heusler Alloys: A First-Principles Study. *J. Appl. Phys.* 103, 083908 (2008).
19. X.P. Wei, X.R. Hu, S.B. Chu, G.Y. Mao, L.B. Hu, T. Lei et al., A First Principles Study on the Full-Heusler Compound Mn_2CuSi. *Phys. B: Condens. Matter* 406, 1139 (2011).
20. H. Luo, Z. Zhu, G. Liu, S. Xu, G. Wu, H. Liu et al., Prediction of Half-Metallic Properties for the Heusler Alloys Mn_2CrZ (Z= Al, Ga, Si, Ge, Sb): A First-Principles Study. *J. Magn. Magn. Mater.* 320, 421 (2008).
21. Z. Ren, Y. Liu, S. Li, X. Zhang, and H. Liu, Site Preference and Electronic Structure of Mn_2RhZ (Z = Al, Ga, In, Si, Ge, Sn, Sb): A Theoretical Study. *Mater. Sci. Pol.* 34, 251 (2016).
22. A. Nelson, P. Kharel, Y. Huh, R. Fuglsby, J. Guenther, W. Zhang et al., Enhancement of Curie Temperature in Mn_2RuSn by Co Substitution. *J. Appl. Phys.* 117, 153906 (2015).
23. J. Chen, H. Luo, P. Jia, F. Meng, G. Liu, E. Liu et al., Site Preference and Electronic Structure of Mn_2RuSn: A Theoretical Study. *J. Magn. Magn. Mater.* 365, 132 (2014).
24. D.C. Gupta and I.H. Bhat, Investigation of High Spin-Polarization, Magnetic, Electronic and Half-Metallic Properties in $RuMn_2Ge$ and $RuMn_2Sb$ Heusler Alloys. *Mater. Sci. Eng. B* 193, 70 (2015).
25. D.C. Gupta and I.H. Bhat, A First-Principles Study of $RuMn_2Si$: Magnetic, Electronic and Mechanical Properties. *J. Alloys Compd.* 575, 292 (2013).
26. K. Shimosakaida and S. Fujii, Atomic Arrangement and Magnetic Order in Mn_2RuZ (Z= Sn, Si). *Mater. Trans.* 57, 312 (2016).
27. X. Xu, T. Kanomata, M. Hayasaka, R. Umino, K. Endo, H. Nishihara et al., Magnetic Properties of Mn_2PdSn and Mn_2PdIn. *J. Magn. Magn. Mater.* 401, 618 (2016).
28. N. Kaur, V. Srivastava, and S.A. Dar, GGA Based Study on Electronic Structure and Thermoelectric Properties of Mn_2PtCo Full-Heusler Compound. *Indian J. Phys.* 96, 71 (2022).
29. Z. Wu, Y. Zhang, Z. Liu, and X. Ma, Influence of Symmetry from Crystal Structure and Chemical Environments of Magnetic Ions on the Fully Compensated Ferrimagnetism of Full Heusler Cr_2YZ and Mn_2YZ Alloys. *Symmetry* 14, 988 (2022).
30. D.M. Hoat, N.H. Giang, M. Naseri, R. Ponce-Perez, J.F. Rivas-Silva, and G.H. Cocoletzi, Mn_2CoX (X = P and As) Full-Heusler Compounds for Spintronic Applications: Half-Metallicity and Elastic Properties. *Phys. Lett. A* 384, 126589 (2020).
31. L. Feng, X. Feng, E.K. Liu, W.H. Wang, G.H. Wu, J.F. Hu, and W.X. Zhang, Principles, Possible Martensitic Transformation in Heusler Alloy Mn_2PdSn from First Principle. *J. Magn. Magn. Mater.* 419, 543 (2016).
32. V. Alijani, O. Meshcheriakova, J. Winterlik, G. Kreiner, G.H. Fecher, and C. Felser, Increasing Curie Temperature in Tetragonal Mn_2RhSn Heusler Compound Through Substitution of Rh by Co and Mn by Rh. *J. Appl. Phys.* 113, 063904 (2013).
33. A. Nelson, P. Kharel, Y. Huh, R. Fuglsby, J. Guenther, W. Zhang, B. Staten, P. Lukashev, S. Valloppilly, and D.J. Sellmyer, Enhancement of Curie Temperature in Mn_2RuSn by Co Substitution. *J. Appl. Phys.* 117, 153906 (2015).
34. J. Winterlik, S. Cadov, A. Gupta, V. Alijani, T. Gasi, K. Filsinger, B. Balke, and G.H. Fecher, Design Scheme of New Tetragonal Heusler Compounds for Spin-Transfer Torque Applications and Its Experimental Realization. *Adv. Mater.* 24, 6283 (2012).
35. O. Meshcheriakova, S. Chadov, A.K. Nayak, U.K. Rößler, J. Kübler, G. André, A.A. Tsirlin, J. Kiss, S. Hausdorf, A. Kalache, and W. Schnelle, Large Noncollinearity and Spin Reorientation in the Novel Mn_2RhSn Heusler Magnet. *Phys. Rev. Lett.* 113, 087203 (2014).
36. D. Bensaid, T. Hellal, M. Ameri, Y. Azzaz, B. Doumi, and Y. Al-Douri, First-Principle Investigation of Structural, Electronic and Magnetic Properties in Mn_2RhZ(Z=Si, Ge, and Sn) Heusler Alloys. *J. Supercond. Novel Magn.* 29, 1843 (2016).
37. K. Endo, T. Kanomata, H. Nishihara, and K.R.A. Ziebeck, Magnetic Properties of New Compounds $RuMn_2Sn$ and $RuMn_2Si$. *J. Alloys Compd.* 510, 1 (2012).
38. P. Blaha, K. Schwarz, G.K. Madsen, D. Kvasnicka, and J. Luitz, *wien2k. An Augmented Plane Wave+ Local Orbitals Program for Calculating Crystal Properties* (Techn. Universitat, 2001), p. 60.
39. J.P. Perdew, K. Burke, and M. Ernzerhof, Generalized Gradient Approximation Made Simple [Phys. Rev. Lett. 77, 3865 (1996)]. *Phys. Rev. Lett.* 78, 1396 (1997).
40. V.I. Anisimov, I.V. Solovyev, M.A. Korotin, M.T. Czyzyk, and G.A. Sawatzky, Density-functional Theory and NiO Photoemission Spectra. *Phys. Rev. B* 48, 16929 (1993).
41. A. Dahani, S. Kacimi, A. Boukortt, M. Bououdina, and A. Zaoui, DFT + *U* Analysis of Structural, Electronic, and Magnetic Properties of Mn–As–Sb Ternary Systems. *J. Supercond. Novel Magn.* 27, 2263 (2014).
42. S. Krishnaveni and M. Sundareswari, Band Gap Engineering in Ruthenium-Based Heusler Alloys for Thermoelectric Applications. *Int. J. Energy Res.* 42, 764 (2017).
43. F.Z. Benkhelifa, A. Lekhal, and S. Méçabih, GGA and GGA+U Description of Structural, Magnetic, and Elastic Properties of Rh_2MnZ (Z=Ge, Sn, and Pb). *J. Supercond. Novel Magn.* 26, 2573 (2013).
44. B. Hamri, B. Abbar, A. Hamri, O. Baraka, A. Hallouche, and A. Zaoui, Electronic Structure and Mechanical Properties of X_2MnSn (X= Cu, Ni, Pd) Under Hydrostatic Pressure: GGA+U Calculations. *Comput. Condens. Matter* 3, 14 (2015).
45. Y. Han, Z. Chen, M. Kuang, Z. Liu, X. Wang, and X. Wang, Scandium-Based Full Heusler Compounds: A Comprehensive Study of Competition Between XA and L21 Atomic Ordering. *Results Phys.* 12, 435 (2019).
46. Wu. Mengxin, F. Zhou, R. Khenata, M. Kuang, and X. Wang, Phase Transition and Electronic Structures of All-d-Metal Heusler-Type X_2MnTi Compounds (X = Pd, Pt, Ag, Au, Cu, and Ni). *Front. Chem.* 8, 546947 (2020).
47. D. Amari, M. Mokhtari, F. Dahmane, T. Belfarh, A. Tabeti, M. Elkeurti et al., A Comparative Study Between Hg_2CuTi and Cu_2MnAl Type Structures for Zr_2CoZ (Z= Al, Ga, In) Heusler Alloys. *Chin. J. Phys.* 60, C450 (2019).
48. H. Zenasni, H. Faraoun, and C. Esling, First-Principle Prediction of Half-Metallic Ferrimagnetism in Mn-Based Full-Heusler Alloys with Highly Ordered Structure. *J. Magn. Magn. Mater.* 333, 162 (2013).
49. T. Song, X. Sun, J. Tian, X. Wei, and G. Wan, The Effect of Pressure on the Structural, Electronic, Magnetic, and Thermodynamic Properties of the Mn_2RuGe Inverse Heusler Alloy. *J. Magn. Magn. Mater.* 428, 287 (2017).
50. L. Yang, B. Liu, H. Luo, F. Meng, H. Liu, E. Liu et al., Investigation of the Site Preference in Mn_2RuSn Using KKR-CPA-LDA Calculation. *J. Magn. Magn. Mater.* 382, 247 (2015).

51. L. Yang, B. Liu, F. Meng, H. Liu, H. Luo, E. Liu et al., Magnetic Properties of Heusler Alloy Mn_2RuGe and Mn_2RuGa Ribbons. *J. Magn. Magn. Mater.* 379, 1 (2015).
52. N. Kervan, S. Kervan, O. Canko, M. Atiş, and F. Taşkın, Half-Metallic Ferrimagnetism in the Mn_2NbAl Full-Heusler Compound: A First-Principles Study. *J. Supercond. Novel Magn.* 29, 187 (2016).
53. H. Luo, B. Liu, Y. Xin, P. Jia, F. Meng, E. Liu et al., Martensitic Transformation in Heusler Alloys Mn_2YIn (Y= Ni, Pd and Pt): Theoretical and Experimental Investigation. *J. Magn. Magn. Mater.* 395, 190 (2015).
54. Y.-N. Duan, X.-X. Fan, A. Kutluk, X.-J. Du, Z.-W. Zhang, and Y.-L. Song, Possible Martensitic Transformation and Ferrimagnetic Properties in Heusler Alloy Mn_2NiSn. *J. Magn. Magn. Mater.* 386, 102 (2015).
55. F. Murnaghan, The Compressibility of Media Under Extreme Pressures. *Proc Natl Acad Sci USA* 30, 244 (1944).
56. A. Nelson, P.K., Y. Huh, R. Fuglsby, J. Guenther, W. Zhang, B. Staten, P. Lukashev, S. Valloppilly, D.J. Sellmyer, Enhancement of Curie temperature in Mn_2RuSn by Co substitution. *J. Appl. Phys.* 117, 153906 (2015)
57. G.J. Ackland, High-Pressure Phases of Group IV and III–V Semiconductors. *Rep. Prog. Phys.* 64, 483 (2001).

Condensed Matter Physics, 2021, Vol. 24, No. 2, 23703: 1–9
DOI: 10.5488/CMP.24.23703
http://www.icmp.lviv.ua/journal

CONDENSED MATTER PHYSICS

First-principles investigation of half-metallic ferromagnetism of Fe_2YSn (Y=Mn, Ti and V) Heusler alloys

M. Sayah[1], S. Zeffane[1], M. Mokhtari[1,2], F. Dahmane[1,3], L. Zekri[2], R. Khenata[3], N. Zekri[2]

[1] Département de SM, Institut des Sciences et des Technologies, Centre Universitaire de Tissemsilt, 38000 Tissemsilt, Algérie

[2] Université des Sciences et de la Technologie d'Oran Mohamed Boudiaf, USTO-MB, LEPM, BP 1505, El M' Naouar, 31000 Oran, Algeria

[3] Laboratoire de Physique Quantique et de Modélisation Mathématique (LPQ3M), Département de Technologie, Université de Mascara, 29000 Mascara, Algérie

Received April 28, 2020, in final form February 22, 2021

In this paper, we use the first-principles calculations based on the density functional theory to investigate structural, electronic and magnetic properties of Fe_2YSn with (Y = Mn, Ti and V). The generalized gradient approximation (GGA) method is used for calculations. The Cu_2MnAl type structure is energetically more stable than the Hg_2CuTi type structure. The negative formation energy is shown as the evidence of thermodynamic stability of the alloy. The calculated total spin moment is found as $3\mu_B$ and $0\mu_B$ at the equilibrium lattice constant for Fe_2MnSn and Fe_2TiSn respectively, which agrees with the Slater-Pauling rule of $M_t = Z_t - 24$. The study of electronic and magnetic properties proves that Fe_2MnSn and Fe_2TiSn full-Heusler alloys are complete half-metallic ferromagnetic materials

Key words: *Heusler alloy, electronic structure, first-principle calculations, half-metallicity*

1. Introduction

In 1983, de Groot et al [1] established the half-metallicity in NiMnSb half Heusler alloy. Later, through theoretical calculations and experiments, many compounds were found to be half-metals, including Heusler alloys [2, 3], alkali metal or transition metal chalcogenides [4], doped diluted magnetic semiconductors [5, 6], zinc-blende and wurtzite structural compounds [7]. Considering the standing great potential advantages, spintronics still faces some challenges, such as generation of high spin injectors [8]. In recent years, Heusler alloys received an insistent attention due to their interesting physical properties [9–11], their remarkable electronic structure makes it possible to use them in various spintronic devices such as spin-transfer torque and large magneto-resistance spinvalves devices [12]. Heusler alloys are ternary inter-metallic compounds, which were first discovered by Heusler in 1903 [13]. This remarkable material and its relatives, which by now comprise a vast collection of more than 1000 compounds, are now known as Heusler compounds. They are ternary semiconducting or metallic materials with a 1:1:1 (also known as "half-Heusler") or a 2:1:1 stoichiometry (also known as "full-Heusler") [13]. Several Fe-based Heusler alloys have already been studied, though due to the differences in their experimental and theoretical results further investigations are still being carried out [3, 13]. This paper is structured as follows: in section 2, we briefly describe the computational method used in this work. Results and discussions of our study are presented in section 3. Finally, a summary of the work is given in section 4.

2. Method of description

The first-principle calculations of Fe_2YSn (Y = Mn, Ti, and V) alloys are performed based on the density functional theory (DFT) [14], which is implemented in WIEN2k code [15]. The solution of the Kohn-Sham equation [14] is done using the full potential linearized augmented plane wave (FP-LAPW) method [15]. The exchange correlation potential is calculated using the Perdew-Burke-Ernzerhof parameterization of the generalized gradient approximation PBE-GGA [16]. In the calculations reported in this paper, we use a parameter $RMT \times K_{\max} = 8$, which defines the matrix size convergence, where $K_{\max}$ is the plane wave cut-off and RMT is the smallest of all atomic sphere radii. In the full potential scheme, the whole crystal is divided into two different parts: the first part is the atomic sphere while the second part includes the interstitial regions. Moreover, the valence wave function inside the muffin-tin (MT) sphere was expanded up to $I_{\max} = 10$, while the charge density was Fourier expanded up to $G_{\max} = 12$ a.u^{-1}. The self-consistent calculations are considered to be converged when the total energy of the system is stable within 10^{-4} Ry.

3. Results and discussions

There are three distinct families of Heusler compounds: the first one with the composition 1:1:1 and the second one with 2:1:1 stoichiometry and the third is 1:1:1:1. The compounds of the first family have the general formula XYZ and crystallize in a non-centro symmetric cubic structure; the second family of Heusler alloys has a formula X_2YZ with two types of structures the Hg_2CuTi and Cu_2MnAl. The two phases consist of four inter-penetrating fcc sub-lattices, which have four crystal sites, A(0, 0, 0), B(0.25, 0.25, 0.25), C(0.50, 0.50, 0.50) and D(0.75, 0.75, 0.75). For Hg_2CuTi type structure, the chain of atoms occupies the four sites of unit cell X-X-Y-Z and for Cu_2MnAl the Y and the second X atom exchange sites. In the Hg_2CuTi type structure, the X atoms entering sites A and B are denoted as X(1) and X(2), respectively [13]. The third family has a formula of XX'YZ and crystallize in the LiMgPdSn type crystal structure. For the Heusler alloys X_2YZ, the X and Y are both a transition metal, and Z is the main group element. In order to establish a stable structure and equilibrium structural parameters of Fe_2ZSn (Z = Mn, Ti and V) compounds, structural optimizations were performed on these alloys for both Cu_2MnAl and Hg_2CuTi type structures and their total energy-volume curves are shown in figure 1. In X_2YZ Heusler alloys, if the Y atomic number is superior to that of X atom from the same period, an inverse Heusler structure with Hg_2CuTi type as the prototype is observed. It is seen from these E-V curves that the Cu_2MnAl type structure is more stable than the Hg_2CuTi phase for the Fe_2YSn with Y = Mn, Ti, V compounds at ambient conditions. The nuclear charge of X atom (Fe) is larger than Y atom (Y = Mn, Ti and V). Consequently, the Cu_2MnAl structure will be visibly observed as can be seen from figure 1. The minimum of the curve is the calculated equilibrium lattice constant. The lattice constant a, bulk modulus B and its pressure derivative B' at zero pressure, for the structures Cu_2MnAl and Hg_2CuTi are calculated using Murnaghan equation of state [17].

$$E(V) = E_0(V) + \frac{BV}{B'(B'-1)}\left[B\left(1-\frac{V_0}{V}\right) + \left(\frac{V_0}{V}\right)^{B'} - 1\right]. \tag{3.1}$$

Here E_0 is the minimum energy at $T = 0$ K, B is the bulk modulus, B' is the bulk modulus derivative and V_0 is the equilibrium volume. The results are listed in table 1. The calculated lattice constants of Fe_2YSn with (Y = Mn, Ti and V) are in good agreement with the previously theoretically optimized lattice constants reported by other researchers.

We study the phase stability of Fe_2YSn with (Y = Mn, Ti, V) based on the formation energy (ΔE_f). This can help to envisage whether these alloys can be prepared experimentally. Here, the formation energy (ΔE_f) is calculated by comparing the total energies of the Fe_2YSn (Y = Mn, Ti, and V) Heusler alloys with the sum of the total energies of the constituting elements. The formation energy of the Fe_2YSn (Y = Mn, Ti, and V) materials is computed following the expression given below:

$$\Delta E_f = E^{\text{total}}_{Fe_2YSn} - \left[E^{\text{bulk}}_{Fe} + E^{\text{bulk}}_{Y} + E^{\text{bulk}}_{Sn}\right]. \tag{3.2}$$

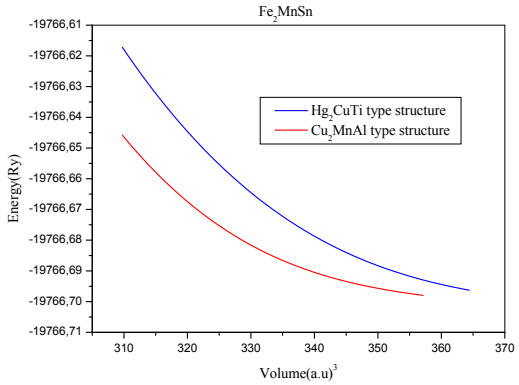

(a)

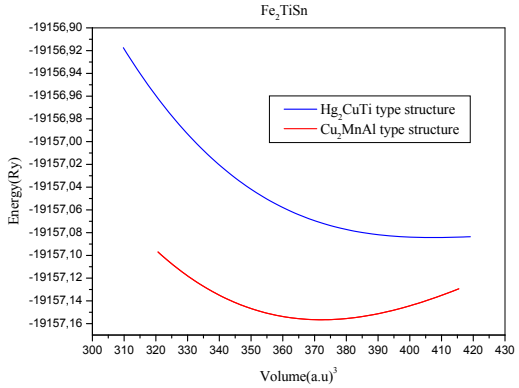

(b)

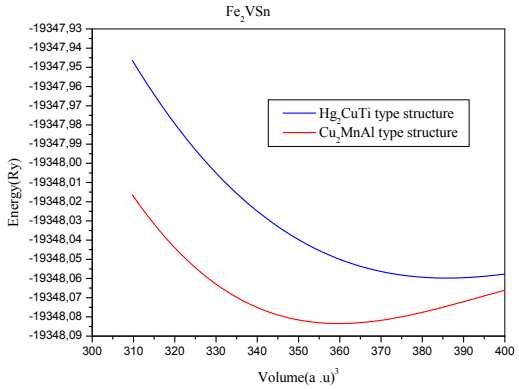

(c)

Figure 1. (Colour online) The calculated total energy of Fe_2YSn (Y = Mn, Ti and V) alloys with both Cu_2MnAl and Hg_2CuTi types structures as a function of the lattice constants for magnetic states.

Table 1. The calculated equilibrium lattice constant a (Å), the bulk modulus B (GPa), the minimum energy (Ry) and the formation energy E_f (Ry) of Fe_2YSn with (Y = Mn, Ti and V).

		a (Å)	B (GPa)	B'	Energy (Ry)	E_f (Ry)
Fe_2TiSn	Hg_2CuTi	6.2173	124.0086	4.9226	−19157.08477	−1.2578
	Cu_2MnAl	6.0436 6.03 [18] 6.04 [19] 6.04 [20]	191.5580	3.7601	−19157.15643	−1.2783
Fe_2VSn	Hg_2CuTi	6.1239 6.06 [21]	133.9734	5.0141	−19348.05986	−1.6761
	Cu_2MnAl	5.9824 5.99 [21]	142.7406	9.9780	−19348.08220	−1.6985
Fe_2MnSn	Hg_2CuTi	6.0843	110.4683	6.0807	−19766.69924	−1.3350
	Cu_2MnAl	5.9584 5.70 [22] 6.01 [23]	178.1479	5.2306	−19766.69677	−1.3425

Here $E^{\text{total}}_{Fe_2YSn}$ is the energy of the Hg_2CuTi type and Cu_2MnAl type structure under their equilibrium lattice constant for the Fe_2YSn with (Y = Mn, Ti and V) full Heusler alloys, and E^{bulk}_{Fe}, E^{bulk}_{Y}, E^{bulk}_{Sn} represent the total energy per atom for Fe, Y (Y = Mn, Ti, V), and Sn elements in the bulk form, respectively. The negative values of the formation energy specify that Fe_2YSn with (Y = Mn, Ti and V) full Heusler alloys are chemically stable, and these materials can be synthesized experimentally. The computed results of the Cu_2MnAl type structures are found more negative than those of the Hg_2CuTi types structures, proving that Cu_2MnAl type structures are more stable compared to the Hg_2CuTi type structures. In half-metallic Heusler compounds, the gap takes place in one spin state, whereas in the other spin state, EF cuts through the bands [24]. The d-band is principally responsible for the position of Fermi level lying in it. The responsibility of transition metals $3d$-states is very important in the description of spin polarized electronic band structures and densities of sates calculations [24]. At the equilibrium lattice constants, we have studied the electronic band structure calculations for all three compounds and have extracted the density of states (DOS) per f.u., which is presented in figure 2, figure 3 and figure 4. The electronic band structure shows the bonding and character of the electron bands. DFT is a standard tool for calculating the band structure for materials in order to determine different properties of solids [25, 26]. The responsibility of transition metals $3d$-states is very essential in the description of spin polarized electronic band structures and densities of sates calculations [24]. The electron spin polarization (SP) at EF of a material is defined as follows [23]

$$SP = \frac{\rho_{\uparrow}(E_f) - \rho_{\downarrow}(E_f)}{\rho_{\uparrow}(E_f) + \rho_{\downarrow}(E_f)}. \tag{3.3}$$

Here $\rho_{\uparrow}(E_f)$, $\rho_{\downarrow}(E_f)$ are the majority and minority densities of states at E_f. When the value of the electron spin polarization (SP) is 100%, alloys are supposed to be true half-metallic, and this is realized when any one of the DOS from the majority and minority spins is equal to zero and the other one is not equal to zero at EF [23]. Figure 2 presents the total density of states and band structure of Fe_2MnSn for both Cu_2MnAl and Hg_2CuTi type structures. From this figure, one can observe that the alloy exhibits half-metallic behavior with Cu_2MnAl type structure, described by an overlap between the bottom of the conduction band and the top of the valence band in spin-up. For spin-down, we can see a gap between the maximum of the valance band and the minimum of the conduction band, this gap being indirect between Γ and X points. For Hg_2CuTi type structure, both the majority and minority spin bands have metallic intersections at the Fermi level. We can see from figure 3 that the total DOS in spin-up and spin-down spin channels for Fe_2TiSn, is symmetrical in the majority and minority spin directions. Therefore, the non-magnetic character of these alloys can be estimated. In both spin directions, the energy gap is open

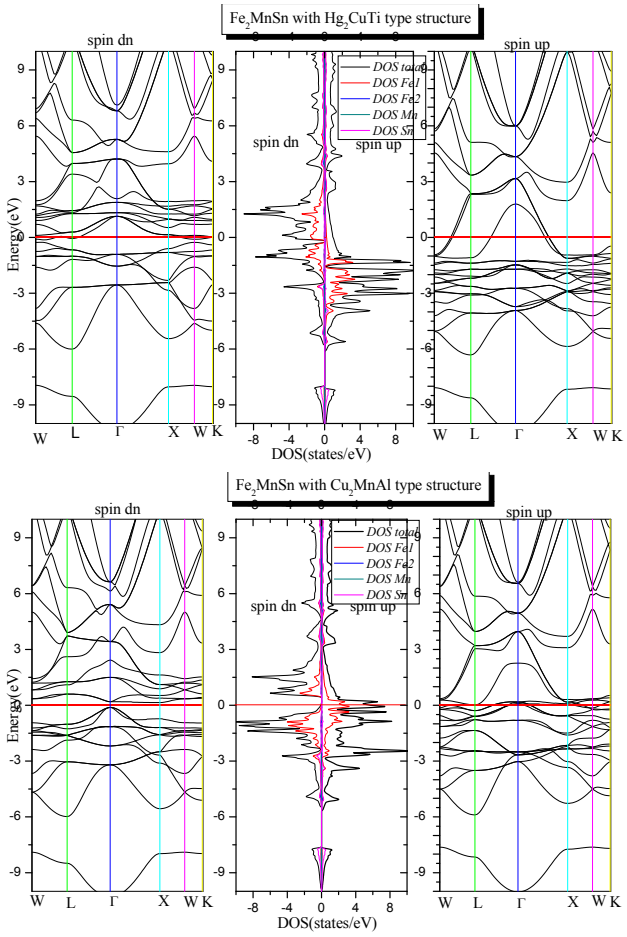

Figure 2. (Colour online) The calculated spin-polarized total and partial density of states and band structure of Fe_2MnSn with both Cu_2MnAl and Hg_2CuTi types structures.

around the Fermi level EF and divides the total DOS into bonding and anti-bonding parts. The formation of this gap is related to the hybridization of Fe and Ti d electrons. There is no contribution from titanium (Ti) and tin (Sn) to the density of states at the Fermi level. We presented the energy bands of Fe_2TiSn in figure 3. It can be seen that the energy gap in Fe_2TiSn is an indirect gap and the Fermi level locates just above the top of the valence band at the Γ point. The electronic band structures and the DOS of the Fe_2VSn compounds for both the Hg_2CuTi and Cu_2MnAl type structures are given in figure 4, the density of states of spin-up and spin-down occurs at Fermi level; as a result, Fe_2VSn is of a metallic character. Both the conduction and valence bands cross the Fermi level, thus diminishing the gap at EF. The metallic nature in this compound is principally due to the interaction between Sn-p and transition metal (TM)-3d states. The Fe-3d and Y-3d (Y = Mn, Ti, V) states are mainly occupied around the Fermi level with a maximum contribution towards the total DOS and, as a result, the corresponding bonding-anti-bonding states control the energy gap formation [27]. At the same time, the Sn atomic states are less active around the Fermi level in these materials. Thus, the observed band gap in these alloys is due to the typical $d - d$ hybridization between the valence states of Fe and Y atoms (Y = Mn, Ti and V). Skaftouros et al. [28] have presented fascinating arguments regarding possible hybridizations between d-orbitals of transition metals in the case of the X_2YZ Inverse Heusler compounds, e.g., Sc-based Heusler compounds. According to their report, the same symmetry of the X [1] and the Y atoms causes their d-orbitals to hybridize together creating five bonding d ($2 \times e_g$ and $3 \times t_{2g}$) and five non-bonding ($2 \times e_u$ and $3 \times t_u$) states. Then, the five X(1)-Y bonding d states hybridize with the d-orbital of the X(2) atoms and create bonding and anti-bonding states again (3).

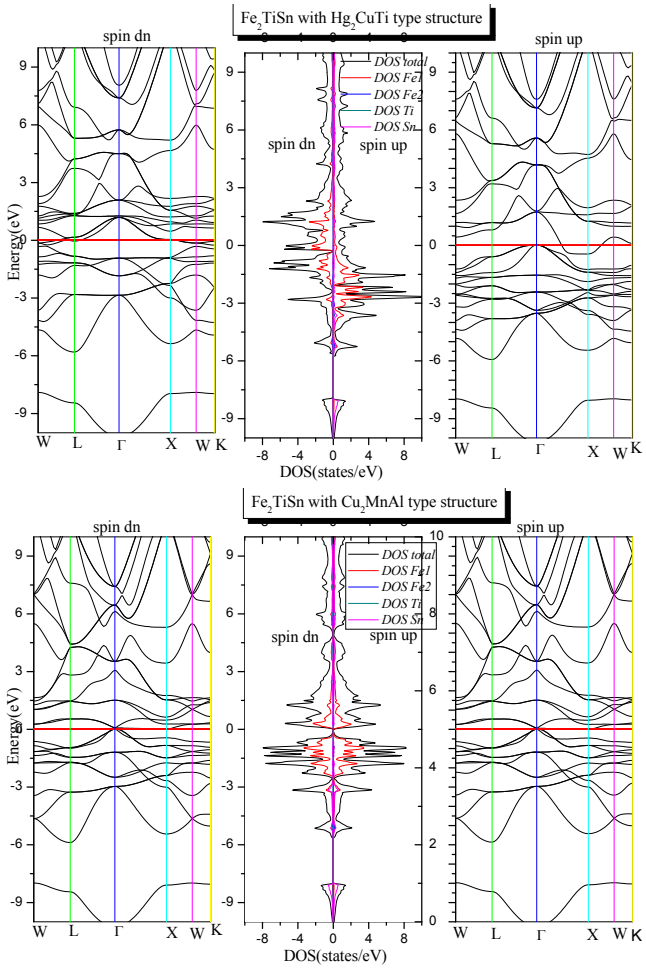

Figure 3. (Colour online) The calculated spin-polarized total and partial density of states and band structure of Fe_2TiSn with both Cu_2MnAl and Hg_2CuTi types structures.

Table 2. The calculated magnetic moments values (μ_B) of the of Fe_2YSn (Y = Mn, Ti and V) Heusler compounds.

		M_{Fe_1}	M_{Fe_2}	M_Z	M_{Sn}	$M_{interstitial}$	M_{total} (M_t)
Fe_2MnSn	Hg_2CuTi	2.47398	2.66903	3.29914	-0.06182	-0.05092	8.32940
	Cu_2MnAl	−0.20534	−0.16421	3.37041	−0.00477	0.01605	3.00014
Fe_2TiSn	Hg_2CuTi	2.34182	2.49429	−0.46420	−0.00535	−0.21745	4.14910
	Cu_2MnAl	0.00092 0.00 [29]	0.00053	0.00023 0.00 [29]	0.00001 0.00 [29]	0.00014	0.00000 0.00 [29]
Fe_2VSn	Hg_2CuTi	2.07363	2.73598	−1.63655	−0.00579	−0.40861	2.75866
	Cu_2MnAl	2.19361	2.19754	−1.06404	−0.01341	−0.28226	3.23143

We present the total magnetic moment, the local magnetic moments on Fe, Y (Y = Mn, Ti, and V), Sn atoms and interstitial moments which are given per unit cell. The calculated local and total magnetic moments in interstitial region for a Heusler compound Fe_2YSn with (Y = Mn, Ti and V) are presented in table 2. It must be noted that the total magnetic moment is very sensitive to both types of structures. For Fe_2YSn with (Y = Mn, Ti and V) with Hg_2CuTi type structure, the magnetic moment is mostly located

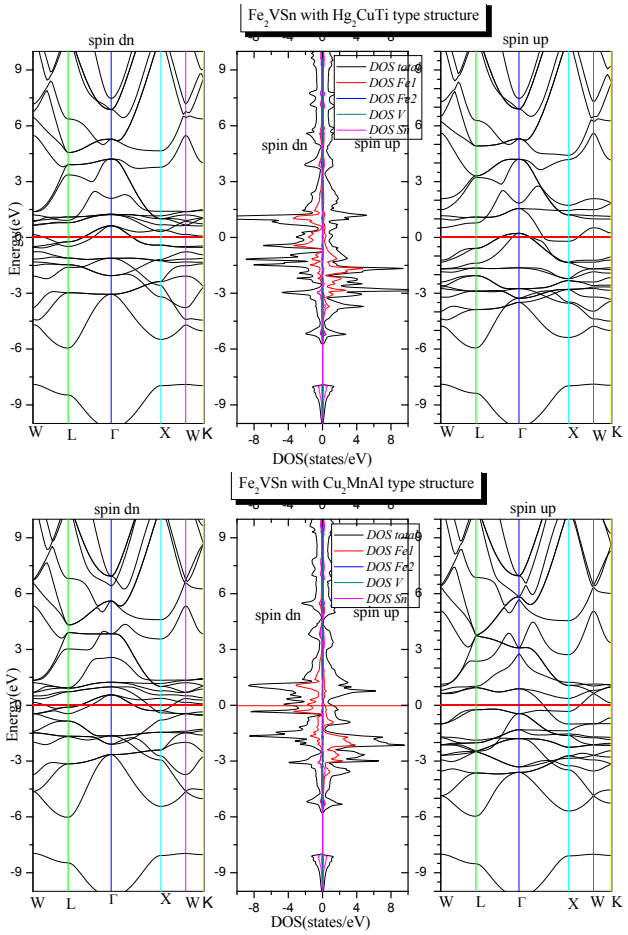

Figure 4. (Colour online) The calculated spin-polarized total and partial density of states and band structure of Fe_2VSn with both Cu_2MnAl and Hg_2CuTi types structures.

on the Fe atoms. Indeed, a great part of the total magnetic moment results from this atom. Therefore, the Sn atom has a minor magnetic moment, which does not give a lot to the total magnetic moment. The found values of the magnetic moment are dependent on the Slater-Pauling curve (SPC) [30] for full Heusler alloys, in which the magnetic moment per unit cell in multiples of Bohr magnetons (μ_B) can be calculated as follows:

$$M_{tot} = N - 24. \tag{3.4}$$

Here M_{tot} represents the total magnetic moment and N represents the total valence electrons in the unit cell. N is equal to 27 for Fe_2MnSn $[(8 \times 2) + 7 + 4 = 27]$, it is equal to 24 for Fe_2TiSn and $[(8 \times 2) + 4 + 4 = 24]$. The value of calculated magnetic moment have an integer value of $0\mu_B$ and $3\mu_B$ for Fe_2TiSn and Fe_2MnSn respectively with Cu_2MnAl type structure, which matches well with moments predicted from Slater-Pauling rule and evidences that these have potential to be half metallic. The magnetic moment of Fe_2TiSn is zero, the interaction between $3d$ electron of Fe and $3d$ electrons of Ti are in opposite directions and cancel the over-all moment. The Heusler alloy Fe_2TiSn has 24 valence electrons. These electrons occupy the majority and minority spin bands equally (12 up and 12 down), which results in a nonmagnetic semiconductor-like band structure [29]. These results agree well with preceding studies in Fe_2TiSn [29]. The total magnetic moment of Fe_2VSn is equal to $2.75866\mu_B$ and $3.23143\mu_B$ for Hg_2CuTi and Cu_2MnAl type structure very far from the integer value witch confirm that this alloys have not half metallic behavior.

4. Conclusion

We have performed ab-initio calculations to investigate the structural, electronic, magnetic properties of Fe_2YSn (Y = Mn, Ti and V) Heusler alloys with both Cu_2MnAl and Hg_2CuTi type structure. The negative formation energy is shown, as an evidence of the thermodynamic stability of Fe_2YSn (Y = Mn, Ti, and V) alloy. The Cu_2MnAl type structure is energetically more stable than the Hg_2CuTi type structure. Our calculations indicate that the 6.08 Å, 5.98 Å and 5.95 Å are the equilibrium lattice constant of Fe_2TiSn, Fe_2VSn and Fe_2MnSn with Cu_2MnAl, respectively. Furthermore, Fe_2MnSn and Fe_2TiSn in the ground state is considered to be a true half-metallic based on the calculations of the band structure and density of states. It is also predicted that Fe_2MnSn and Fe_2TiSn compounds are half-metallic with 100% spin polarization with an integer magnetic moments making these compounds a good candidates for spintronic devices applications.

5. Acknowledgement

This work has been supported by DGRST-ALGERIA.

References

1. De Groot R. A., Muller F. M., van Engen P. G., Buschow K. H., Phys. Rev. Lett., 1983, **50**, 2024–2027, doi:10.1103/PhysRevLett.50.2024.
2. Dahmane F., Mesri D., Tadjer A., Khenata R., Benalia S., Djoudi L., Doumi B., Boumia L., Aourag H., Mod. Phys. Lett. B, 2016, **30**, 1550265, doi:10.1142/S0217984915502656.
3. Dahmane F., Mogulkoc Y., Doumi B., Tadjer A., Khenata R., Bin Omran S., Rai D. P., Murtaza G., Varshney D., J. Magn. Magn. Mater., 2016, **407**, 167–174, doi:10.1016/j.jmmm.2016.01.074.
4. Abbouni N., Amari S., Sadouki H., Belkadi A., Zaoui Y., Obodo K. O., Beldi L., Bouhafs B., Spin, 2018, **8**, 1850020, doi:10.1142/S2010324718500200.
5. Dahmane F., Tadjer A., Doumi B., Mesri D., Aourag H., Sayede A., Mater. Sci. Semicond. Process., 2014, **21**, 66–73, doi:10.1016/j.mssp.2014.01.037.
6. Addadi Z., Doumi B., Mokaddem A., Elkeurti M., Sayede A., Tadjer A., Dahmane F., J. Supercond. Novel Magn., 2017, **30**, 917–923, doi:10.1007/s10948-016-3894-3.
7. Wen-Hui Xie, Ya-Qiong Xu, Bang-Gui Liu, Pettifor D. G., Phys. Rev. Lett, 2003, **91**, 037204, doi:10.1103/PhysRevLett.91.037204.
8. Li Fan, Feng Chen, Chun-mei Li, Xun Hou, Xin Zhu, Jiang-lei Luo, Thi-Qian Chen, J. Magn. Magn. Mater., 2020, **497**, 166060, doi:10.1016/j.jmmm.2019.166060.
9. Liu G. D., Dai X. F., Yu S. Y., Zhu Z. Y., Chen J. L., Wu G. H., Zhu H., Xiao J. Q., Phys. Rev. B, 2006, **74**, 054435, doi:10.1103/PhysRevB.74.054435.
10. Dai X., Liu G., Chen L., Chen J., Wu G., Solid State Commun., 2006, **140**, 533, doi:10.1016/j.ssc.2006.09.030.
11. Abu Baker D. N., Abu-Jafar M. S., Mousa A. A., Jaradat R. T., Ilaiwi K. F., Khenata R., Mater. Chem. Phys., 2020, **240**, 122122, doi:10.1016/j.matchemphys.2019.122122.
12. Shukla V., Kumar S. O., J. Magn. Magn. Mater., 2020, **498**, 166111, doi:10.1016/j.jmmm.2019.166111.
13. Graf T., Felser C., Parkinc S. S. P., Prog. Solid State Chem., 2011, **39**, 1–150, doi:10.1016/j.progsolidstchem.2011.02.001.
14. Kohn W., Sham L. J., Phys. Rev. A, 1965, **140**, 11331138, doi:10.1103/PhysRev.140.A1133.
15. Blaha P., Schwarz K., Luitz J., WIEN97: A Full Potential Linearized Augmented Plane Wave Package for Calculating Crystal Properties, Techn. Universitat Wien, Austria, 1999.
16. Perdew J. P., Burke K., Ernzerhof M., Phys. Rev. Lett., 1996, **77**, 3865, doi:10.1103/PhysRevLett.77.3865.
17. Murnaghan F. D., Proc. Natl. Acad. Sci. U.S.A., 1944, **30**, 244, doi:10.1073/pnas.30.9.244.
18. Luo H., Liu G., Meng F., Li J., Liu E., Wu G., J. Magn. Magn. Mater., 2012, **324**, 3295–3299, doi:10.1016/j.jmmm.2012.05.033.
19. Shastri S. S., Pandey S. K., Comput. Mater. Sci, 2018, **143**, 316–324, doi:10.1016/j.commatsci.2017.10.053.
20. Ślebarski A., J. Phys. D: Appl. Phys., 2006, **39**, 856–864, doi:10.1088/0022-3727/39/5/S12.
21. Dahmane F., Doumi B., Khenata R., Wang X. T., Bin Omran S., Rai D. P., Tadjer A., Indian J. Phys., 2018, **92**, 1403–1411, doi:10.1007/s12648-018-1243-z.

22. Hamad B., Charifi Z., Baaziz H., Soyalp F., J. Magn. Magn. Mater., 2012, **324**, 3345–3350, doi:10.1016/j.jmmm.2012.05.052.
23. Jain V. K., Lakshmi N., Jain R., Chandra A. R., J. Supercond. Novel Magn., 2019, **32**, 739–749, doi:10.1007/s10948-018-4751-3.
24. Rauf S., Arif S., Haneef M., Amin B., J. Phys. Chem. Solids, 2015, **76**, 153–169, doi:10.1016/j.jpcs.2014.07.021.
25. Ahmed N., Nisar J., Kouser R., Nabi A. G., Mukhtar S., Saeed Y., Nasim M. H., Mater. Res. Express, 2017, **4**, 065903, doi:10.1088/2053-1591/aa75fc.
26. Khan S., Ahmad N., Ahmed N., Safeer A., Iqbal J., Han X. F., J. Magn. Magn. Mater., 2018, **465**, 462–470, doi:10.1016/j.jmmm.2018.05.013.
27. Khandy S. A., Islam I., Gupta D. C., Khenata R., Laref A., Sci. Rep., 2019, **9**, 1475, doi:10.1038/s41598-018-37740-y.
28. Skaftouros S., Özdoğan K., Şaşioğlu E., Galanakis I., Phys. Rev. B, 2013, **87**, 024420.
29. Luo H., Liu G., Meng F., Li J., Liu E., Wu G., J. Magn. Magn. Mater., 2012, **324**, 3295–3299, doi:10.1016/j.jmmm.2012.05.033.
30. Hongzhi Luo, Yuepeng Xin, Bohua Liu, Fanbin Meng, Heyan Liu, Enke Liu, Guangheng Wu , J. Alloys Compd., 2016, **665**, 180–185, doi:10.1016/j.jallcom.2015.11.207.

Першопринципне моделювання напівметалічного феромагнетизму сплавів Гейслера Fe_2YSn (Y=Mn, Ti та V)

М. Саях[1], С. Зеффане[1], М. Мохтарі[1,2], Ф. Дахмане[1,3], Л. Зекрі[2], Р. Хената[3], Н. Зекрі[2]

[1] Інститут науки і техніки, університетський центр Тіссемсілта, 38000 Тіссемсілт, Алжир

[2] Університет науки і техніки ім. Мухаммеда Будіафа в Орані, Ель Нуар, 31000 Оран, Алжир

[3] Лабораторія квантової фізики та математичного моделювання, Технологічний факультет Університету Маскара, 29000 Маскара, Алжир

У роботі для дослідження структурних, електронних та магнітних властивостей Fe_2YSn з (Y = Mn, Ti та V) використовується першопринципне моделювання на основі функціоналу густини у рамках узагальненого градієнтного наближення. Структури типу Cu_2MnAl є більш енергетично стійкими, ніж Hg_2CuTi. Від'ємна енергія утворення є свідченням термодинамічної стійкості сплаву. Для рівноважного значення сталої гратки розрахований повний спіновий момент складає $3\mu_B$ та $0\mu_B$ для сплавів Fe_2MnSn та Fe_2TiSn, відповідно, що узгоджується з правилом Слейтера-Паулінга $M_t = Z_t - 24$. Вивчення електронних та магнітних властивостей підтверджує, що повні гейслерівські сплави Fe_2MnSn і Fe_2TiSn є типовими напівметалічними феромагнітними матеріалами.

Ключові слова: *сплави Гейслера, електронна структура, першопринципне моделювання, напівметалічність*